

MATERIAL FACTORS INFLUENCING METALLIC WHISKER GROWTH

Except where reference is made to the work of others, the work described in this dissertation is my own or was done in collaboration with my advisory committee. This dissertation does not include proprietary or classified information.

Chad L. Rodekohr

Certificate of Approval:

George T. Flowers, Co-Chair
Professor
Mechanical Engineering

Michael J. Bozack, Co-Chair
Professor
Physics

Jeffrey C. Suhling
Quina Professor
Mechanical Engineering

Pradeep Lall
Thomas Walter Professor
Mechanical Engineering

Joe F. Pittman
Interim Dean
Graduate School

MATERIAL FACTORS INFLUENCING METALLIC WHISKER GROWTH

Chad L. Rodekohr

A Dissertation

Submitted to

the Graduate Faculty of

Auburn University

in Partial Fulfillment of the

Requirements for the

Degree of

Doctor of Philosophy

Auburn, Alabama
December 19, 2008

MATERIAL FACTORS INFLUENCING METALLIC WHISKER GROWTH

Chad L. Rodekohr

Permission is granted to Auburn University to make copies of this dissertation at its discretion, upon request of individuals or institutions and at their expense. The author reserves all publication rights.

Signature of Author

Date of Graduation

VITA

Chad L. Rodekohr is the son of Donn and Becky Rodekohr and was born on November 12, 1973 in Norfolk, Nebraska (USA). He obtained a Bachelor of Science degree in Aviation Management from Auburn University in December 1997 and subsequently taught science in secondary school. Later, he returned to Auburn University as a research assistant in the Physics Department, earning a Master of Science degree in Physics in May 2006. His scientific interests include electronics packaging, solder reliability, tin whiskers, and electron microscopy.

DISSERTATION ABSTRACT

MATERIAL FACTORS INFLUENCING METALLIC WHISKER GROWTH

Chad L. Rodekohr

Doctor of Philosophy December 19, 2008
(M.S., Auburn University, 2006)
(B.S., Auburn University, 1997)

173 pages typed

Directed by Michael J. Bozack and George T. Flowers

Whiskering refers to the formation of slender, long, metallic filaments, much thinner than a human hair, that grow on a metallic thin film surface. They are readily observed for pure and alloyed zinc (Zn), silver (Ag), cadmium (Cd), indium (In), and tin

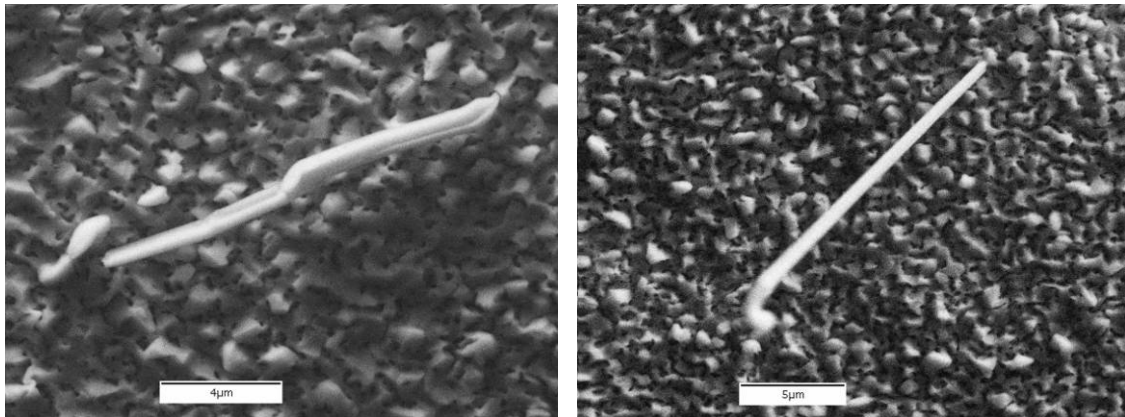


Figure 1 Micrographs of typical Sn whiskers

(Sn) surfaces. The longest reported whisker length is 4.5 mm long but most high-aspect ratio whiskers range from 1-500 μm . The focus of this research is upon Sn whiskers. Sn whiskers pose serious reliability problems for the electronics industry and are known to be the source of failure in a wide range of electronic devices, such as nuclear power facilities, heart pacemakers, commercial satellites, aviation radar, telecommunication equipment, and desktop computers. The problem with whiskering has been recently exacerbated by the worldwide shift to lead (Pb) free electronics and the continuing reduction in electrical contact pitches. A thorough understanding of the growth mechanism of Sn whiskers is urgently needed. Currently, there is no universally accepted model that explains the broad range of observations on whiskering.

The goals of this research are: 1) to develop a more detailed understanding of the physical mechanisms leading to the initiation and growth of Sn whiskers and 2) to outline reasonable mitigation strategies that could be followed to reduce or eliminate the problem of Sn whiskers. The major contributions of this work are:

- A reliable method for growing Sn whiskers with predictable incubation times has been developed and tested.
- A surface oxide is not necessary for whisker growth.
- Intermetallic compounds (IMC) are not necessary for whisker growth.
- Smoother, not rougher, substrate surfaces promote whisker growth.
- Whiskers grow under both compressive and tensile thin film stress states.
- Whisker growth increases with externally applied compression and tension forces.
- Sn whiskers are composed of pure Sn except for the expected thin, native Sn oxide on their surface.

- For Sn on brass, the atom feedstock for whiskers lies within the film exclusively; the brass substrate does not contribute to whisker production.
- The volume of film consumed by a metallic whisker is a simple volumetric calculation.
- There are likely to be multiple mechanisms of whisker growth depending on the substrate – thin film system.
- In general, the thickness of a metallic film does not have an effect on whisker growth qualities.

ACKNOWLEDGMENTS

Throughout my tenure as a student at Auburn University, Dr. Bozack has been my mentor and a constant source of wisdom. He is my reason for coming back to school in pursuit of advanced degrees. My path through graduate education would not be possible without the consistent love and support of my wife Rachel, who (among many other things) fearlessly and selflessly took on the challenge of being at home with our children during this time. Special thanks goes to my parents who taught me Christian values and whose legacy I can only hope to follow. All glory belongs to the God of heaven and earth who has saved me through His Son Jesus Christ.

This dissertation would not be possible without the expert guidance of my committee members. Thanks also to the scientists and engineers who make up the industrial partners of the Center for Advanced Vehicle Electronics (CAVE), who have provided valuable direction and support for this work.

Style manual or journal used: IEEE Transactions on Electronics Packaging
Manufacturing

Computer software used: Microsoft Word, Microsoft Excel, Microsoft Power Point,
Mathematica 4.1, ERDAS Imagine 8.7, OriginPro7, Adobe Photo Shop 7.0.1

TABLE OF CONTENTS

LIST OF FIGURES.....	xiii
LIST OF TABLES	xix
CHAPTER 1 INTRODUCTION AND BACKGROUND.....	1
1.1 Problems in Electronics Components.....	1
1.2 Failure Modes	1
1.3 Timeliness of the Issue	2
1.4 Thin Film Deposition	3
1.5 Research Objectives	5
CHAPTER 2 REVIEW OF LITERATURE.....	6
2.1 The Oxidation Factor.....	7
2.2 The Crystallography Factor.....	7
2.3 The Extrusion Factor	11
CHAPTER 3 EXPERIMENTAL INVESTIGATIONS	14
3.1 Reproducibility of Sn Whisker Incubation.....	14
3.2 Role of Surface Oxides.....	17
3.3 Role of Compressive Stress from Intermetallic Growth	19
3.4 Effect of Surface Smoothness	21
3.5 Role of the Film Stress State	28
3.6 Composition of the Whisker Surface	32

3.7 Feedstock Origin of Sn Atoms	39
3.8 Whisker Growth from Metallic Films Other Than Sn.....	41
3.8.1 Zinc Metallic Films	43
3.8.2 Cadmium Metallic Films.....	47
3.8.3 Silver Metallic Films	52
3.8.4 Zinc Metallic Films	57
3.9 Influence of Known Extrinsic Stresses.....	60
3.9.1 6000Å of Tin on Brass Substrates	63
3.9.2 1500Å of Tin on Aluminum Substrates.....	68
3.9.3 6000Å of Tin on Aluminum Substrates.....	73
3.10 Influence of Film Thickness on Whisker Growth	81
CHAPTER 4 CONCLUSIONS	84
CHAPTER 5 SUGGESTIONS FOR AND DEVELOPMENT OF FUTURE WORK.....	88
5.1 Intermetallic Development in a Thin Film-Substrate System	88
5.2 Intrinsic Stresses in a Thin Film-Substrate System.....	89
5.3 A Multi-Media Time Elapsed Comparison of Whisker Growth, Intrinsic Stress, and Intermetallic Development.....	105
5.4 Do Alloyed Whiskers Exist?	105
5.5 Development of a Working Model of Whisker Incubation, Initiation, and Growth.....	106
5.6 Confirmation of Model Validity Using a Finite Element Method	106
REFERENCES	107
APPENDIX 1 DERIVATION OF STRESS IN A THIN FILM	110

A1.1 Introduction	110
A1.2 Derivation of Intrinsic Stresses.....	112
A1.3 Derivation of Externally Imposed Stresses	121
APPENDIX 2 DERIVATION AND JUSTIFICATION OF THE RADIUS OF CURVATURE FROM A MEASURED DISPLACEMENT IN A CURVED BEAM	126
APPENDIX 3 A DISCUSSION ON THE ORIGINS OF FILM STRESS	129
A3.1 Introduction	129
A3.2 Atomic Peening	130
A3.3 Coefficient of Thermal Expansion Mismatch	131
A3.4 Microstructure stabilization.....	134
A3.5 Surface Oxidation.....	135
A3.6 Oxidation Within the Grain Boundaries.....	135
A3.7 Intermetallic Development	135
A3.8 Externally Applied Stress	136
A3.9 Intrinsic Stress State	136
APPENDIX 4 EXTERNAL STRESS FIXTURE DESCRIPTIONS, DIMENSIONS, AND DIAGRAMS	142
APPENDIX 5 PLOTS OF TOTAL STRESS STATE VS. QUALITIES OF WHISKER GROWTH WHEN EXTERNAL STRESS IS VARIED	147
A5.1 6000Å of Tin on a 0.125 mm Brass Substrate.....	147
A5.2 6000Å of Tin on a 0.25 mm Aluminum Substrate	149
A5.3 1500Å of Tin on a 0.25 mm Aluminum Substrate	151

LIST OF FIGURES

Figure 1 (Abstract) Micrographs of typical Sn whiskers	v
Figure 1.1 Input output (I/O) connectors of a QFP with a pitch of 20 μ m.....	3
Figure 2.1 Columnar grains pushing a whisker out at an imperfect grain	8
Figure 2.2 A grain being destroyed and recrystallized into a whisker	10
Figure 2.3 Growth orientation and kink orientation.....	10
Figure 2.4 The copper-tin phase diagram.....	12
Figure 2.5 A whisker with a striation along its length	13
Figure 3.1 Pictorial representation of native oxide removal by an Ar ⁺ ion beam and the resulting whiskers	17
Figure 3.2 Micrographs of whiskers on cleaned (left) and un-cleaned (right) sections of the sample.....	18
Figure 3.3 Al-Sn phase diagram, with no eutectic point and hence no IMC layer	20
Figure 3.4 Bubble in the Sn film on an Al substrate	20
Figure 3.5 How a rough IMC produces a compressive stress parallel to the surface.....	21
Figure 3.6 Electro-chemical etching showing how sharp points are smoothed	23
Figure 3.7 Thornton and Hoffman's chart, modified to show Sn's threshold pressure ...	29
Figure 3.8 Micrographs of three Sn films before incubation, deposited at 2,7, and 9 mTorr, respectively.....	31

Figure 3.9 Micrographs showing the whiskers that grew on the samples shown in Figure 3.8.....	31
Figure 3.10 High resolution micrographs showing the whisker base (1), film (2), whisker middle (3), and whisker tip (4) analyzed using AES.....	35
Figure 3.11 Auger spectra of the surfaces of the Sn film and the whisker base	36
Figure 3.12 Auger spectra of the surfaces of a central portion of the whisker and its tip.....	37
Figure 3.13 Auger spectra at point #3 after 250Å and 500Å of the whisker had been removed using an Ar ⁺ ion beam	38
Figure 3.14 Auger Spectrum at point #3 after 1000Å of the whisker had been removed.....	39
Figure 3.15 High resolution micrograph showing a small area of depletion for a large whisker	41
Figure 3.16 Small whisker found on the sample with 1500Å of Zn	43
Figure 3.17 Whisker on sample with 1500Å of Ag on a polished substrate.....	53
Figure 3.18 Direction of external moment required to create a uniform tangential compressive stress state in a thin film.....	61
Figure 3.19 Direction of external moment required to create a uniform tangential tensile stress state in a thin film.....	61
Figure 3.20 Fixtures used to create a uniform tangential compressive (left) and tensile (right) stress state in a thin film	62
Figure 3.21 Whisker found after 85 days	63

Figure 3.22 Surface of sample (left) incubated at -215 MPa, with whiskers from side (right) and surface (bottom) of surface	64
Figure 3.23 Surface of sample (left) incubated at -107 MPa (magnification ~490x) with close-up of whisker (right)	64
Figure 3.24 Surface of sample (left) incubated at -71 MPa (magnification ~490x) with close-up of whisker (right)	64
Figure 3.25 Close-up of whisker on sample incubated at -43 MPa.....	65
Figure 3.26 Whiskers on sample incubated at 43 MPa	65
Figure 3.27 Micrographs of grooves on samples stored under tensile stress	65
Figure 3.28 Surface of sample (upper left) incubated at 107 MPa magnified at ~490x. Remaining micrographs show whiskers on this surface	66
Figure 3.29 Surface of sample incubated at 107 MPa (magnification ~490x) close to the source of compressive normal stress exerted by the clamp.....	66
Figure 3.30 Surface of sample incubated at 213 MPa magnified at ~490x (left) showing vertical ‘stretch marks and horizontal relief marks, with a typical whisker (right)	67
Figure 3.31 Whisker population density (left) and average whisker length (right) as a function of stress.....	68
Figure 3.32 Micrographs of whiskers incubated at -432.8 MPa	69
Figure 3.33 Collage showing micrograph of longest whisker (543 μm) found, on sample incubated at -215.3 MPa	70
Figure 3.34 Long whiskers on sample incubated at -142.5 MPa	70
Figure 3.35 Typical whiskers on sample incubated at -85.5 MPa.....	71

Figure 3.36 Typical whiskers on sample incubated at 85.5 MPa.....	71
Figure 3.37 Typical whiskers on sample incubated at 142.6 MPa.....	71
Figure 3.38 Short (left) and long (right) whiskers on sample incubated at 213.3 MPa ...	72
Figure 3.39 Micrographs of whiskers from samples incubated at 425.1 MPa.....	72
Figure 3.40 Population density (left) and average whisker length (right) as a function of stress.....	73
Figure 3.41 Typical whiskers on sample incubated at -432.4 MPa.....	74
Figure 3.42 Typical whiskers on sample incubated at -215.1 MPa.....	74
Figure 3.43 Typical whiskers on sample incubated at -142.3 MPa.....	74
Figure 3.44 Typical whiskers on sample incubated at -85.4 MPa.....	75
Figure 3.45 Typical whisker on sample incubated at 85.4 MPa	75
Figure 3.46 Typical whiskers on sample incubated at 142.5 MPa.....	76
Figure 3.47 Typical whiskers on sample incubated at 213.1 MPa.....	76
Figure 3.48 Detailed micrographs of typical whiskers on sample incubated at 424.6 MPa.....	77
Figure 3.49 Additional micrographs of sample in previous figure	78
Figure 3.50 Whisker population density (left) and average whisker length (right) as a function of stress.....	79
Figure 5.1 The IMC layer developed in a solder-substrate system	88
Figure 5.2 Effect of an intrinsic compressive stress on a thin film-substrate system	89
Figure 5.3 Effect of an intrinsic tensile stress on a thin film-substrate system	90
Figure 5.4 Dimensions of samples used to measure intrinsic stresses in a deposited film	91

Figure 5.5 Fixture used to mount samples.....	91
Figure A1.1 Exaggerated bend in a substrate–thin film system and measurements used to determine the stress in the film	110
Figure A1.2 Difference between ‘exact’ stress (derived in this appendix) and Stoney’s approximated stress in the film.....	111
Figure A1.3 Difference between ‘exact’ stress (derived in this appendix) and Stoney’s approximated stress in the substrate	111
Figure A1.4 Thin film-substrate system that has not undergone bending.....	112
Figure A1.5 Thin film-substrate system that has undergone bending.....	113
Figure A1.6 Cross section of a substrate–thin film system, viewed along the width.....	114
Figure A1.7 Stress gradients and equivalent forces associated with a substrate–thin film system that has undergone bending	115
Figure A1.8 Substrate - thin film system, with R and ρ labeled	117
Figure A1.9 Dimensions needed to determine Q of the film at the interface between the film and the substrate.....	123
Figure A2.1 Measurement of Δx relative to each leaf of the samples.....	126
Figure A3.1 Definition of Cartesian Coordinate system used for samples in this study	130
Figure A3.2 The σ_{xx} component of intrinsic stress as a function of time in 1500Å of Sn on an aluminum substrate	138
Figure A4.1 Computer aided drawing of fixture used to impose external compressive stress	143

Figure A4.2 Computer aided drawing of fixture used to impose external tensile stress	144
Figure A4.3 Physical dimensions of fixture used to produce externally applied compressive stress	145
Figure A4.4 Physical dimensions of fixture used to produce externally applied tensile stress.....	146
Figure A5.1 Whisker growth as a function of the σ_{xx} component of total stress.....	147
Figure A5.2 Whisker growth as a function of the σ_{yy} component of total stress.....	147
Figure A5.3 Whisker growth as a function of the σ_{zz} component of total stress.....	148
Figure A5.4 Whisker growth as a function of the σ_{xy} component of total stress.....	148
Figure A5.5 Whisker growth as a function of the σ_{xx} component of total stress.....	149
Figure A5.6 Whisker growth as a function of the σ_{yy} component of total stress.....	149
Figure A5.7 Whisker growth as a function of the σ_{zz} component of total stress.....	150
Figure A5.8 Whisker growth as a function of the σ_{xy} component of total stress.....	150
Figure A5.9 Whisker growth as a function of the σ_{xx} component of total stress.....	151
Figure A5.10 Whisker growth as a function of the σ_{yy} component of total stress.....	151
Figure A5.11 Whisker growth as a function of the σ_{zz} component of total stress.....	152
Figure A5.12 Whisker growth as a function of the σ_{xy} component of total stress.....	152

LIST OF TABLES

Table 3.1	Micrographs of whiskers grown using the new preparation process	16
Table 3.2	Extremes of roughness measurements, their characteristics, and the resulting histograms.....	24
Table 3.3	Surface conditions used, surface roughness, and the associated histogram from AFM analysis.....	26
Table 3.4	The impact of surface roughness on whisker growth.....	27
Table 3.5	Area of Sn film necessary for whisker growth.....	40
Table 3.6	Investigation matrix for metallic whiskers other than Sn.....	42
Table 3.7	Micrographs of surfaces with Zn film.....	46
Table 3.8	Data for whiskers found on Zn film samples	47
Table 3.9	Micrographs of surfaces with Cd film.....	51
Table 3.10	Data for whiskers on Cd film samples	52
Table 3.11	Predicted radius and area of film needed to grow the whisker in Figure 3.17	54
Table 3.12	Micrographs of surfaces with Ag film	56
Table 3.13	Data for whiskers on Ag film samples	57
Table 3.14	Micrographs of surfaces with In film.....	59

Table 3.15 Data for whiskers on In film samples.....	60
Table 3.16 Externally applied stress on brass substrates: raw data.....	67
Table 3.17 Population density and average whisker length at each stress level	73
Table 3.18 Population density and average whisker length at each stress level	79
Table 3.22 Population density and average whisker length from the study in Dection 3.9	81
Table 3.23 Population density and average whisker length from the study in Section 3.3	82
Table 3.24 Population density and average whisker length for the study in Section 3.8	82
Table 5.1 Sample matrix used for preliminary study	92
Table 5.2 Stress change over time in a brass substrate–Ag film system.....	93
Table 5.3 Stress change over time in a brass substrate–Zn film system	94
Table 5.4 Stress change over time in a brass substrate–Cd film system	95
Table 5.5 Stress change over time in a brass substrate–In film system	96
Table 5.6 Stress change over time in a brass substrate–Sn (6000Å) film system.....	97
Table 5.7 Stress change over time in a brass substrate–Sn (1500Å) film system.....	98
Table 5.8 Stress change over time in an Al substrate–Sn (6000Å) film system	99
Table 5.9 Stress change over time in an Al substrate–Sn (1500Å) film system	100
Table 5.10 Whisker data for final stress states for 6000Å Sn on Brass	102
Table 5.11 Whisker data for final stress states for 6000Å of Sn on Al.....	103
Table 5.12 Whisker data for final stress states for 1500Å of Sn on Al.....	104

Table A1.1. Equations describing the effect of internal tensile stress(es) in a thin film that force the system to conform to a concave curve.....	119
Table A1.2. Equations describing the effect of internal compressive stress(es) in a thin film that force the system to conform to a convex curve.....	120
Table A1.3 Equations describing the normal and shear stress that arise when an external source is used to force a compressive stress state in the thin film.....	124
Table A1.4 Equations describing the effect of an external moment applied to force a tensile stress state in a thin film.....	125
Table A2.1 Extreme measured values of Δx	128
Table A3.1 Characteristics of materials used in this study	137

CHAPTER 1 INTRODUCTION AND BACKGROUND

1.1 Problems in Electronic Components

Metallic whiskers have been anecdotally observed in electronic components for decades. In the first published paper on this topic, Cobb [1] (1946) noted the presence of cadmium whiskers on capacitors. Since that time, research on metallic whiskers has been sporadic, with particular attention being devoted to Sn whiskers. Sn whiskers are important because the modern electronics industry depends on Sn for a variety of circuit applications where the growth of Sn whiskers may create short circuits. In a complex electrical circuit, for example, a thin metallic Sn film is frequently used to solder components (resistors, capacitors, inductors) to printed circuit boards (PCBs). Due to its ideal wetting characteristics and low capital investment, Sn is an ideal metal for board finishes, but it is from Sn that whiskers are most likely to grow.

1.2 Failure Modes

There are at least four ways a Sn whisker may cause a failure in an electronic system. When a whisker grows between two electrically isolated contact points, a short circuit occurs. If the current is low, the whisker will form a 1) *stable short circuit*, but if the current is high enough, Joule heating will cause the whisker to fuse and form a 2) *transient short circuit*. This occurs when its current density is greater than 4.5 mA/cm^2 (calculated from data collected by Dunn [2]). By contrast, if the ambient pressure is low

say as in a vacuum chamber or in the vacuum of space, the fused whisker can sublime to the plasma state and become significantly more conductive (> 200 amps), causing a catastrophic meltdown of the entire electronic system known as 3) *plasma arcing*. Finally, whiskers may break loose from a surface and become 4) *debris or contamination* in the system. The debris becomes a problem when it falls between two electrical connectors, causing one of the other three failures. It could also interfere with a micro electro mechanical (MEMS) type device [3].

1.3 Timeliness of the Issue

The use of Pb in Sn alloys was first introduced as a Sn whisker mitigation technique in 1959 [4]. It is thought that the presence of Pb in the film serves to reduce stress to the point where Sn whiskers are eliminated. This mitigation technique temporarily solved the problem of Sn whiskers, but fears that the Pb in discarded electronic systems will seep into human water sources have lead to global legislation mandating the use of 'green' or 'Pb-free' electronics. The European Union (EU) passed legislation in 2006 known as "The Restriction of the Use of Certain Hazardous Substances in Electrical and Electronic Equipment", or the *RoHS Directive* [5]. This legislation and related market drivers are causing the electronics industry to abandon the best defense against Sn whiskers.

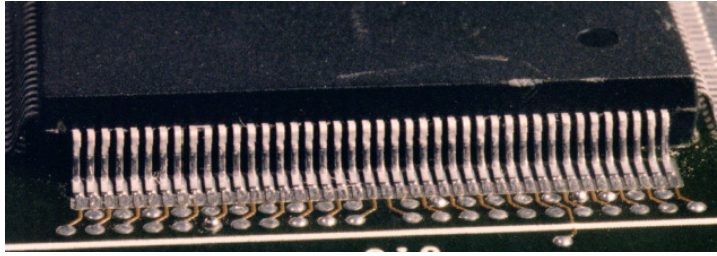


Figure 1.1 Input output (I/O) connectors of a QFP with a pitch of $20\mu\text{m}$ [6].

A second factor that has increased the need for a better understanding of Sn whiskers is the electronics packaging industry, who continues to decrease the input/output connector pitch. The original DIP (dual in line package) had a pitch of 100 mils (0.1 inches, or $2500\mu\text{m}$), but current QFPs (quad flat packages) and flip chip packages can have pitches as low as 6-8 mils ($150\text{-}200\mu\text{m}$). Since Sn whiskers can approach $1\text{-}500\mu\text{m}$ in length, this means that Sn whiskers have to be completely eliminated, not just confined to a limited growth length.

Due to the worldwide elimination of Pb and the continuing decrease in packaging dimensions, the area of Sn whiskers is currently being pursued vigorously. There have been more published papers on the subject of whiskering in the past 6 years than in the previous 54 [7].

1.4 Thin Film Deposition

There are many ways to produce thin films with variations that can drastically change the characteristics of the deposited film from which whisker grow. It is important to be aware of the thin film methods and interpret their results accordingly. In industry, the most common way to deposit a thin film is by electroplating. This is the process of using a Sn anode and the substrate as the cathode in an acidic liquid solution,

commonly a sulfuric acid solution. The length of time, applied voltage, and the specific acid solution control the thickness of the film and affect the stress state of the Sn.

Impurities in the acid solution may lead to impurities in the film, which then modifies the stress within the matrix of the film's atomic structure.

Sputter deposition is a method of film deposition common in academic laboratory studies. In sputter deposition, single atoms of Sn are removed (sputtered) from a target of solid Sn by a plasma [8] (typically Ar). The Sn atoms leave the solid and adhere to an adjoining substrate. Sputter deposition is conducted in a vacuum chamber with a low atmosphere of pure Ar. The gas pressure, which determines the mean free path of the Sn atoms, gas purity, the degree of bias between the solid Sn cathode and the substrate anode, and the possible use of magnetic fields all have effects on the stress state and grain structure of the deposited Sn layer.

Deposited Sn films are conveniently grouped into three categories based on their final appearance. *Matte* Sn describes deposited Sn that is dull gray in appearance and has a large non-uniform grain structure. *Bright* Sn reflects light better than matte Sn and is characterized by the smallest grain structures. *Satin* Sn falls between matte and bright Sn in reflectance. Board finish manufacturers prefer to have a bright Sn coating because it is more visually appealing, but bright Sn suffers from the highest incidence of whisker formation [9].

A related issue for thin films involves adhesion to the supporting substrate. Many factors contribute to film adhesion [10], including chemical and mechanical bonding, diffusion rates, built-in stresses, thermal stresses, surface topography, surface impurities, and surface preparation. A few studies [11] have suggested that whisker

growth is directly correlated to adhesion, so it is important for researchers to ensure adequate adhesion in their studies.

1.5 Research Objectives

The objectives of this research were to:

- 1) develop more detailed understanding of the physical mechanisms leading to the initiation and growth of Sn whiskers; and
- 2) find ways to reduce whiskering, particularly in Pb-free electronic components.

The experimental design to pursue these objectives led to the following set of investigations:

- Determine a method to predictably grow Sn whiskers through manipulation of background Ar pressure during the sputter deposition process.
- Determine the effects of surface oxides on whisker growth.
- Determine the effects of IMC growth on whisker growth.
- Determine the effectiveness of surface polishing as a mitigation practice.
- Evaluate the film stress state required for whisker growth.
- Determine the surface and bulk composition of Sn whiskers grown from Sn on brass.
- Find general characteristics of whisker growth by studying other types of metallic whiskers (ie. Zn, Ag, Cd, and In).
- Experimentally quantify the effects of varying amounts externally applied stress.
- Determine the effects of film thickness on whisker growth.

CHAPTER 2 REVIEW OF LITERATURE

Early research on Sn whiskers largely consisted of anecdotal observations of whiskering. A complete understanding of how Sn whiskers are formed has eluded investigators for over fifty years; this understanding has been dubbed ‘the end game.’ [11] In order for a single, comprehensive theory to end the game, it must reconcile the abundance of empirical observations on whiskering that have been reported throughout the literature. The observations are the listed here [12]. The end game theory must describe:

1. Why Sn whiskers are made of pure Sn.
2. Why Sn whiskers are composed of a single crystal.
3. Why Sn whiskers are not observed immediately, but instead require unpredictable incubation times.
4. Why Sn whiskers do not continue to grow indefinitely, but instead reach a point at which growth completely stops.
5. How Sn is transported to the whisker.

So far there have been no models that fully correlate these observations. End game theories typically include three primary whiskering factors; namely, *oxidation*, *crystallography*, and *extrusion*. A complete description of end game theories is beyond the scope of this chapter; instead, a general understanding of the important ideas will be presented here.

2.1 The Oxidation Factor

Several research groups believe oxidation drives whisker formation [11, 13, 14]. Proponents of oxidation-based models of whiskering argue that the growth of whiskers can be forestalled or eliminated by simply preventing oxygen from entering the Sn film. The oxygen exists as native Sn-oxide at the surface of the Sn film and the oxygen or Sn-oxide within the grain boundaries of the Sn film. The Sn-oxide surface layer is believed to seal the Sn into place and form a pressure normal to the Sn film. A crack, hole, or weak spot in this oxidation layer subsequently provides a way for the Sn to escape the pressurized Sn layer, initiating a whisker.

Others believe that the stress within the Sn is caused by oxygen seeping into the grain boundaries of the deposited Sn film. These oxygen atoms occupy a previously unoccupied volume within the film pushing on the surrounding atoms to create an overall internal tangential compressive stress. Formation of Sn-oxide (either SnO or SnO₂) in the grain boundaries of the film also increases the internal compressive stress tangentially to the surface and is thought to serve as the driving force that pushes the whiskers out.

2.2 The Crystallography Factor

Papers from the 1950's were captivated with the role of crystallographic dislocation in whiskering [11]. Some recent research supports its validity [15]. This factor posits that Sn atoms migrate to the whisker along crystallographic dislocations, although the suggested driver for the migration varies from theory to theory. One study assumed atomic migration through screw dislocations in the whisker center, where each atom worked its way through the core of the whisker to deposit itself at the end of the

whisker [16]. Others have suggested that screw dislocations move each atom to the base of the whisker. The Burger vector is frequently used to calculate the growth rate of the

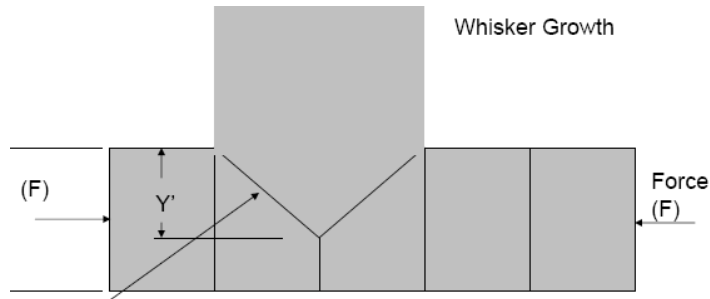


Figure 2.1 Columnar grains pushing a whisker out at an imperfect grain [11].

whisker.

Edge, slip, or glide dislocations are thought to cause atoms to migrate from the bulk or surface of the Sn to the whisker nucleation point. A study by Smetana [11] examined the sliding of one grain along the boundary of two or three others, suggesting that the compressive stress acting parallel to the surface pushes on the columnar Sn grain boundaries, with slippage beginning at any grain boundary that is not perfectly vertical. Figure 2.1 shows that stress parallel to the surface is evenly applied in columnar tin grains, but at the boundaries that are not vertical, the stress is lower than in the surrounding areas. As the crooked grain slips in the vertical direction, vacancies are formed beneath it. The vacancies and the surrounding stress gradient drive the Sn atoms to the nucleation point of the whisker. Smetana then explains why some whiskers are straight while others are curly, which he ascribes to imperfect crystal structure. If a row

of atoms are missing, there is a kink in the whisker, while if a series of rows are missing, effect is magnified and a curl forms.

It has also been suggested that strain energy density plays a role [14]. Strain energy density is defined in equation 2.1,

$$U = \frac{1}{2} \underline{\sigma} \cdot \underline{\varepsilon} \quad (\text{Equation 2.2.1})$$

where the nine element (six of which are independent) stress and strain tensors are written in six dimensional vector form as, equation 2.2 and equation 2.3 respectively.

$$\underline{\sigma} \equiv \begin{pmatrix} \sigma_{11} \\ \sigma_{22} \\ \sigma_{33} \\ \sigma_{12} \\ \sigma_{13} \\ \sigma_{23} \end{pmatrix} \quad (\text{Equation 2.2.2})$$

$$\underline{\varepsilon} \equiv \begin{pmatrix} \varepsilon_{11} \\ \varepsilon_{22} \\ \varepsilon_{33} \\ \varepsilon_{12} \\ \varepsilon_{13} \\ \varepsilon_{23} \end{pmatrix} \quad (\text{Equation 2.2.3})$$

Stress and strain are also linked through Hooke's law (equation 2.4),

$$\underline{\varepsilon} = \underline{\underline{S}} \cdot \underline{\sigma} \quad (\text{Equation 2.2.4})$$

where $\underline{\underline{S}}$ is the 36 element symmetric (assuming that the Sn grains exhibit elastic characteristics) compliance matrix. Sn grains are orthotropic in nature and there are 9 independent elements in the symmetric compliance matrix. The strain energy density can be calculated at any grain boundary, which can be represented by 3 grain boundary

points assuming that $(h_1, k_1, l_1) \neq (h_2, k_2, l_2) \neq (h_3, k_3, l_3)$. The energy can be calculated as each grain is rotated through the 360 degrees of θ for each 180 degrees of φ , expressed in spherical coordinates. To aid in the calculations, Hoffman et al. fixed φ , and stepped θ through the full rotation in 20° increments. The results revealed that when the strain energy density reached a critical value, one of the grains began to be destroyed by neighboring grains and the pieces could possibly recrystallize into a uniform crystal, effectively lowering the strain energy by escaping in the form of a whisker.

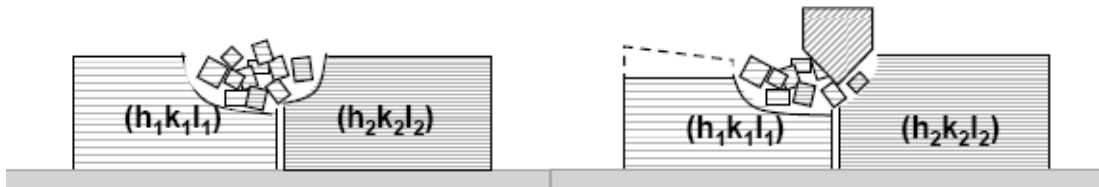


Figure 2.2 A grain being destroyed and recrystallized into a whisker [15].

The crystallography factor is often used to explain how the crystallographic orientation of the whisker growth is related to the orientation of the grains from which the whisker grows [17]. Lee and Lee suggested that whiskers prefer to grow at angles of 63° and 27° to the surface and thus the kinks in the whiskers can only be at either 90° or

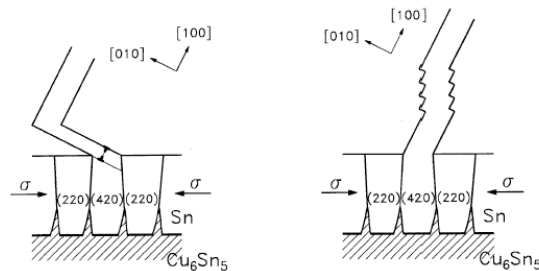


Figure 2.3 Growth orientation and kink orientation [17].

27° to the growth direction. The angles of 63° and 27° are formed by the recrystallization of Sn atoms along the [100] direction (63°) or the [010] direction (27°). Lee and Lee determined the preferred orientation of deposited Sn by comparing XRD measurements of the film to those for powdered tin, which made it possible to relate the voltage of the electro-deposition to the preferred orientation of the grain structure. By using TEM, they measured the preferred angle of whisker growth by measuring the projected length of whiskers at two known angles of observation and the direction of the whisker growth axis. They argued that whiskers only grow when the planar orientation of an individual grain is different from that of the majority of the grains around it (for example, if the grain is (420), while the preferred direction is (220)). They suggested that this difference in orientation causes an increase in the out-of-plane strain, which forces a crack in the oxide layer. The crack permits a whisker to escape in order to relieve the internal stress in the bulk Sn. They argued that the Sn atoms are transported to the crack via a Bardeen-Herring dislocation, which provides the source of Sn atoms for the whisker until the stress is relieved.

2.3 The Extrusion Factor

Extrusion advocates argue that the whisker is literally squeezed through a hole similar to the way toothpaste is squeezed out of a tube. In metallurgy, this process is known as cold extrusion [18, 19]. Sn can be extruded in two ways—from the (IMC) layer and through cracks in the grain boundaries.

For Sn films on a copper (Cu) substrate, a combination often used in the electronics industry, there are two possible IMC alloys: Cu₃Sn, and Cu₆Sn₅ (Fig. 2.4). Cu₆Sn₅ forms readily at room temperature, while Cu₃Sn occurs at higher temperatures.

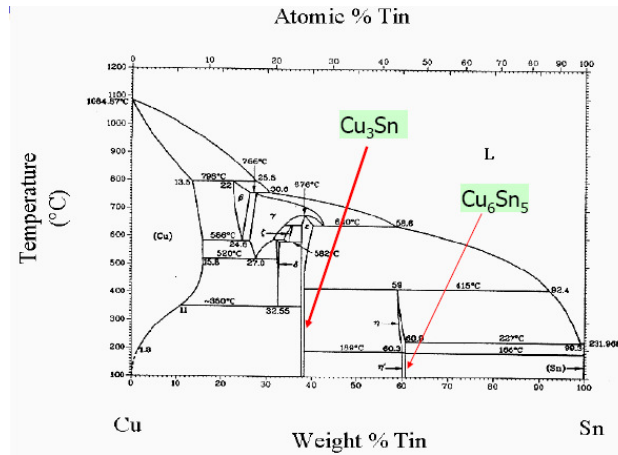


Figure 2.4 The copper-tin phase diagram [9].

During IMC formation, although there is diffusive movement of atoms in both directions, the diffusion rate of Cu into Sn is higher than the diffusion rate of Sn into Cu and it is through this inter-diffusion that the IMC layer is formed. Proponents of this school of thought claim that the IMC layer causes an increase in compressive film stress tangential to the surface because both Cu₆Sn₅ and Cu₃Sn occupy a larger molar volume than either Sn or Cu. Since diffusion processes are slow in condensed matter, the process takes time, which is why the whiskers do not appear immediately. Because the IMC layer does not form in a uniform manner, the stress is not spatially uniform (i.e., $\sigma = \sigma(x, y)$) and stress gradients form within the Sn. The tin is transported by the stress gradients to areas where the stress is least. At these points, the Cu₆Sn₅ grows nearly to the surface (Galyon and Palmer referred to this thick hill of Cu₆Sn₅ as a “pedestal” [18]) and it is from these pedestals that the whiskers are extruded. Any remaining bulk Sn or surface Sn oxide between the pedestal and free space is pushed aside by the growing whisker.

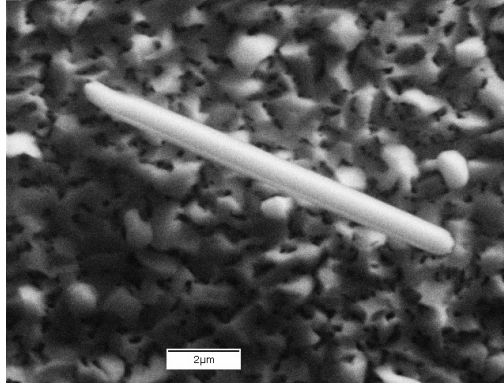


Figure 2.5 A whisker with a striation along its length, possibly explained by the shape of the hole through which it was extruded

It is also possible that whiskers are extruded from the Sn film through tin grain boundaries. Here, the presence of surface oxide is irrelevant. The argument is based on Le Chatelier's Principle, which states in this context, that when a tangential compressive stress is induced in the Sn film, whiskers form to relieve the stress via extrusion through the grain boundaries. This idea is supported by striations that are often observed along the sides of whiskers, such as the one shown in Figure 2.5, indicating the shape of the hole or crack in the grain boundary from which it originated.

CHAPTER 3 EXPERIMENTAL INVESTIGATIONS

To organize our work in this dissertation, ten key issues fundamental to the whiskering process were identified. An experiment was then devised to explore each issue. The issues and experiments are fully described in the following sections.

3.1 Reproducibility of Sn Whisker Incubation

The development of Sn whiskers can be conveniently described in three distinct phases. During the initial *incubation* phase no whiskers are visible. After the whiskers begin to appear, *growth* is observed for a time, after which an *equilibrium point* appears to be reached once the whiskers have reached their maximum growth. Little is known about the timeline of whisker development, however. There is no agreement among researchers about the length or cause of the incubation period; the length, cause, or growth rate during the growth phase; the establishment of the equilibrium point; or even if growth ends at all.

Most reports of whiskers are anecdotal, with few details on the time that elapses before whiskers are observed. Few groups have been able to reproducibly grow whiskers with consistent incubation times. Reported incubation periods vary from a few hours [19], to one year [13], to as long as multiple years [20]. Only in a special Sn-Mn alloy not used by industry has reproducible whisker formation been observed [19].

A major goal of this section of our work was to find a whisker production method with a reproducible incubation time using films composed of pure Sn.

Achieving this goal was a necessary prerequisite for the remaining objectives of this study. The process allows whiskers to be reproducibly grown in 90-110 days.

The process is detailed here. A metallic substrate (brass, Cu, Ag, Zn, Al, and Ni were all found to be satisfactory) is first degreased, washed (soap and water), and rinsed with acetone. The substrate is then placed in a cylindrical magnetron sputtering system ~ 12cm directly above a 99.999% pure Sn sputter target (Kurt J. Lesker™). The chamber is pumped down to $< 10^{-6}$ torr using a turbo molecular pump. At this point the turbo molecular pump is partially restricted and a measured flow of Ar is introduced and a potential difference is applied to produce a DC diode plasma. The Ar flow is then slowly reduced while the discharge voltage is adjusted to maintain the plasma until the background Ar pressure in the system is ~ 2 mtorr. The substrate is then introduced to the bombarding Sn atoms and the film deposited. Once the desired thickness of Sn has been deposited, the sample is removed from the chamber and allowed to incubate in an undisturbed location at standard temperature and pressure for 90-110 days.

Representative samples of the whiskers produced are shown in Table 3.1 below. This process was applied to all the whisker growths reported in this thesis.



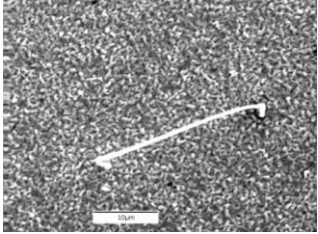
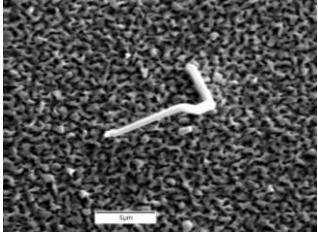
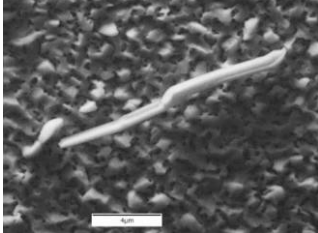
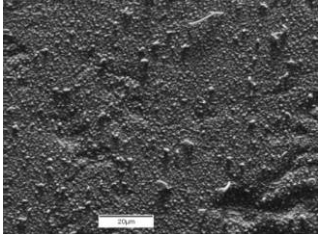
Whisker(s)	Conditions of production	Incubation time
	<p>Brass substrate, ~3000Å of Sn deposited at 2 mTorr background Ar Pressure</p>	<p>110 days</p>
	<p>Brass substrate, ~3000Å of Sn deposited at 10 mTorr background Ar Pressure</p>	<p>110 days</p>
	<p>Brass substrate, ~3000Å of Sn deposited at 2 mTorr background Ar Pressure</p>	<p>110 days</p>
	<p>Brass substrate, ~5000Å of Sn deposited at 2 mTorr background Ar Pressure</p>	<p>110 days</p>
	<p>Zinc substrate, ~5800Å of Sn deposited at 2 mTorr background Ar Pressure</p>	<p>110 days</p>
	<p>Silver substrate, ~5800Å of Sn deposited at 2 mTorr background Ar Pressure</p>	<p>98 days</p>

Table 3.1 Micrographs of whiskers grown using our reproducible process.

Key Result: A method for reproducibly growing Sn whiskers with predictable incubation times has been developed and tested.

- This technique has been used throughout these studies.
- The incubation time is 90-110 days.
- To our knowledge, there have been no previous reports of a reproducible method of whisker production from pure Sn films.

3.2 Role of Surface Oxide

Sn forms two oxides, SnO₂ and SnO, and many researchers [17, 13] have postulated that whiskering and oxidation are directly related. The suggested mechanism is that the surface oxide, or oxygen seeping into the grain boundaries, causes a compressive (normal and tangential respectively) stress which drives whisker growth. This is inferred from the fact that oxides have molar volumes which are greater than those of either Sn or Cu (SnO₂ = 21.84 cm³, SnO = 20.89 cm³, Sn = 16.29 cm³, and Cu = 7.11 cm³).

The surface oxide theory was tested as follows. Using the sample preparation method described in the previous section, a 1” square brass sample with ~3000 Å of Sn

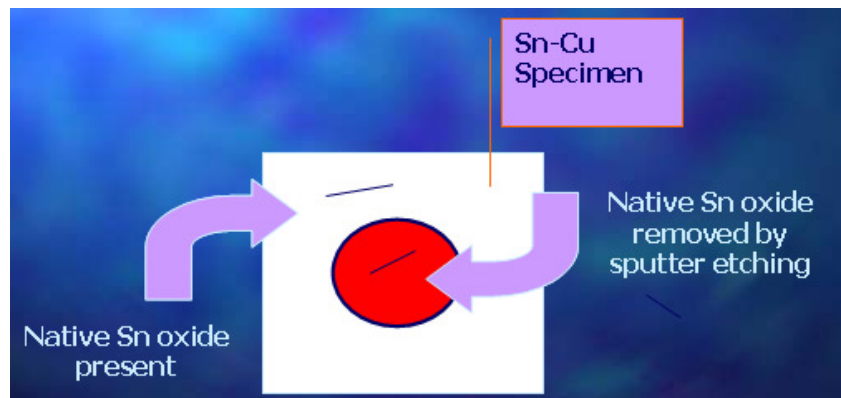


Figure 3.1 Pictorial representation of native oxide removal by an Ar⁺ ion beam and the resulting whiskers.

was produced and placed immediately in an Auger electron spectroscopy (AES) system and pumped to a background pressure of 10^{-9} Torr. Subsequently, an oval section of the surface was cleaned with an Ar^+ ion beam to remove any native O_2 , SnO , or SnO_2 that may have formed on the surface during the transfer time from the sputtering system to the AES system. Auger analysis verified that no oxygen was present on the cleaned Sn film area, although it was present on the surrounding un-cleaned area. The samples were left to incubate in the Auger chamber at 10^{-9} Torr for 110 days, after which the samples were examined in an SEM. Whiskering was found on both the cleaned surface and the un-cleaned surface (Fig. 3.2). Repeating this experiment produced the same results, which are in agreement with findings reported by Moon et al. [20] for a Sn-Cu alloy film.

This result clearly shows that surface oxides are not necessary for whisker growth and that the normal stress caused by surface oxides cannot be the primary

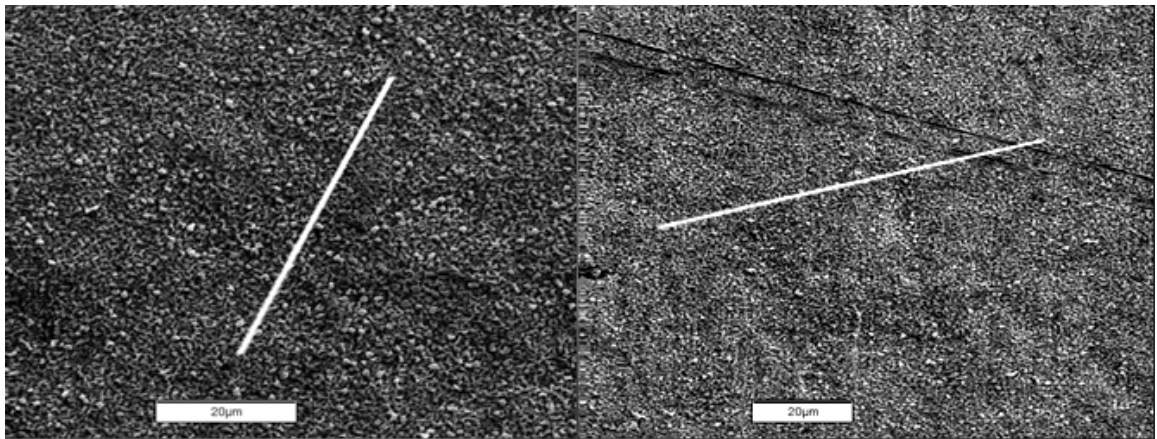


Figure 3.2 Micrographs of whiskers on cleaned (left) and un-cleaned (right) sections of the sample.

driving force for whisker growth. Since oxygen seepage into the grain boundaries was minimized but not eliminated, oxidation within the grain boundaries may still be a contributor to whisker growth through tangential stress. Barsoum et al. [21] used finite element analysis (FEA) to show that Sn oxide formation at grain boundaries was capable of providing sufficient tangential stress to drive whisker growth. Further experiments are necessary to verify this work.

Key Result: A surface oxide is not necessary for whisker growth.

- This result does not support the hypothesis set forth by Tu. [13].
- This result supports the findings of Moon et al. [20].

3.3 Role of Compressive Stress from Intermetallic Compound Growth

It has been suggested [17, 18, 23] that the IMC layers which form between the film and the substrate are the primary source of the internal stress in the thin film and thus the cause of whisker growth. The experiments reported here were designed to test this theory.

The Al-Sn phase diagram in Fig. 3.3 shows that there is no Al-Sn IMC that forms in this binary system at equilibrium. Since no IMC is formed, clearly IMC growth cannot contribute to any compressive or tensile stresses that may be exhibited in the thin film.

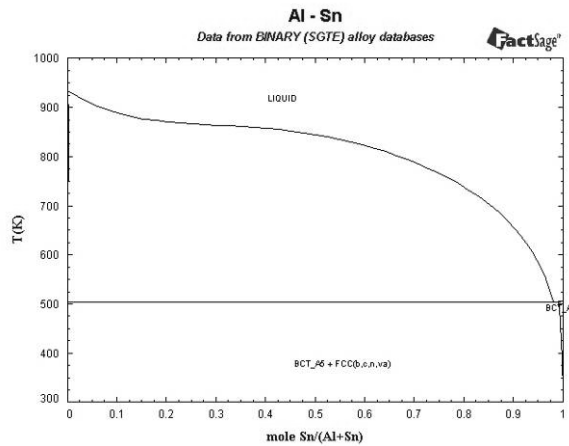


Figure 3.3 Al-Sn phase diagram, with no IMC indicated.

We produced a 1 cm square Al sample with $\sim 5800 \text{ \AA}$ of Sn. After 96 days of incubation, substantial whisker growth was found. In fact, measurements revealed a whisker density of 154 whiskers per square centimeter, with an average length of $13 \mu\text{m}$.

These results show that IMC growth is not necessary for whisker development. Parenthetically, an interesting ‘bubble’ of Sn was found upon examining the sample,

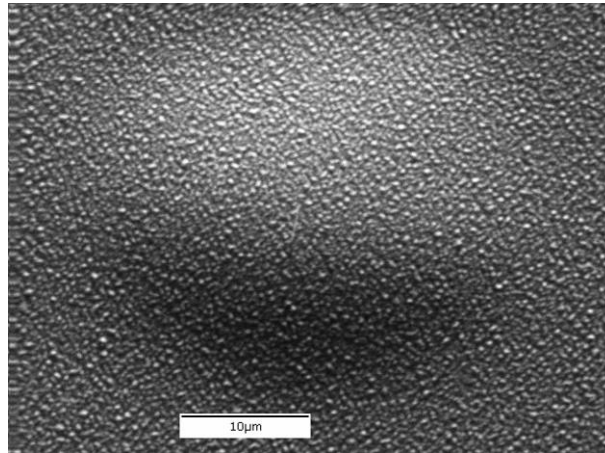


Figure 3.4 Bubble in the Sn film on an Al substrate.

indicating weak adhesion between the Sn and Al (and hence no IMC layer) and direct evidence of a compressive stress state in the Sn film.

Key Result: IMC growth is not necessary for whisker growth.

- Thousands of whiskers were grown in a Sn-Al thin film system that can have no IMC.
- This result does not support the hypothesis set forth by Galyon et al. [18].

3.4 Role of Surface Smoothness

Galyon and Palmer [18] argue that non-uniform or rough IMC growth causes an increase in tangential compressive stress within the thin film (Fig. 3.5). This implies that a rough surface leads to greater compressive stress and the formation of more whiskers.

In order to investigate this theory, we fabricated three types of substrate surfaces.

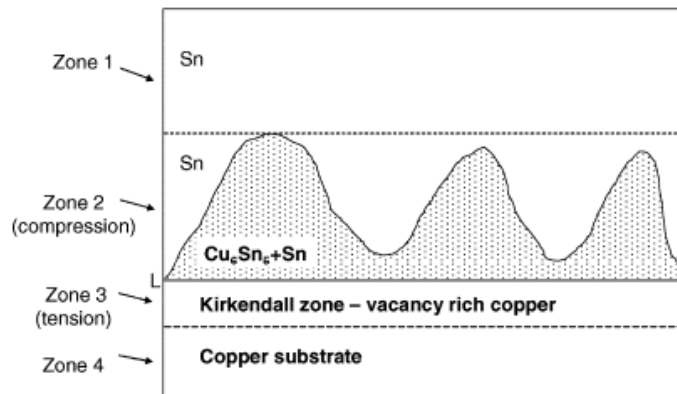


Figure 3.5 How a rough IMC produces a compressive stress parallel to the surface [from 18].

A 1-cm square brass (Goodfellow) substrate with three surface roughness conditions was used: *as received*, *mechanically polished*, and *electrochemically polished*. The as received samples served as the rough (control) samples. To attain a mechanically polished surface, samples were potted in a resin-catalyst solution to provide a convenient way to handle the sample while polishing. The samples were then mounted in a modified Buhler polishing attachment and ground using SiC paper, progressing from 320 grit through 1200 grit, and then using a 3 μm diamond suspension on a woven nylon polishing pad. Finally, the samples were polished using a gritless polishing compound and a polishing pad. The electrochemically polished samples were connected to the anode end of a DC low voltage source and lowered into a sulfuric acid solution. Since charge tends to accumulate at sharp points, the metal ionizes best at the corners and thus leaves the metal surface from the roughest points, thus smoothing the surface.

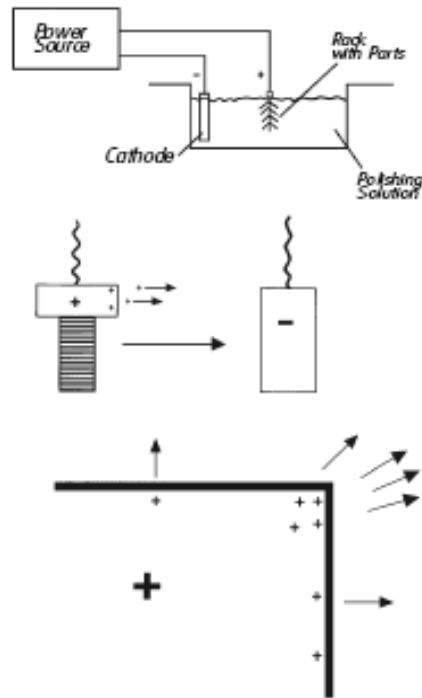


Figure 3.6 Electrochemical etching showing how sharp points are smoothed.

Once the roughness conditions were prepared, the roughness of each was carefully analyzed using an Atomic Force Microscope (AFM). To obtain a roughness measurement the thickness of the sample is recorded at each measuring point and the results compiled into a histogram whose standard deviation is, by definition, the roughness. Table 3.2 shows the extremes of possible surface roughness, their characteristics and a sample histogram for each. Table 3.3 shows a 3-D computer generated picture of the three roughness conditions, and the associated histogram for each surface.

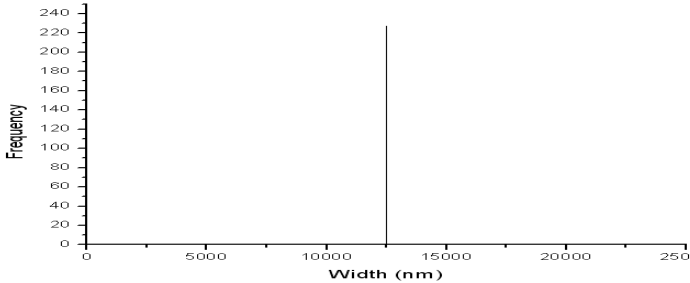
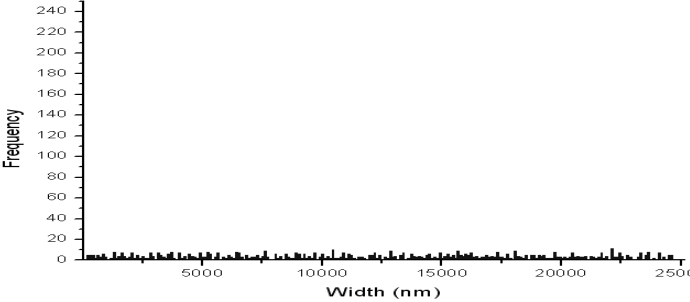
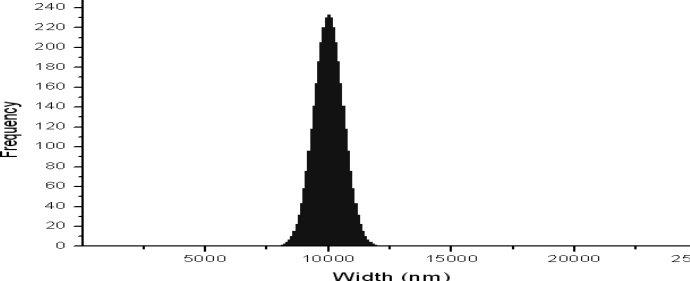
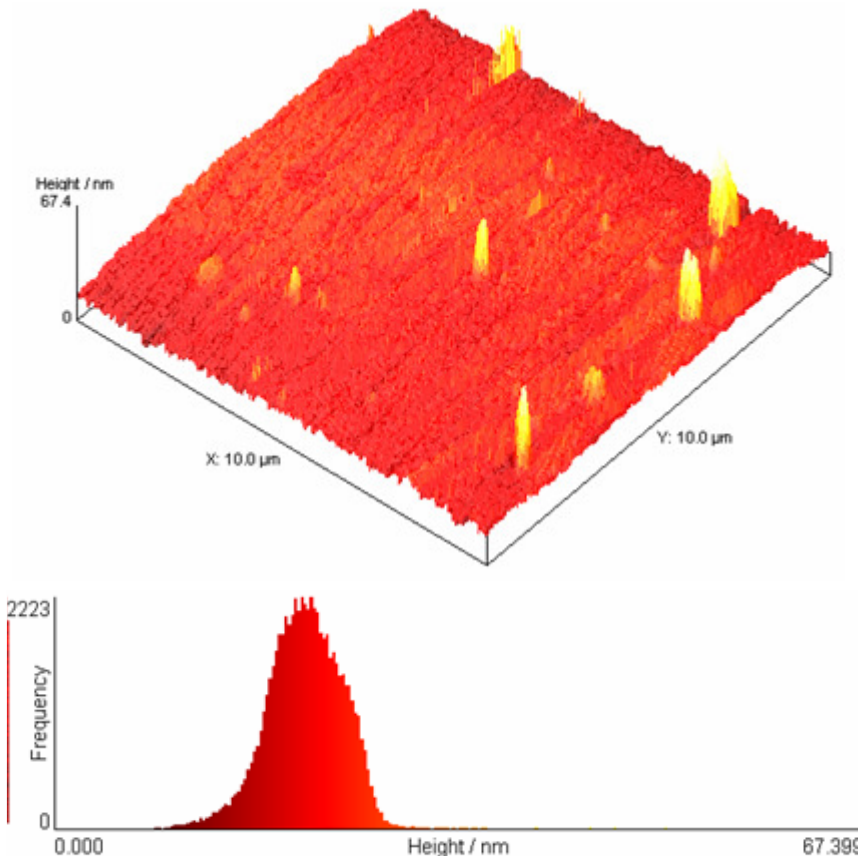
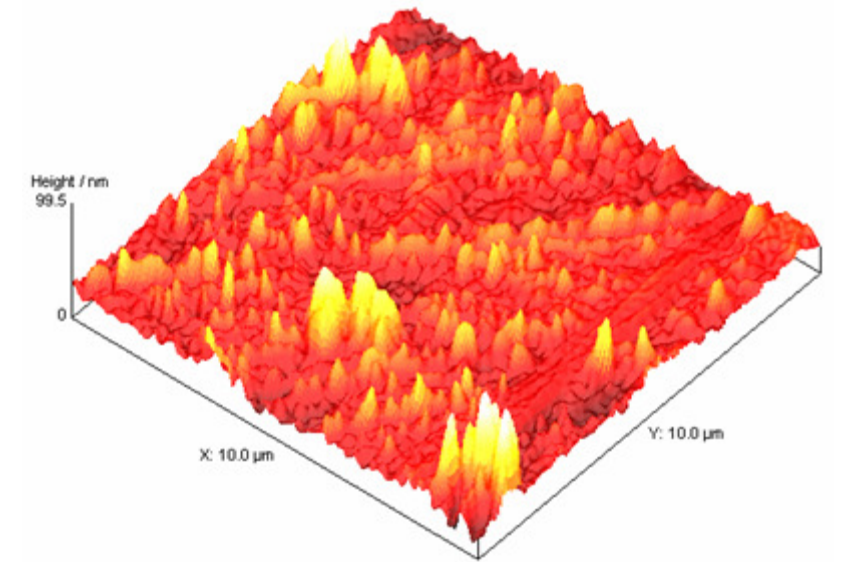
Extreme Measurement	Characteristics	Sample Histogram
Perfectly Smooth	<ul style="list-style-type: none"> All measurements are exactly the same thickness at every point Resulting histogram is a delta function Not realistic for this work 	 <p>Roughness = 0 nm/100 μm^2</p>
Perfectly Rough	<ul style="list-style-type: none"> Nearly every point has a different thickness measurement Resulting histogram has contributions at all thicknesses Not realistic for this work. 	 <p>Roughness = 7200 nm/100 μm^2</p>
Ideally Smooth	<ul style="list-style-type: none"> Each measurement is similar to the maximum or minimum thickness Resulting histogram is a Gaussian function 	 <p>Roughness = 600 nm/100 μm^2</p>

Table 3.2 Extremes of roughness measurements, their characteristics, and the resulting histograms.

Surface Condition (Roughness)	3-D Image and Histogram
<p>Electrochemically polished</p> <p>(2.62 nm/100 μm^2)</p>	 <p>The figure displays a 3-D surface topography image and its corresponding histogram for an electrochemically polished surface. The 3-D image shows a surface with a height scale from 0 to 67.4 nm and a 10.0 μm x 10.0 μm area. The surface appears relatively smooth with some small peaks. The histogram below shows a narrow peak with a maximum frequency of 2223, indicating a low surface roughness.</p>
<p>Mechanically Polished</p> <p>(6.42 nm/100 μm^2)</p>	 <p>The figure displays a 3-D surface topography image and its corresponding histogram for a mechanically polished surface. The 3-D image shows a surface with a height scale from 0 to 99.5 nm and a 10.0 μm x 10.0 μm area. The surface is significantly rougher than the electrochemically polished surface, with many larger peaks. The histogram below shows a broader peak, indicating a higher surface roughness.</p>

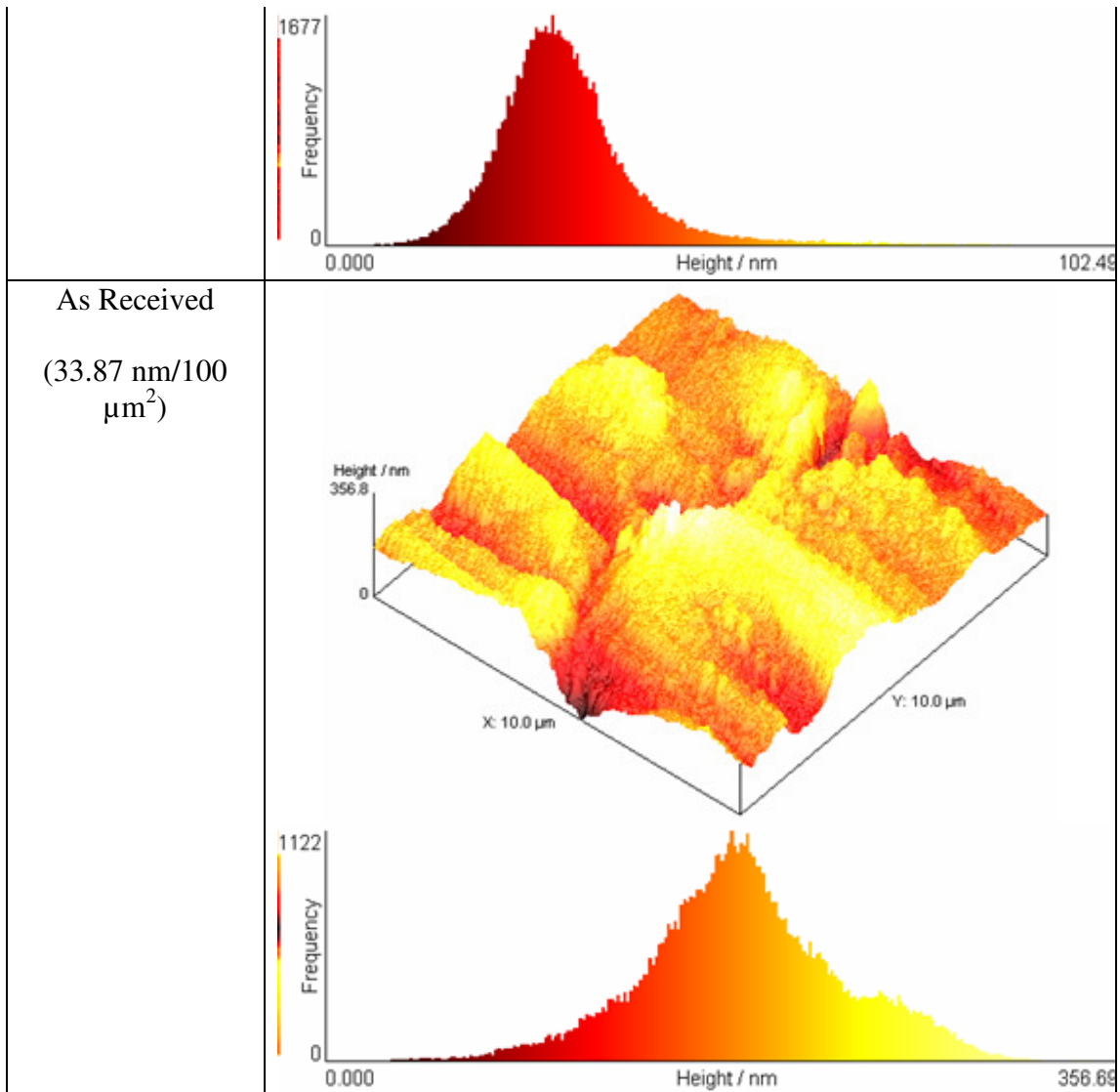


Table 3.3 Surface conditions used, surface roughness, and the associated histogram from AFM analysis.

Once Sn is deposited on the brass surfaces, IMC begin to develop. It is reasonable to suppose that the resulting IMC would be roughest on the as received (roughest) samples, leading to the greatest stress gradients and hence, based on Galyon and Palmer’s hypothesis [18], the most Sn whiskers. A 6000Å layer of Sn was sputter – deposited on each sample and the samples incubated under ambient conditions for 114 days. The results are shown in Table 3.4.

Surface Condition	Whisker Population Density (cm ⁻²)	Average Length (µm)	Longest Whisker(s) (µm)
Electrochemically Polished	2265	15-20	80 (of which there were 5)
Mechanically Polished	598	8	100, 60, 60
As Received	55	5	14

Table 3.4 The impact of surface roughness on whisker growth.

The results of this experiment are opposite to Galyon and Palmer's supposition. Repeating the experiment twice with brass substrates and a variety of other substrates (Al, Ni, Cu, and Zn) showed similar results. More details are provided in Section 3.10. The results support the experimental findings of Takeuchi et al. [23].

Key Result: Smoother substrate surface finishes promote whisker growth; polishing the substrate is not an effective whisker mitigation technique, although making the substrate rougher can be effective.

- Whisker growth (both in population density and average length) are enhanced by smoother substrates.
- This work complements and provides evidence to support results reported by Takeuchi et al. [23].
- This result does not support the hypothesis set forth by Galyon et al.[18].

3.5 Role of the Film Stress State

In most models, whisker growth is attributed to compressive stress within the thin film, where growth serves as the stress relief mechanism. Whisker growth is assumed to stop when the stress within the film has been sufficiently lowered [18, 19]. In this section the role of compressive stress in the formation of Sn whiskers is examined. Three samples on brass substrates were prepared using the method described in Section 3.1, except that the background Ar pressure was altered. Thornton and Hoffman [24] showed that the internal stress in a sputter deposited film can be controlled by the background Ar pressure. When the background Ar pressure is low there are fewer particles (Ar atoms) between the sputter target (cathode) and the substrate (anode). The sputtered atoms thus travel further without colliding into other atoms in the system (i.e., they have a longer mean free path) and therefore have more kinetic energy when they arrive at the substrate surface. The resulting impulse that is experienced by the developing film at the surface is then greater:

$$impulse \equiv \Delta P = \sqrt{2mT}, \quad (\text{Equation 3.4.1})$$

where T is the kinetic energy of sputtered atom just before impact with the sample surface, ΔP is change in momentum of sputtered atom during the impact with the surface, and m is mass of sputtered atom. Consequently, as each new Sn atom bombards the film's surface, the film's crystalline structure becomes tighter and compressive stress results. As the Ar pressure increases, the resulting impulse is reduced because more kinetic energy is lost to collisions with Ar molecules along the way (which lowers T in equation 3.4.1), and the film's internal stress becomes more tensile. Thornton and

Hoffman found experimentally that the Ar pressure at which the stress state was neutral (threshold pressure) was roughly linearly proportional to the square root of the atomic mass of the sputtered element (threshold pressure $\propto \sqrt{m}$, as is impulse shown in equation 3.4.1), likening this process to the peening process used by metallurgists.

Figure 3.7 shows Thornton and Hoffman's results [24], with the addition of the atomic mass of Sn to allow the threshold pressure of Sn to be inferred. Their results indicate a threshold pressure for Sn of between 7 and 9 mTorr for Sn, so the Ar pressure at which most of the samples for these studies (2 mTorr) have been deposited is well into the compressive stress range. It is important to note that this chart cannot be used to obtain a quantitative value for internal stress; there are as yet no reports in the literature of these

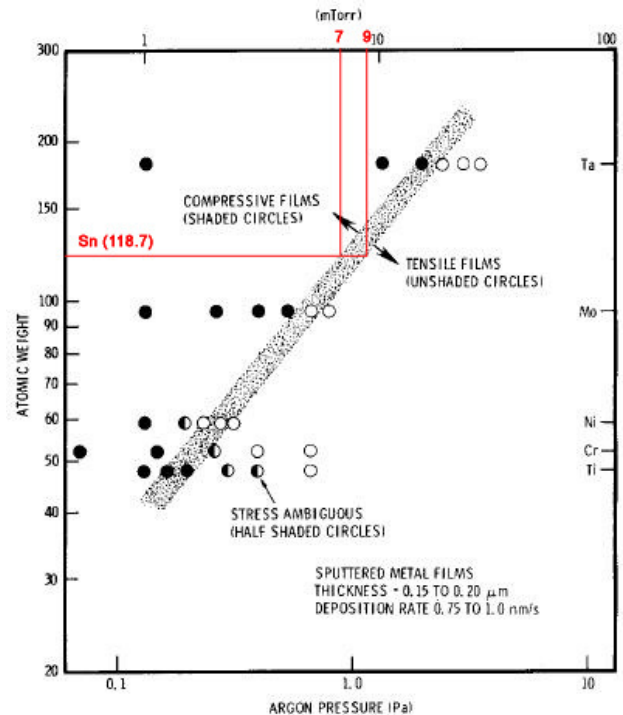


Figure 3.7 Thornton and Hoffman's chart, modified to show Sn's threshold pressure [24].

internal stress values for Sn, however a method for quantifying this information has been identified and carried out in Section 5.2.

In our work, the background Ar pressure was varied in order to change the intrinsic stress state of the Sn film. Samples were deposited at 2 mTorr (compressive stress state), 7 mTorr (neutral stress state) and 10 mTorr (tensile stress state). As shown in Figures 3.8-3.9, after 110 days, both the 2 mTorr and 9 mTorr samples produced numerous whiskers, while the 7 mTorr sample produced no whiskers. This study indicates that either compressive or tensile stress states form whiskers and an effective whisker mitigation technique results when thin films with no intrinsic stress are used.

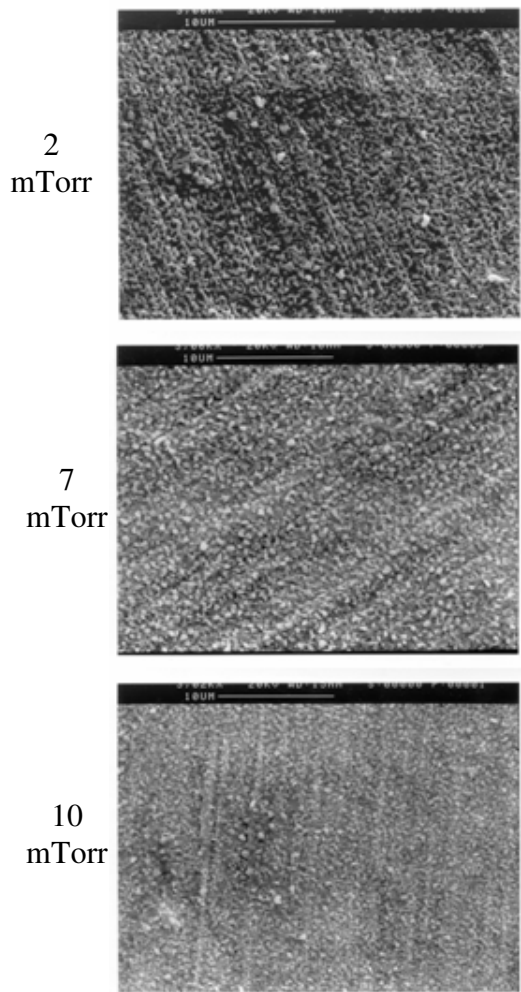


Figure 3.8 Micrographs of three Sn films before incubation, deposited at 2, 7, and 9 mTorr, respectively.

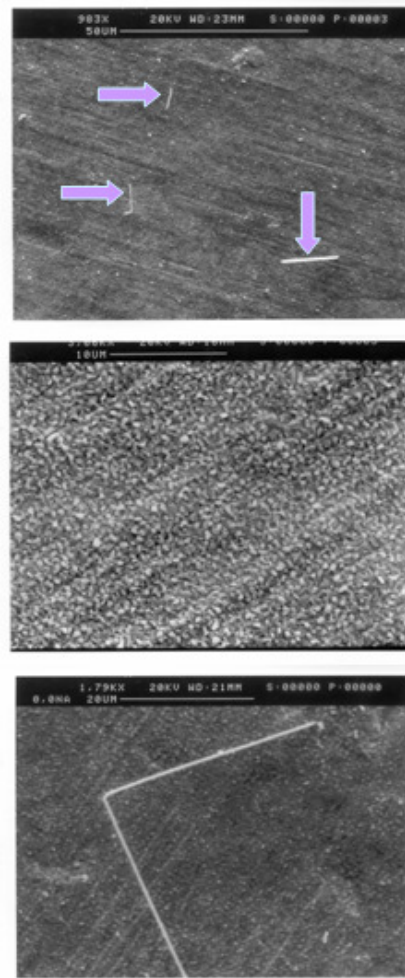


Figure 3.9 Micrographs showing the whiskers that grew on the samples in Figure 3.8.

Key Result: Whiskers grow when either compressive or tensile stress exists in the Sn film.

- This contradicts the many authors who hypothesized that it is exclusively compressive stress which drives whisker growth.

3.6 Composition of the Whisker Surface

The presumption that Sn whiskers are composed of Sn (only) has been derived in part from X-ray techniques [25]. Since the spot size of a conventional X-ray system is substantially larger than a typical Sn whisker, however, conclusions on whisker material properties are based on area-averages over a large portion of the substrate surface covered with whiskers. Micro-focus X-ray techniques have permitted stress and crystalline orientation for single grains, but has only recently been applied to Sn whiskering [26]. A further important question incapable of investigation with diffraction methods is whether the Sn whisker has any unexpected concentrations of surface or bulk elements (such as oxygen), long thought to be a key element in models of whisker growth.

Thus, there has been a lack of direct materials information on the composition of Sn whiskers. In 1980, Fujiwara and Kawanaka [27] et al. reported finding Zn in Sn whiskers grown from Sn films which had been electrodeposited on brass substrates. The question of whether Zn or Cu is found on or within Sn whiskers grown from brass is important because it would help elucidate the growth mechanism of Sn whiskers. In particular, the amount of Zn or Cu pulled up into the whisker from the brass substrate would indicate the relative contribution of the substrate in the whiskering process.

Brass substrates ($1 \text{ cm}^2 \times 0.125 \text{ mm}$ thick) (60Cu/40Zn by weight) were placed in a cylindrical magnetron sputtering system operating with a 99.999% pure Sn sputter target and we deposited a 6000 \AA Sn film on the brass. The sample was then removed from the chamber and allowed to incubate in an undisturbed location at ambient room conditions for 114 days. Our specimens deposited at 2 mTorr were well into the

compressive regime (based on the information presented in section 3.5). After the incubation period, the specimens were introduced into a high-resolution Physical Electronics PHI 680 field emission scanning Auger nanoprobe for surface analysis. For the purposes of this work, we selected several high-aspect ratio (0.5 μm diameter, 10 μm long) Sn whiskers for study. Fixed-beam AES was used to measure the surface composition at the base, middle and tip of various whiskers. AES sputter profiling subsequently generated a depth profile into the whisker. By using this combination of surface and depth analysis, we have been able to determine the composition of Sn whiskers at depths of 250, 500, and 1000 \AA into the whisker.

The clean surface and bulk composition of the whiskers were found to be entirely Sn with an Auger signature identical to the adjoining deposited Sn thin film. Points 1 and 2 on Figure 3.10 show a high-resolution SEM photo of representative AES analysis positions at the base of a whisker and on the underlying deposited Sn film. Only the elements Sn, O, and C are observed (Figure 3.11) on the surfaces before sputter cleaning. O and C are expected on surfaces exposed to atmospheric conditions before sputter cleaning; in fact, the Auger signature is what is expected from a surface of pure Sn after introduction into a vacuum system (native Sn oxide and C). The middle and leading tip of the whisker (points 3 and 4 in Figure 3.10) also showed only Sn, O, and C in the Auger spectra (Figure 3.12). Next, the native Sn oxide was removed by sputtering ~ 200 \AA into the whisker surface (Figure 3.13). With further depth profiling, the Auger spectra continued to yield Sn only and no Zn or Cu was found. The measurements were taken at depths calculated (based on known sputter rates) to be 250 \AA , 500 \AA (Figure 3.13), and 1000 \AA (Figure 3.14) into the whisker shaft. The results show that Sn

whiskers grown on brass from thin sputtered Sn films are pure Sn and contain no evidence of the substrate elements (Zn and Cu), either on their surface or in the whisker bulk.

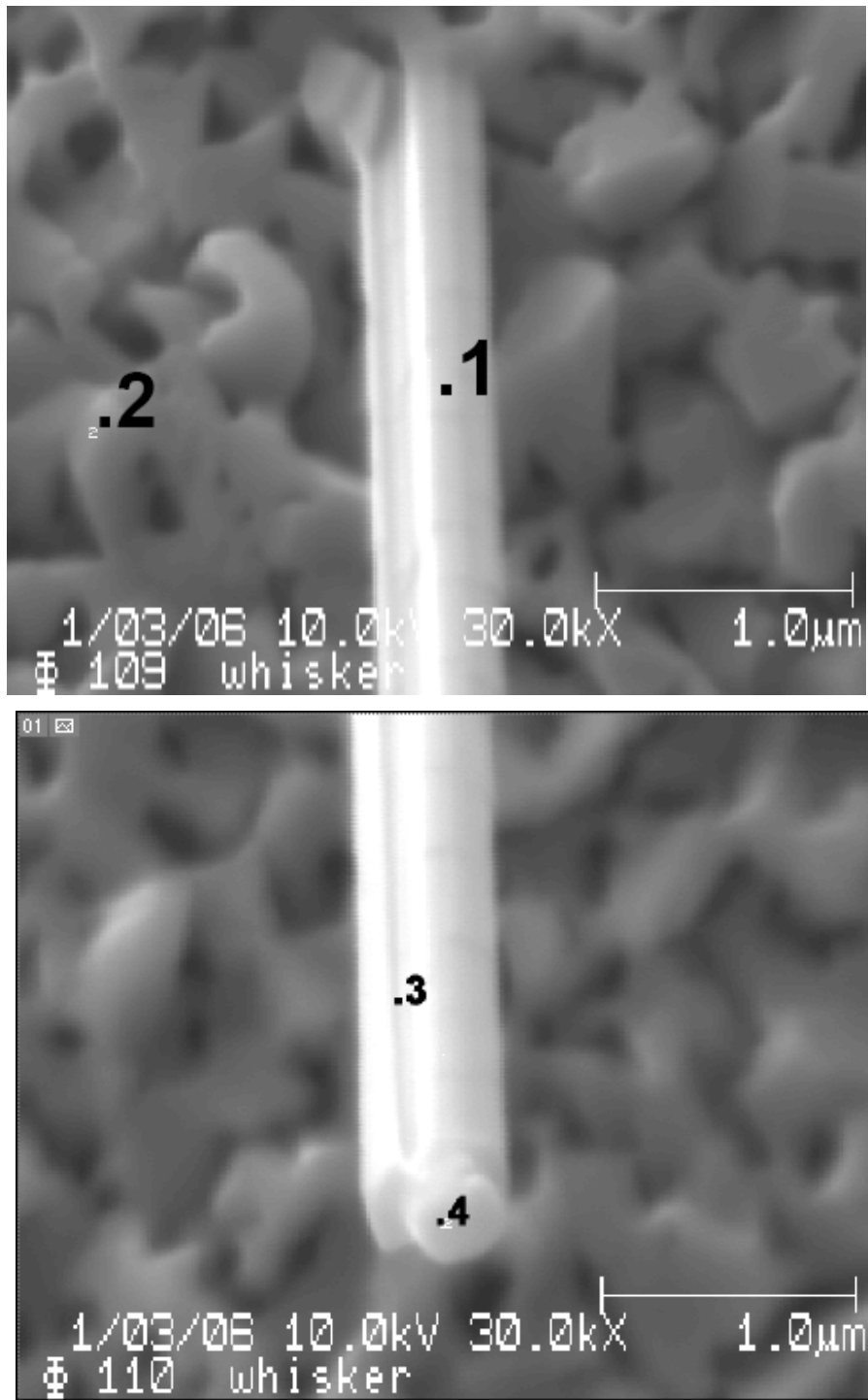


Figure 3.10 High resolution micrographs showing the whisker base (1), film (2), whisker middle (3), and whisker tip (4) analyzed using AES.

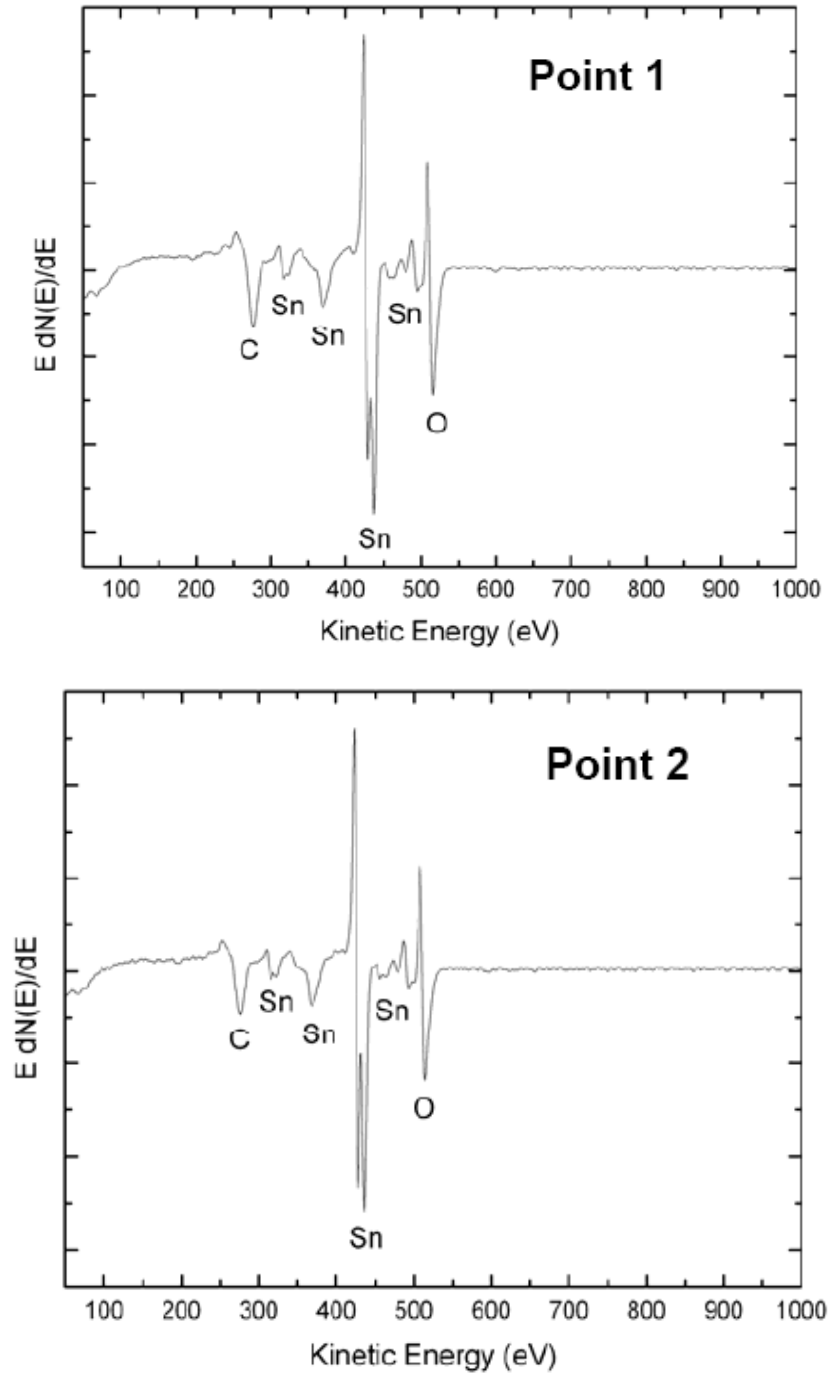


Figure 3.11 Auger spectra of the surfaces of the Sn film and the whisker base.

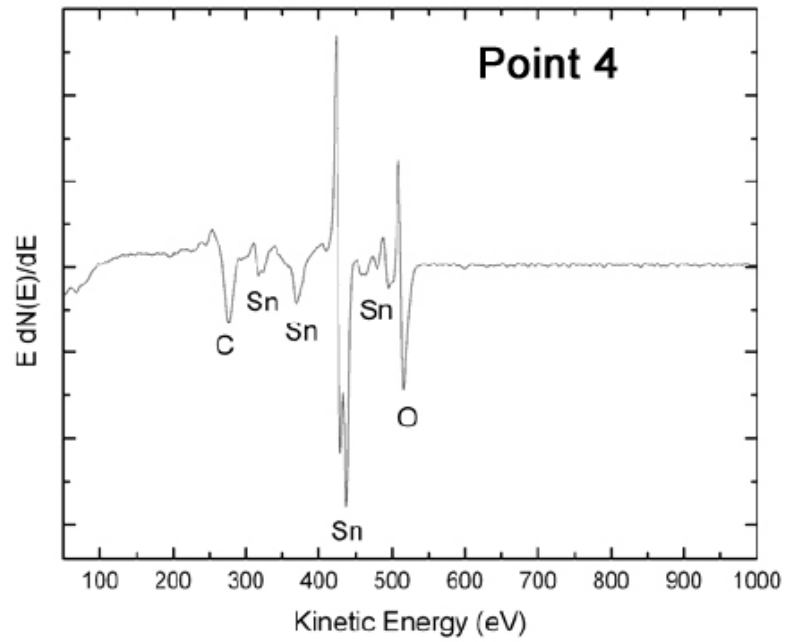
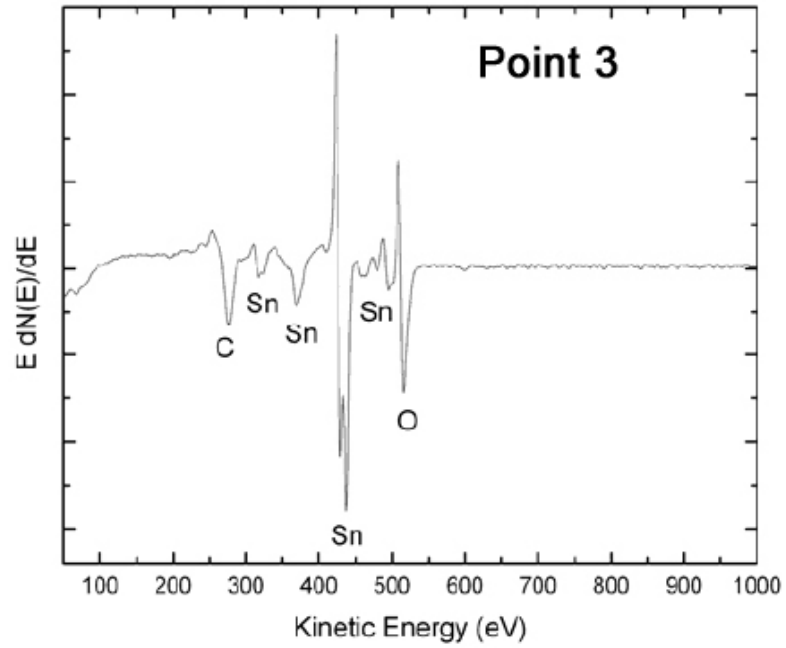


Figure 3.12 Auger spectra of the surfaces of a central portion of the whisker and its tip.

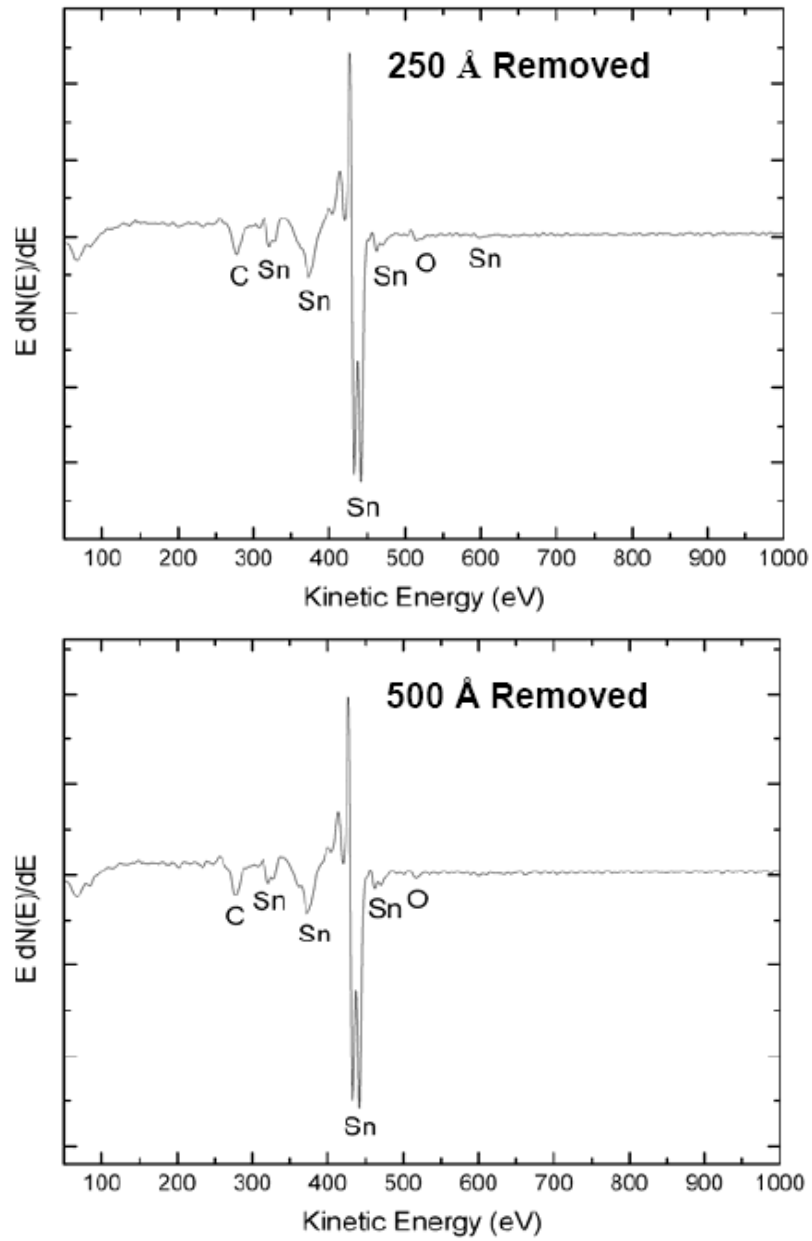


Figure 3.13 Auger spectra at point #3 after 250Å and 500Å of the whisker had been removed using an Ar⁺ ion beam.

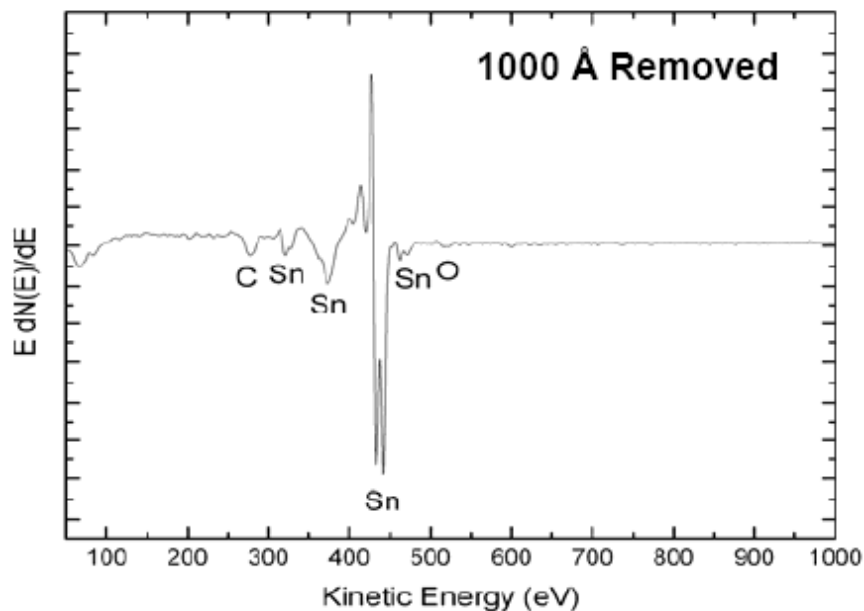


Figure 3.14 Auger Spectra at point #3 after 1000Å of the whisker had been removed.

Key Result: Sn whiskers are composed of pure Sn, both on their surface and in their bulk.

- This is contrary to the findings of Fujiwara and Kawanaka [27] who found that Cu and Zn were found on the whiskers..

3.7 Feedstock Origin of Sn Atoms

The findings in the previous section are significant because this means that Sn whiskers must get their supply of Sn atoms exclusively from the Sn film; the substrate does not contribute to the composition of the whisker. Simple volumetric calculations enable us to calculate how much of the film will be depleted in order to grow a whisker of a given length (Table 3.5).

The calculations imply that there must be a significant migration of Sn atoms from the Sn film to the whisker. The fact that long Sn whiskers are composed of pure

Sn and grow from such thin layers of Sn shows extensive Sn migration is occurring during whisker growth. The migration path could be along the surface, through the IMC, or via grain boundaries within the bulk. Table 3.5 shows that this migration could be expected to yield Sn-deficient regions around Sn whiskers, at least in optimum cases. During our investigations of Sn whiskers on brass, however, we rarely observe depressions around whiskers. The scarcity of these observations may indicate that 1) the area of Sn depletion draws from a significantly larger but shallower area of the film than assumed in Table 3.5 (and therefore unobservable); or 2) there are multiple mechanisms of whisker growth; or 3) the grain structure and thickness of the Sn film does not lend itself to easy observation of the expected Sn depletion. Figure 3.15 shows one whisker with a significant depletion around it.

Whisker Length (μm)	Whisker Volume (μm^3)	Area of 0.6 μm Sn Thin Film Needed to Synthesize Whisker (μm^2)	Radius of Circular Area Around Whisker Base Needed for Whisker Synthesis (μm)
1	0.20	0.33	0.32
10	2.0	3.3	1.0
100	20	33	3.2
1000	200	330	10
10000	2000	3300	32
Whisker radius (μm)	0.25		
Film Thickness (μm)	0.6		
Assumption: Density of Sn whisker is the same as that of the surrounding Sn film			

Table 3.5 Area of Sn film necessary for whisker growth.

As Sn whiskers are formed of a single crystal [7] (and thus dense Sn), while the film is composed of multiple grains, it seems likely that the first option offers a more credible mechanism. If the Sn atoms travel over very large distances, the driving force for this migration must be very strong, which raises the question: what path do the Sn atoms follow? There are four possible avenues, namely along the surface, through the bulk material, along the grain boundaries, or along the IMC/ interface. Clearly more research is needed in this area.

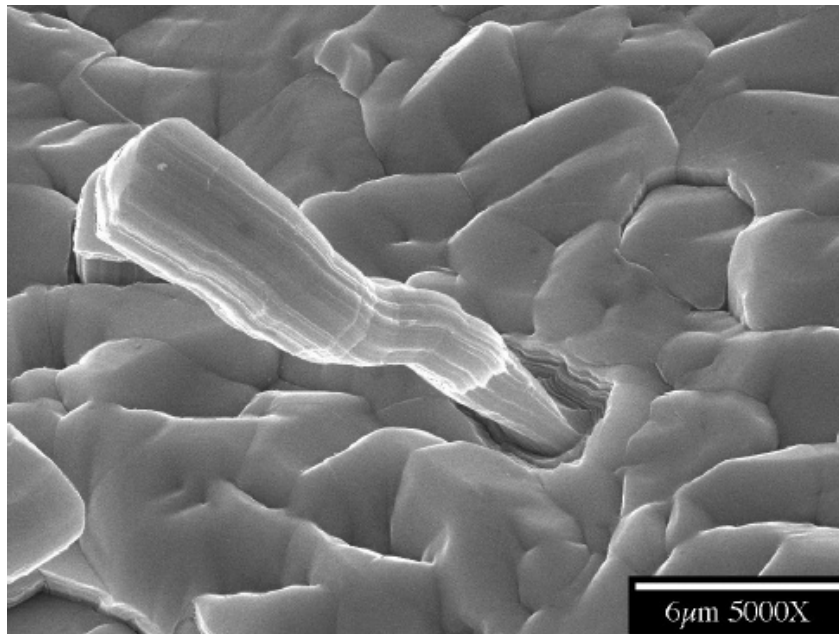


Figure 3.15 High resolution micrograph showing a small area of depletion for a large whisker. (Photograph courtesy of Mr. Peter Bush, SUNY.)

Key Result: For Sn on brass, the feedstock for Sn whiskers lies within the Sn film exclusively; the brass substrate does not contribute to whisker production.

3.8 Whisker Growth From Metallic Films Other Than Sn

To shed further light onto the fundamental causes behind the growth of metallic whiskers, other types of whiskers likely to exemplify interesting characteristics were

examined. Sixteen 1cm square brass samples were prepared, 8 of which were electrochemically polished, and 8 in the as received state. Four sputter targets, Ag, In, Cd, and Zn (metals which have been reported to be whisker prone), were used to build the thin films. The matrix of this experiment is summarized in Table 3.6 below.

Sample Number	Substrate Composition	Substrate Surface Condition	Film Composition	Film Thickness (Å)
1	Brass	As Received	Zinc	6000
2	Brass	As Received	Zinc	1500
3	Brass	Electrochemically Polished	Zinc	6000
4	Brass	Electrochemically Polished	Zinc	1500
5	Brass	As Received	Cadmium	6000
6	Brass	As Received	Cadmium	1500
7	Brass	Electrochemically Polished	Cadmium	6000
8	Brass	Electrochemically Polished	Cadmium	1500
9	Brass	As Received	Silver	6000
10	Brass	As Received	Silver	1500
11	Brass	Electrochemically Polished	Silver	6000
12	Brass	Electrochemically Polished	Silver	1500
13	Brass	As Received	Indium	6000
14	Brass	As Received	Indium	1500
15	Brass	Electrochemically Polished	Indium	6000
16	Brass	Electrochemically Polished	Indium	1500

Table 3.6 Experimental matrix for metallic whiskers other than Sn.

After 85 days the samples were examined and 2 small whiskers were found, one on the 6000Å Zn film and the other on the 1500Å Zn film (Fig. 3.16), both on electrochemically polished substrates. These samples were then allowed to further incubate for a total of 220 days.

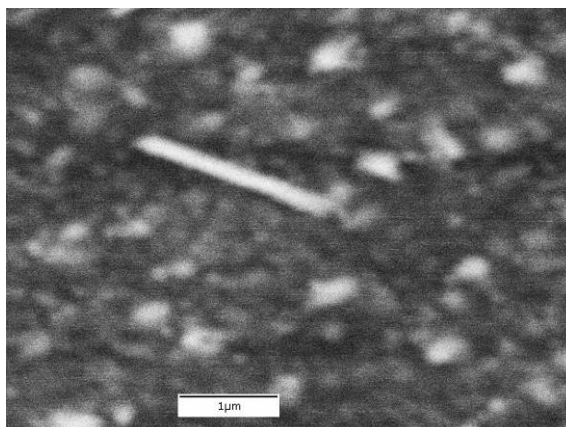


Figure 3.16 Zn whisker found on the sample with 1500Å of Zn after 85 days.

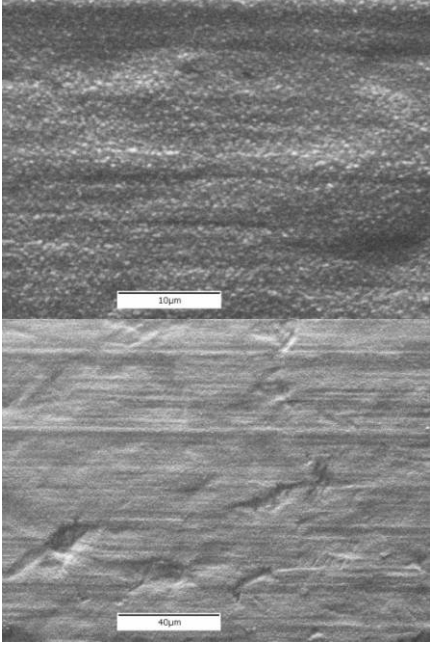
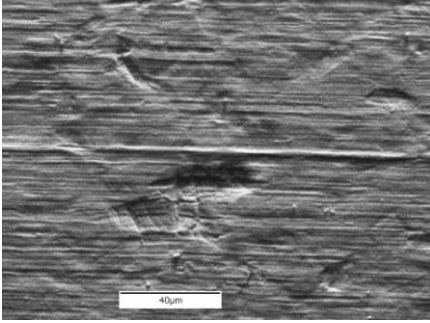
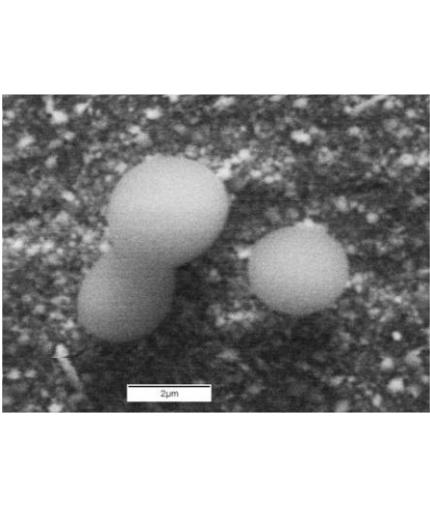
After 220 days of incubation each type of film yielded a wide variety of whiskers. These findings are discussed in turn below.

3.8.1 Zinc Metallic Films

No whiskers were found on the samples which were not polished, but the polished (smoother) samples had high populations of whiskers. This is in agreement with the results obtained for the Sn on brass samples reported in Section 3.4, where whisker growth increased as the substrate smoothness increased. Two types of whiskers (spherical and linear) were observed, both appearing on the sample with 6000Å of Zn, while only the spherical whiskers appeared on the sample with 1500Å of Zn. This may

suggest two different growth mechanisms. One mechanism (the one which produces linear whiskers) requires 6000 Å of film, while the mechanism which produces spherical whiskers works with either film thickness. It seems likely that both mechanisms exist in the other types of films, but only with Zn do they produce different types of whiskers.

To better grasp the types of Zn whiskers two tables have been provided. Table 3.7 qualitatively describes Zn whiskers through exemplary micrographs of all samples with Zn films. Table 3.8 quantitatively describes Zn whiskers by listing the population density and average length of Zn whiskers on each sample.

Sample Description	Exemplary Micrographs	Notes
6000Å of Zn on “as received” (non-polished brass)		no whiskers were found
1500Å of Zn on “as received” (non-polished brass)		no whiskers were found
6000Å of Zn on polished brass Substrate		Two kinds of whiskers were observed, ‘spheres’ and ‘lines’. Average sphere diameter = 2.3 µm; average line length = 2.4 µm. Both types of whiskers appeared in large numbers. The spheres appeared at all locations on the sample, especially along lines of substrate defects. There were 4

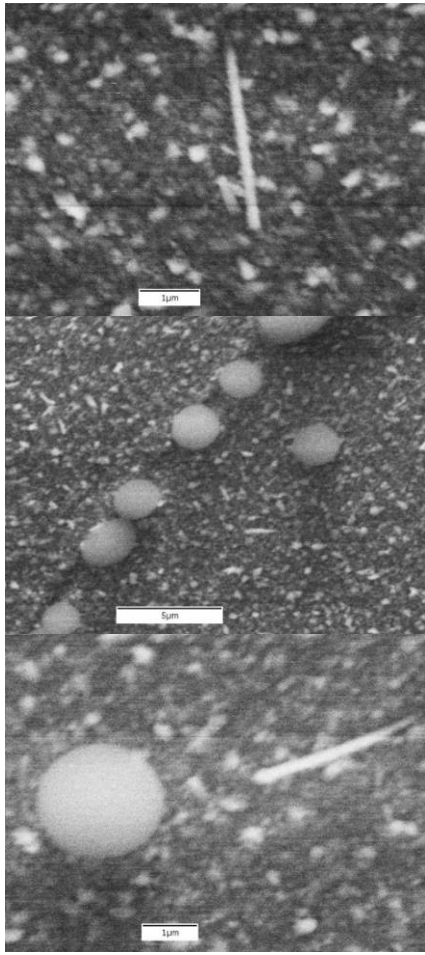
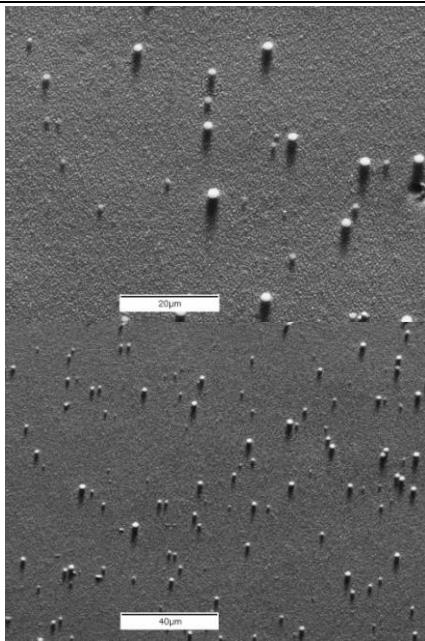
		<p>times as many lines as spheres.</p>
<p>1500Å of Zn on polished brass</p>		<p>Only spheres were found. These spheres appeared in much greater numbers (6 times) than on the 6000Å film.</p>

Table 3.7 Micrographs of surfaces with Zn film.

Surface	Thickness (Å)	Description	Population Density (cm ⁻²)	Average Length (µm)
As Received	6000	No Whiskers	0	
As Received	1500	No Whiskers	0	
Polished	6000	Spheres	47007	2.3 (Diameter)
		Lines	226144	2.4
		<i>Total</i>	<i>273150</i>	
Polished	1500	Spheres only	277783	1.6 Diameter

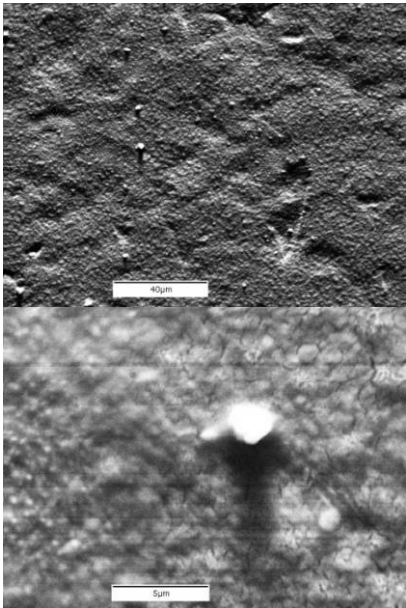
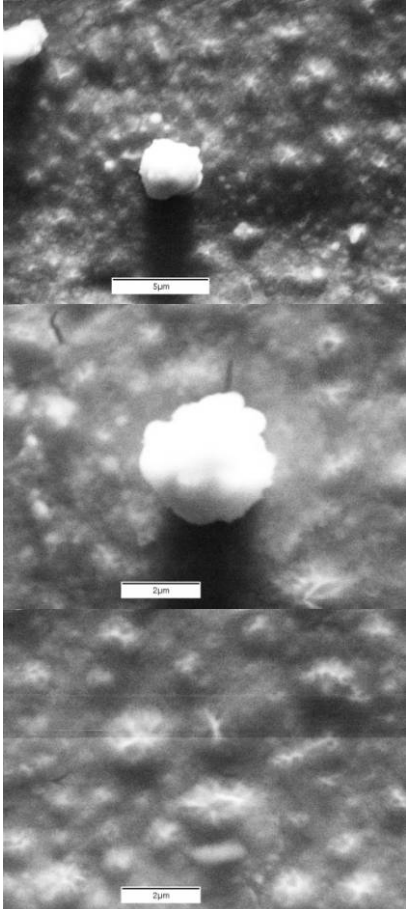
Table 3.8 Data for whiskers found on Zn film samples.

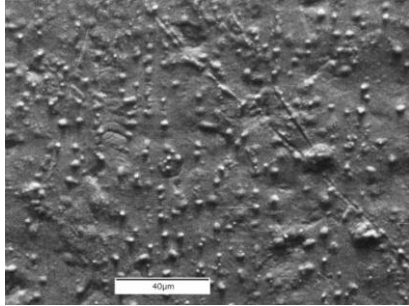
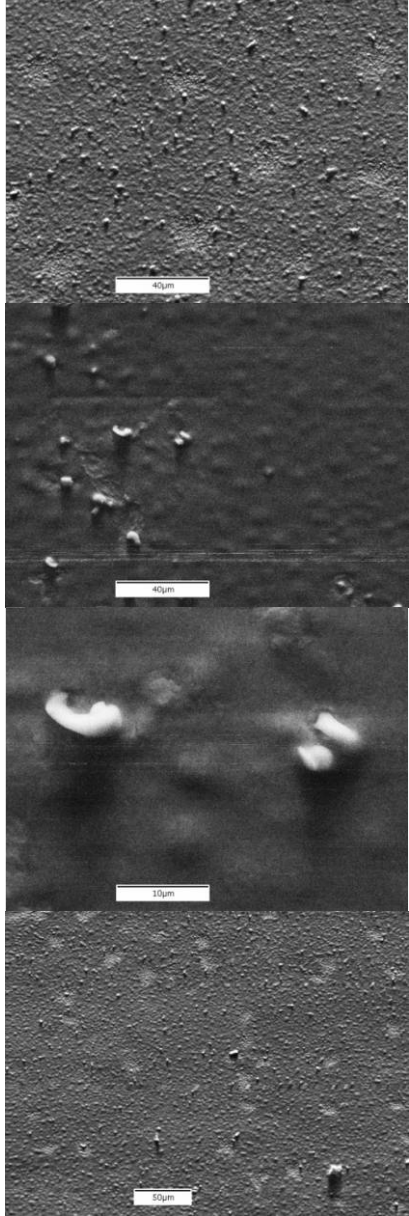
3.8.2 Cadmium Metallic Films

The samples with a metallic film of Cd also produced two types of whiskers: nub-like whiskers and cauliflower-type whiskers. The cauliflower-type whiskers only formed when 1500Å of Cd was deposited to the as-received sample and no other types of whisker occurred on this sample. The other three samples all had nub-like whiskers. The nub-like whiskers that formed with 6000Å of Cd on polished brass tended to be slightly longer than the other nubs, appearing more similar to the high aspect ratio whiskers commonly observed Sn.

The different whisker growth patterns again may indicate different growth mechanisms, with possibly as many as three different mechanisms being in operation. One mechanism occurs in the samples with 1500Å of Cd on a rough substrate (cauliflower-like whiskers); another in samples with 6000Å of Cd on a polished substrate (longer nub-whiskers); and the third in samples with 6000Å on a rough substrate or 1500Å on a polished substrate (normal nub-like whiskers).

To better understand the types of Cd whiskers two tables have been provided. Table 3.9 qualitatively describes Cd whiskers through exemplary micrographs of all samples with Cd films. Table 3.10 quantitatively describes Cd whiskers by listing the population density and average length of Cd whiskers on each sample.

Sample Description	Exemplary Micrographs	Notes
<p>6000 Å of Cd on “as received” (non-polished) brass</p>		<p>Many small nub like whiskers were found</p>
<p>1500 Å of Cd on “as received” (non-polished) brass</p>		<p>Many small cauliflower like whiskers were found.</p> <p>The surface appeared to be bubbling with bumps ready to let a whisker grow through, indicating a sub-surface transport</p>

		
<p>6000Å of Cd on polished brass Substrate</p>		<p>Many small whiskers grew from this surface.</p> <p>There were also many spots on the surface of smaller grain structure.</p>

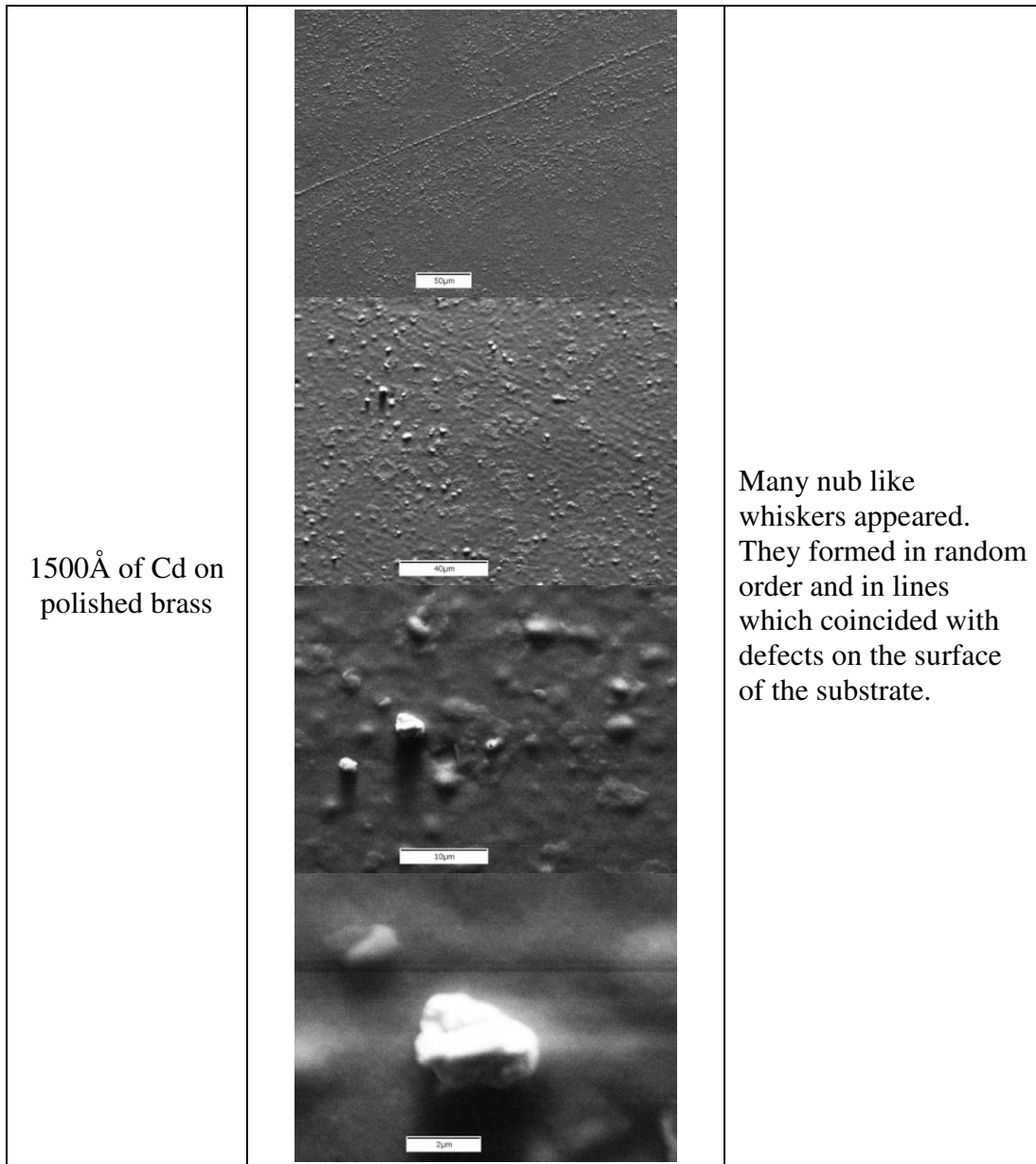


Table 3.9 Micrographs of surfaces with Cd film.

It is interesting to note that the surface of the sample with 1500Å of Cd and a rough substrate is littered with tiny bumps that appear ready to burst, possibly indicating that this substrate will produce many more cauliflower whiskers if allowed further incubation time. These tiny eruptions appear to indicate that the whiskers are coming

from below the surface; since there is little bulk material in this very thin film (1500Å) the atoms may be transporting through the IMC interface.

As with Sn and Zn, the Cd samples also produced more whiskers on the polished surfaces than on the non-polished surfaces. This indicates that the whisker-forming mechanism is more effective when the substrate is polished.

Surface	Thickness (Å)	Description	Population Density (cm ⁻²)	Average Length (µm)
As Received	6000	nub	34590	~1-2 Diameter
As Received	1500	cauliflower	253659	~1-2 Diameter
Polished	6000	longer nub	90466	~1-4
Polished	1500	nub	382262	~1-2

Table 3.10 Data for whiskers on Cd film samples.

3.8.3 Silver Metallic Films

Only a single type of whisker formed on the Ag film samples. Sputtered Ag forms a fine and uniform grain structure that reveals the roughness and imperfections of the underlying substrate and, unlike the other metallic films tested, more Ag whiskers are formed when a rougher substrate is used. Interestingly, the same is true when Sn films are deposited on Ag substrates (Section 3.10). Another notable feature is that microscopic dents in the film were observed around many of the whiskers, particularly in the sample with 1500Å of Ag on a polished substrate, which may be delineating the area from which the feedstock of the whisker is drawn; thicker films or rougher substrates in the other samples appear to mask this trait. *This is an important*

observation because it reveals that bulk material is visibly depleted by the whisker formation process.

ERDAS Imagine software was used to examine one of the whiskers on the sample with 1500Å of Ag on a polished substrate, record the area of the whisker and estimate its height, and measure and label the area of the dent surrounding its base. A calculation similar to the one used in Table 3.5 was performed to predict the area of the circle that would be depleted if the density of the whisker and the film were the same. The radius of the actual dent (Figure 3.17) was only slightly larger than the area of the predicted hole (Table 3.11).

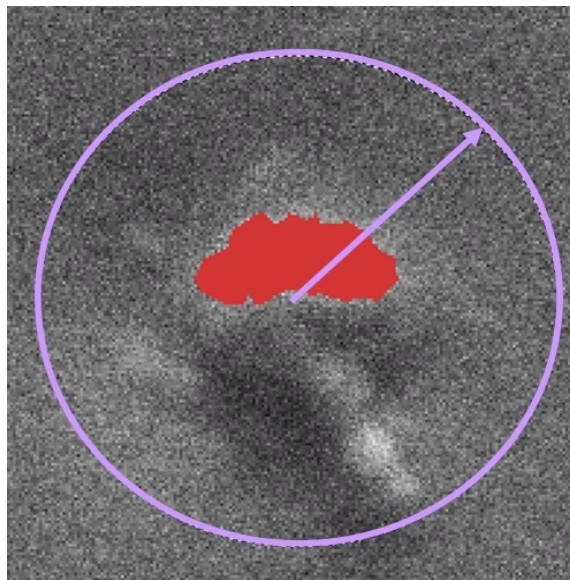
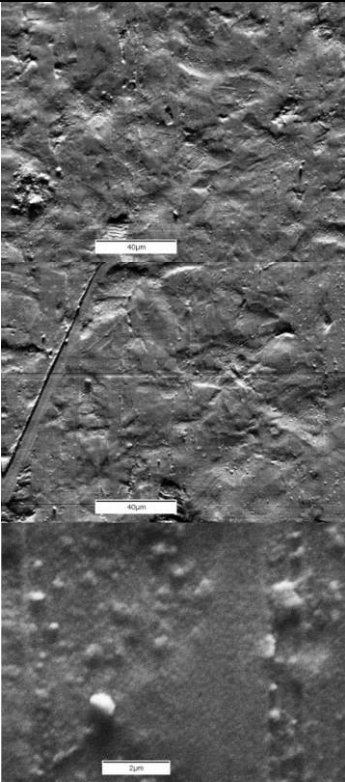
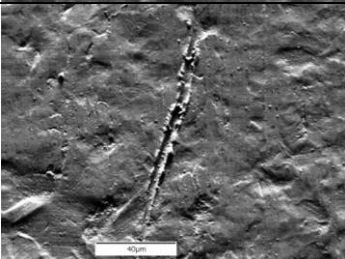
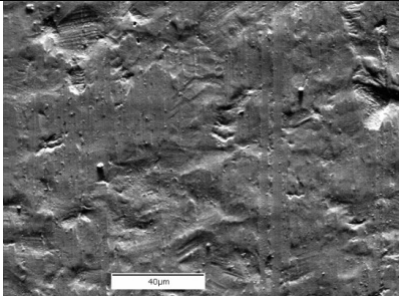
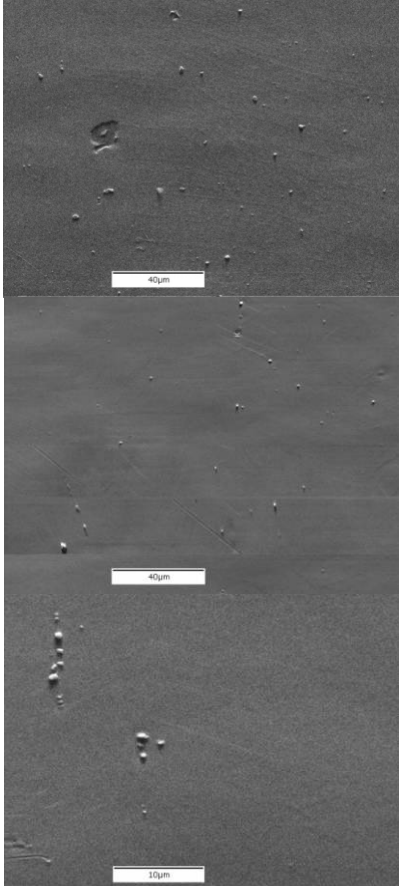
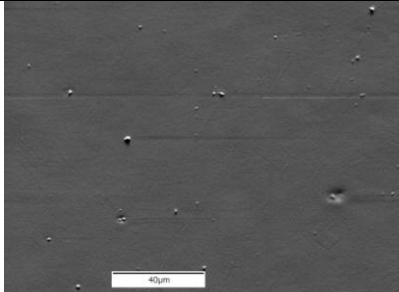


Figure 3.17 The Ag whisker which was measured using ERDAS Imagine software. The radius of the dent was measured at 1.4µm

Estimated Whisker Length (μm)	Whisker Volume (μm^3)	Area of Needed Film (μm^2)	Radius of Potential Hole (μm)
2	0.82	5.45	1.32
Measured Whisker Area (μm^2)	0.41		
Film Thickness (μm)	0.15		

Table 3.11 The calculated radius and area of film which would be needed to grow the whisker in Figure 3.17.

Sample Description	Exemplary Micrographs	Notes
6000Å of Ag on “as received” (non-polished) brass		Many small nub like whiskers were found
1500Å of Ag on “as received” (non-polished) brass		Many small nub like whiskers were found.

		
<p>6000Å of Ag on polished brass Substrate</p>		<p>Many nub like whiskers were found.</p>
<p>1500Å of Ag on polished brass</p>		<p>Many nub like whiskers appeared. There also appeared to be a 'dent' around most of the whiskers</p>

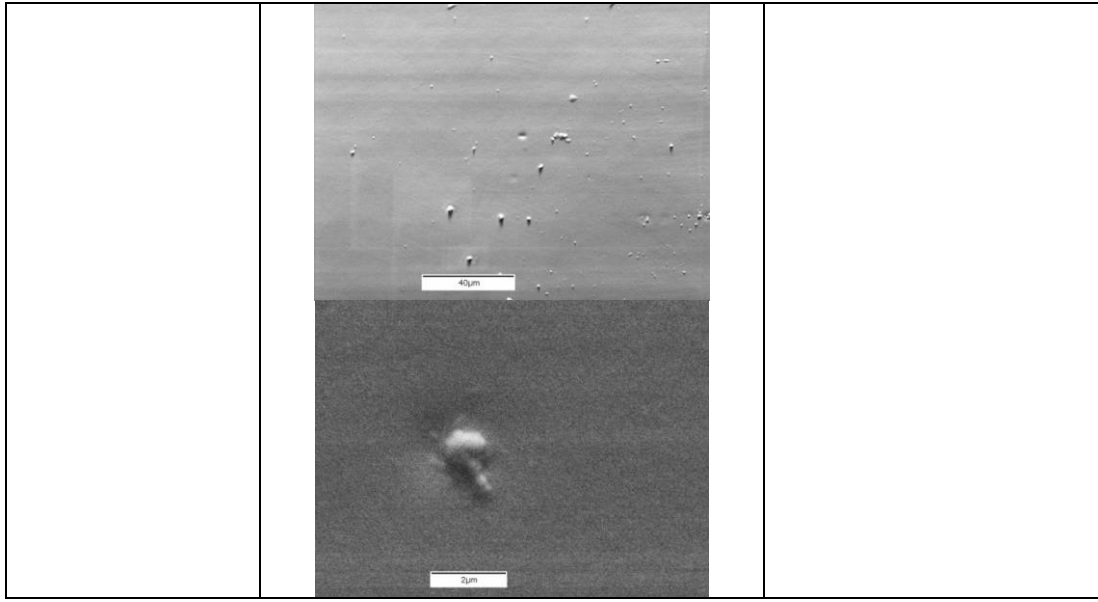


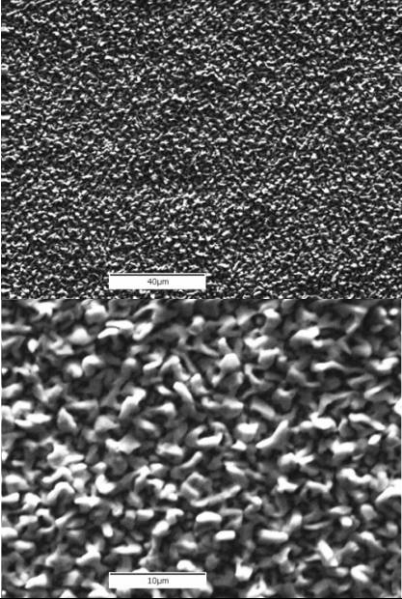
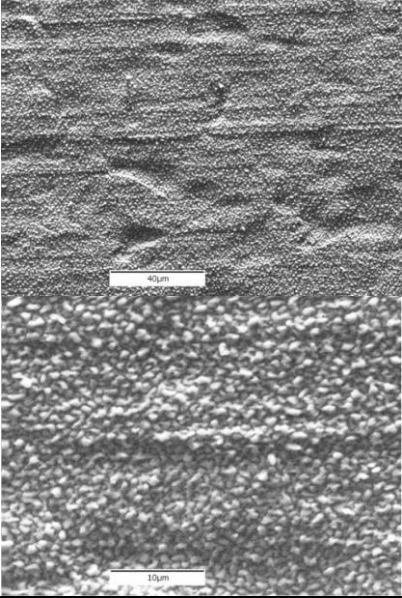
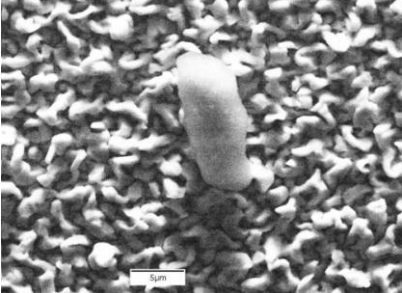
Table 3.12 Micrographs of surfaces with Ag film.

Surface	Thickness (Å)	Description	Population Density (cm ⁻²)	Average Length (µm)
As Received	6000	nub	3168276	0.5
As received	1500	nub	2380397	0.5
Polished	6000	nub	118847	1-2
Polished	1500	nub	179157	1-2

Table 3.13 Data for whiskers on Ag film samples.

3.8.4 Indium Metallic Films

Indium metallic films produced whiskers that most closely resembled those of Sn, with clear striations along the length of the whiskers as frequently observed for many Sn whiskers. Unlike Sn whiskers, however, those formed by In also had striations in the azimuthal direction, giving the whisker the appearance of an extended mariners telescope. The film itself had an unusually large (0.5 – 1 µm) grain structure. The as received (rough) substrates did not grow any whiskers, but the polished substrates did; the 1500Å film produced significantly more whiskers than the 6000Å film. As with Zn, Cd, and Sn; In films also had longer whiskers with higher population densities on the smoother substrates (Ag films and Ag substrates seem to be the exception to this rule). Tables 3.14 and 3.15 show the qualitative and quantitative data from In whiskers.

Sample Description	Exemplary Micrographs	Notes
<p>6000Å of In on “As received” (non-polished brass)</p>		<p>No whiskers were found.</p> <p>A large grain structure was observed.</p>
<p>1500Å of In on “As received” (non-polished brass)</p>		<p>No whiskers were found.</p>
<p>6000Å of In on polished brass Substrate</p>		<p>One whisker was found.</p>

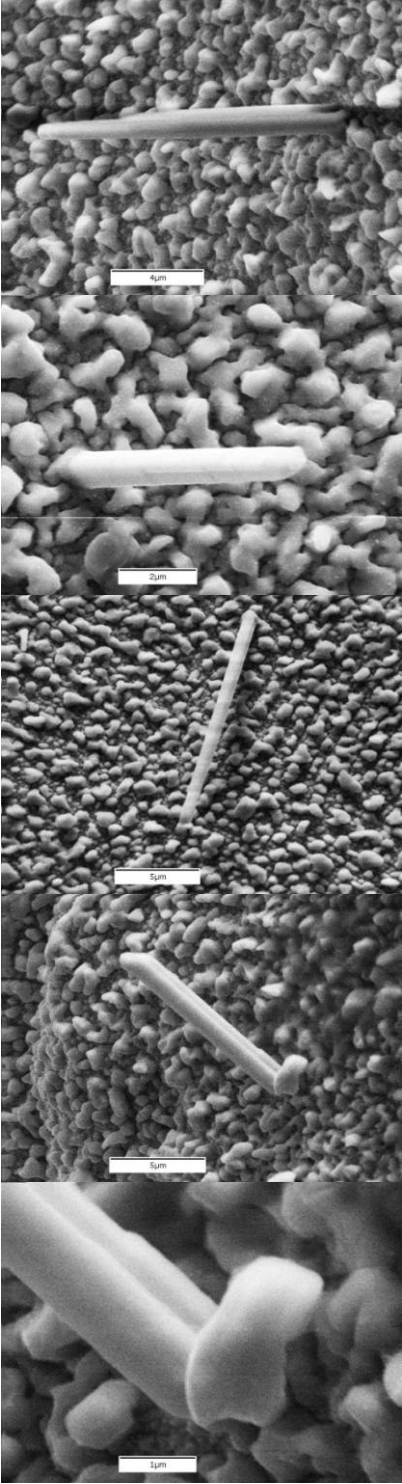
<p>1500Å of In on polished brass</p>		<p>Several 'traditional' whiskers appeared.</p>
--------------------------------------	--	---

Table 3.14 Micrographs of surfaces with In film.

Surface	Thickness (Å)	Description	Population Density (cm ⁻²)	Average Length (µm)
As received	6000	No Whiskers	0	N/A
As received	1500	No Whiskers	0	N/A
Polished	6000	stubby	8	7.0
Polished	1500	whiskers	50	7.3

Table 3.15 Data for whiskers on In film samples.

- *Key Result: There are probably multiple mechanisms of whisker growth depending on the substrate – thin film system.*
- *Key Result: The film volume consumed by the growth of a single whisker can be estimated by a simple volumetric comparison.*
 - This was confirmed by measurement of a Ag film
 - The Ag film had an extremely fine and uniform grain structure, clearly revealing changes beneath the surface and showing the area affected by the growth of individual whiskers.

3.9 Influence of Known Extrinsic Stresses

It has long been observed that whiskers tend to form near surface defects [22]. The assumption is that surface defects cause additional stress in the film, and thus the whiskers tend to develop there. However no research has been done to quantify the additional stress required to accelerate the growth of the whiskers. In an attempt to address this issue, two fixtures were designed (computer aided models with precise dimensions and construction details are shown in Appendix 4) and built to impose varying levels of stress in the thin film of the samples at well known increments. In

order to apply an evenly distributed tangential stress throughout the thin film, samples were forced to conform to a curve, as shown in Figures 3.18 and 3.19.

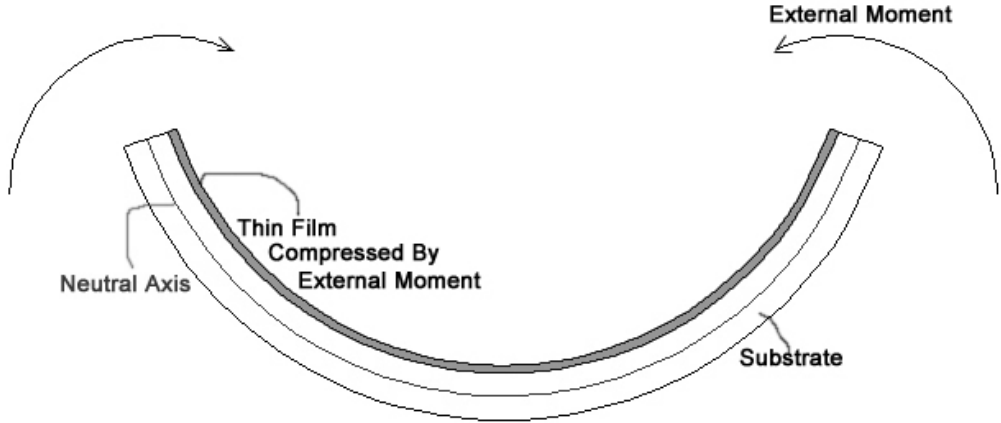


Figure 3.18 Direction of external moment required to create a uniform tangentially compressive stress state in a thin film.

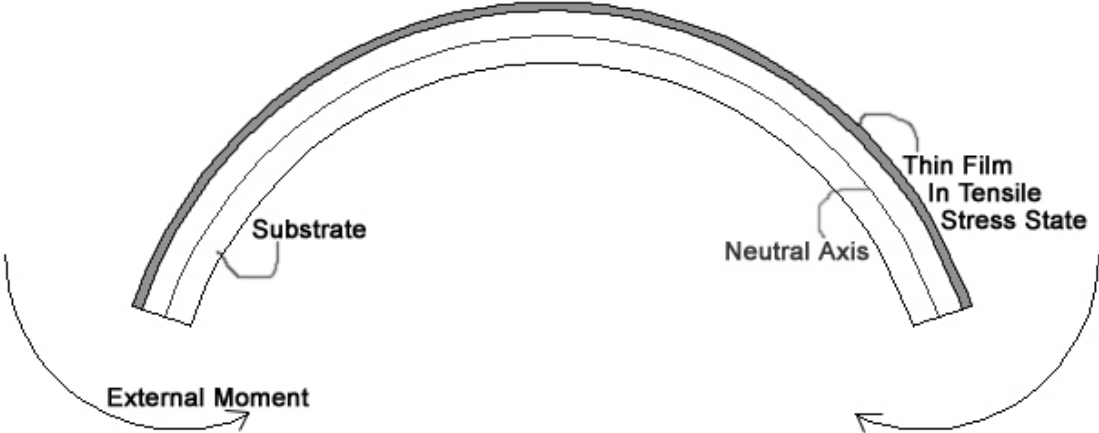


Figure 3.19 Direction of external moment required to create a uniform tangentially tensile stress state in a thin film.

The exact stress value for the known radii of curvature, in the thin film can be calculated from fundamental mechanics (derivation provided in Appendix 1). The calculation depends on the film thickness and Young's modulus of both the film and the

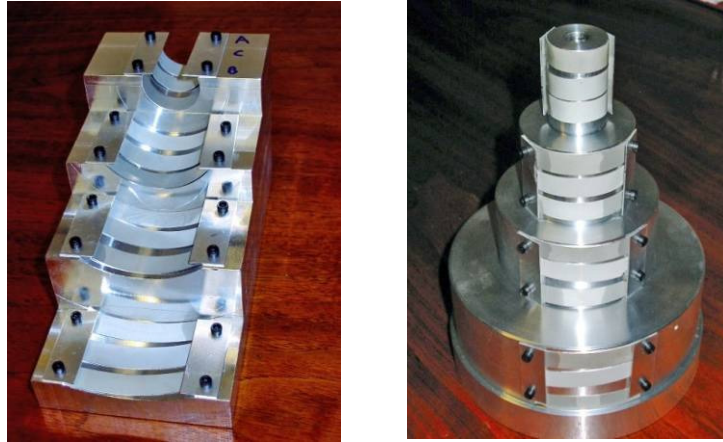


Figure 3.20 Fixtures used to create a uniform tangential compressive (left) and tensile (right) stress state in a thin film.

substrate. The two fixtures designed and manufactured for this study (Figure 3.20), one of which was concave and the other convex, had curvatures with diameters of 5", 3", 2", and 1" (± 19 mils, see Appendix 4 for details), yielding stresses of ± 43 , ± 71 , ± 107 , ± 214 MPa (on brass samples) respectively.

A series of 8 brass and 8 Al substrates with 6000\AA of Sn and 8 Al substrates with 1500\AA of Sn (each 1 x 5 cm) were fabricated and prepared for sputter deposition as described in section 3.1. The samples were mounted in the fixtures and incubated for 85 days under stress, with one of each type of sample at each radius of curvature. After 85 days, only one whisker was found at the very edge of one of the samples where there was a bulge in the Sn due to edge effects and the applied uniform tangential stress was probably ineffective (Figure 3.21). Incubation continued for a total of ~ 220 days, after which time many whiskers were found.

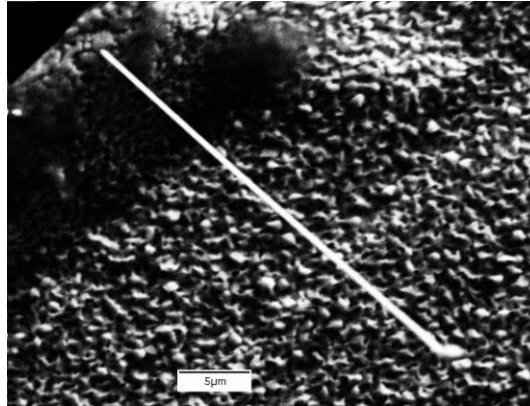


Figure 3.21 Whisker found after 85 days. Notice the bulge of Sn that formed on the very edge of the sample; stresses at an edge are very different from those in the bulk sample.

During production of the external stress fixtures, cutting oil had to be used when the threaded holes were hand tapped. Although careful attempts were made to remove the oil residue using compressed air, acetone and Kim-wipes™, an extremely thin film of oil was observed on these samples that seeped from the threaded holes onto the sample surfaces. It is possible that this thin layer of oil slowed the whisker incubation time to the observed 220 days, which suggests that systematic use of an oil layer on a thin film may be a useful whisker mitigation tool. After the 220 day incubation period, many whiskers were found. The results for samples with brass substrates, samples with Al substrates and 1500Å of Sn, and samples with Al substrates and 6000Å of Sn are discussed in turn below.

3.9.1 6000 Å of Tin on Brass Substrates

The figures in this section show a series of micrographs of representative whiskers on each of the 8 brass samples. The micrographs are in order from most compressive (-) to most tensile (+) stress.

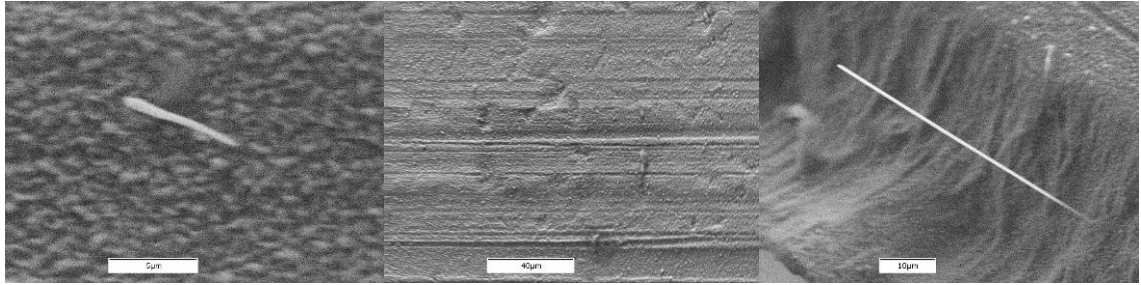


Figure 3.22 Surface of sample (middle) incubated at -215 MPa, with whiskers from side and surface (right and left). The longest whisker (right) was 41µm long. Magnification ~490x.

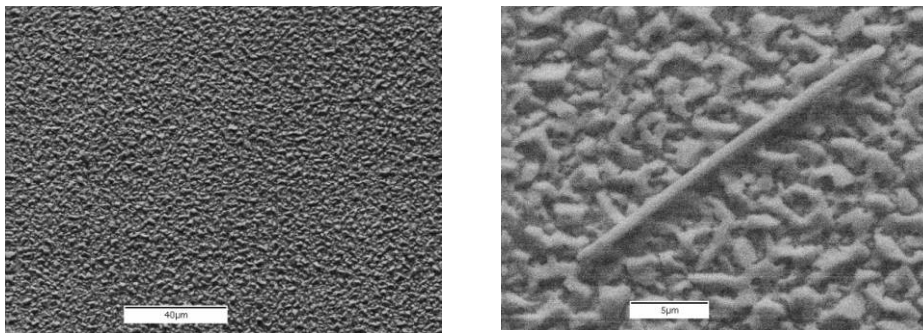


Figure 3.23 Surface of sample (left) incubated at -107 MPa (magnification ~490x), with close-up of whisker (right).

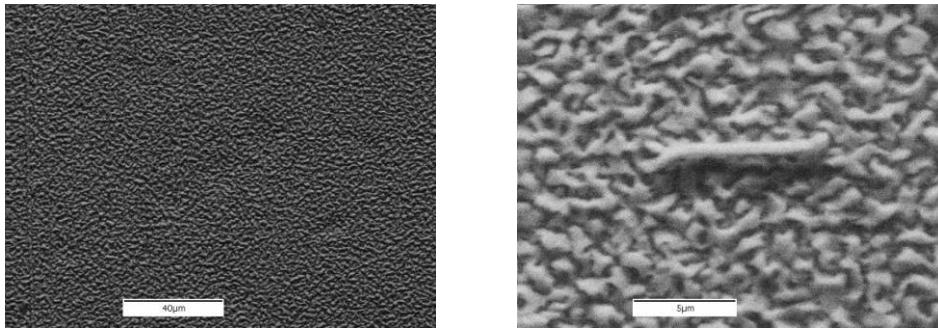


Figure 3.24 Surface of sample (left) incubated at -71 MPa (magnification ~490x), with close-up of whisker (right).

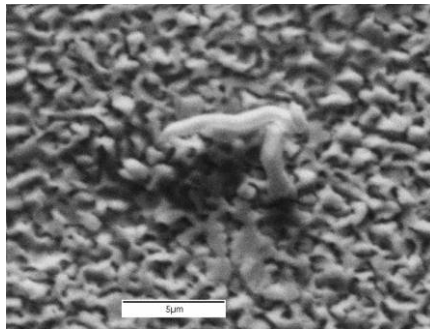


Figure 3.25 Close-up of whisker on sample incubated at -43 MPa.

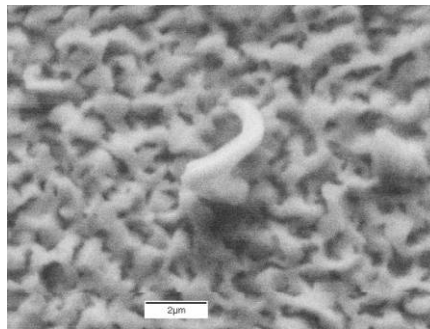
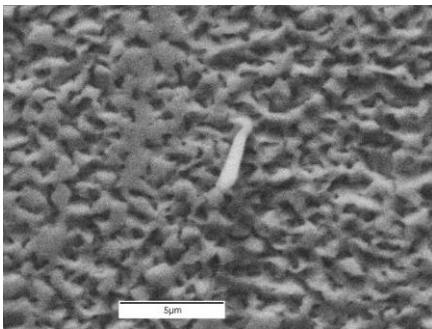


Figure 3.26 Close-ups of whiskers on sample incubated at 43 MPa.

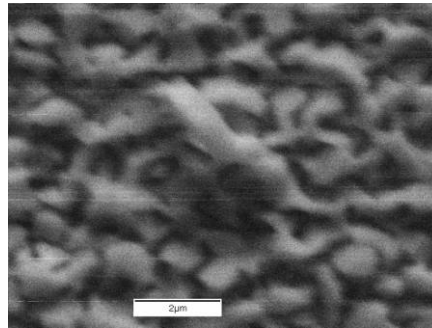
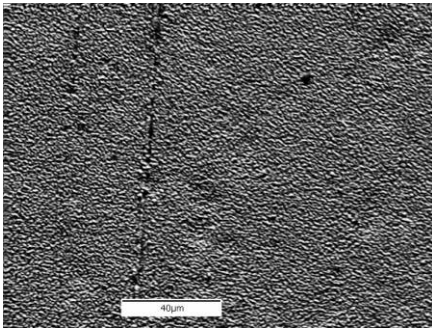


Figure 3.27 Micrographs of grooves on samples stored under tensile stress. These apparent 'stretch marks' were common on these samples; the micrograph on the right shows a whisker found on a sample incubated at 71 MPa.

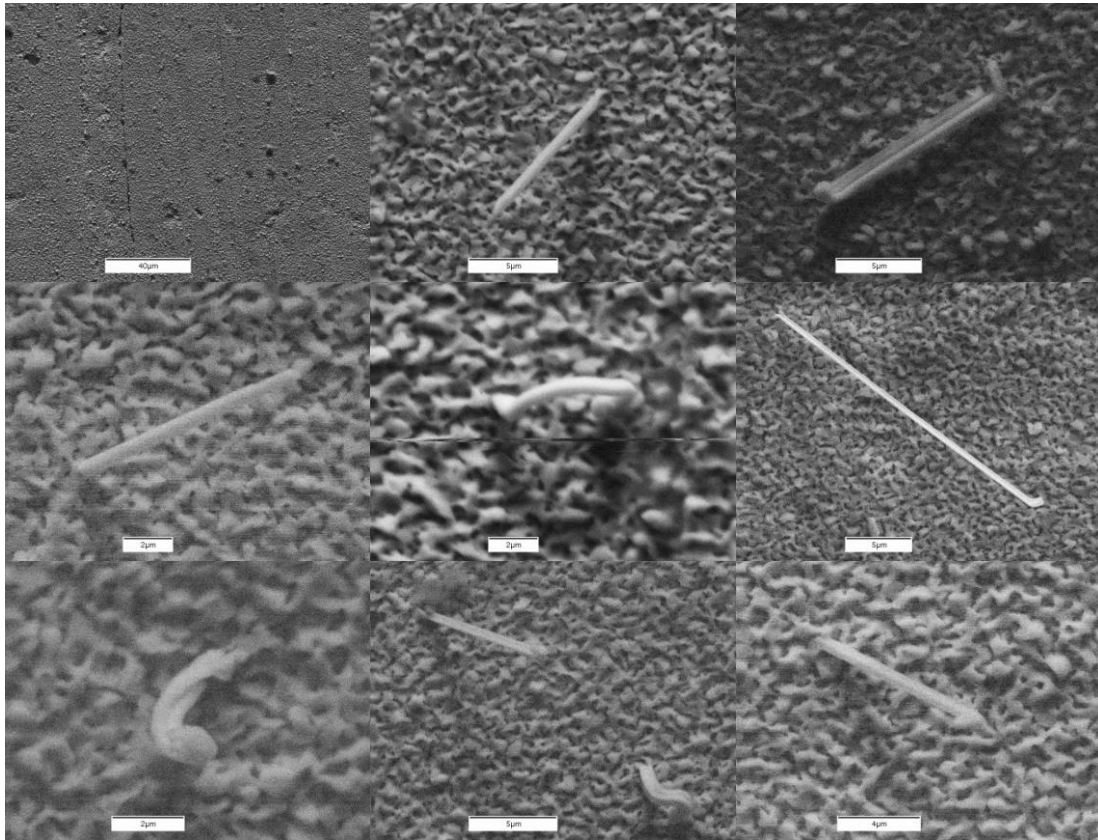


Figure 3.28 Surface of sample (upper left) incubated at 107 MPa (magnification ~490x). Remaining micrographs show whiskers on this surface.

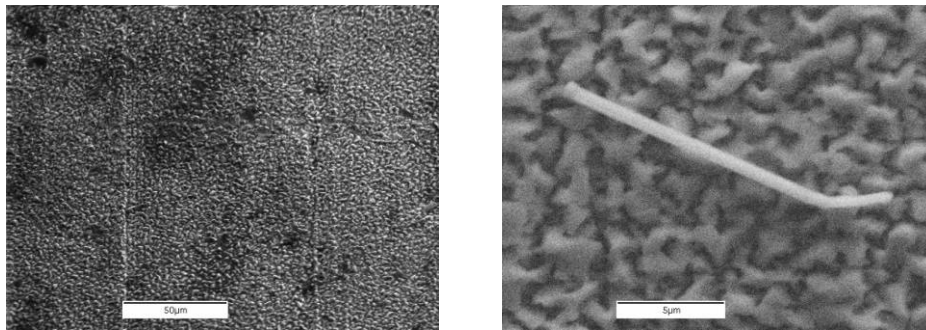


Figure 3.29 Surface of sample (left) incubated at 213 MPa (magnification ~490x) showing vertical 'stretch marks, and horizontal relief marks, with close-up of whisker (right).

The results of the experiment described in Section 3.5 indicated that whisker growth increases as stress in either direction (compressive or tensile) increases. If whisker growth is assessed in terms of whisker length, these results confirm this prediction; however, if whisker growth is assessed in terms of population density these results neither confirm nor contradict it. These two conclusions are shown in Table 3.16 and Figure 3.30.

Externally Applied Stress	Population Density	Average Length
-215	26.5	17.7
-107.2	2.4	19.3
-71	5.5	6.5
-42.7	16.7	7.4
42.7	16.7	3.5
71.3	2.4	1.0
106.8	97.9	5.9
213.3	26.5	10.1

Table 3.16 Externally applied stress on brass substrates: raw data.

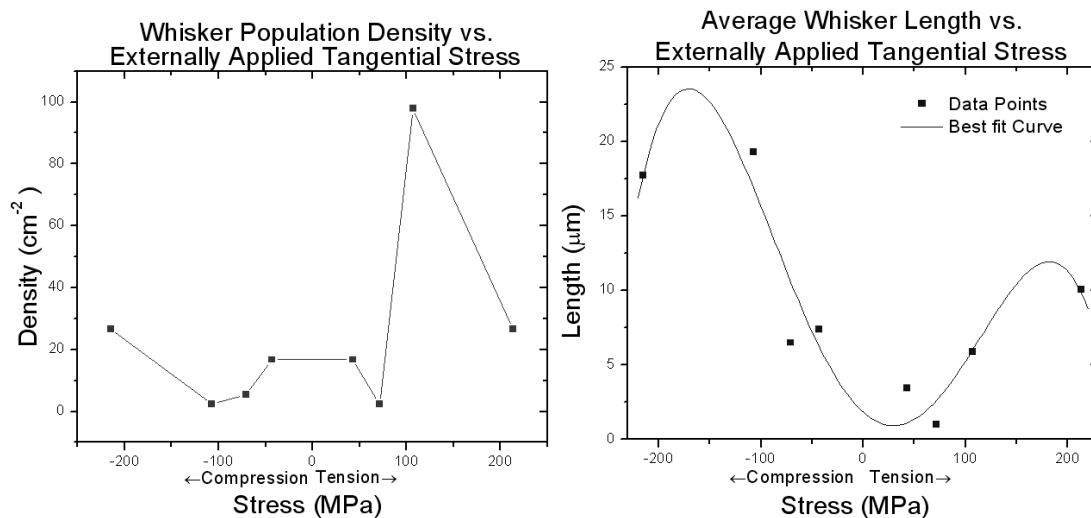


Figure 3.30 Whisker population density (left) and average whisker length (right) as a function of stress. Data presented is for 6000Å of Sn on brass.

Another interesting observation is shown in Figure 3.31, where there is a slight normal stress (imposed by the clamp) as well as the tangential stress (imposed by the curvature). These micrographs reveal an extraordinarily high whisker population density; in this area (approximately 0.19 mm^2) the population density is more than 3500 times greater than in the rest of the sample. It is unclear if this population explosion is due exclusively to the normal compressive stress of the clamp or the complete stress state, which encompasses the normal compressive stress of the clamp, the tangential tensile stress from the curvature, and all the intrinsic stresses. This issue is discussed in more detail in Section 5.2. Clearly further study is needed in this area.

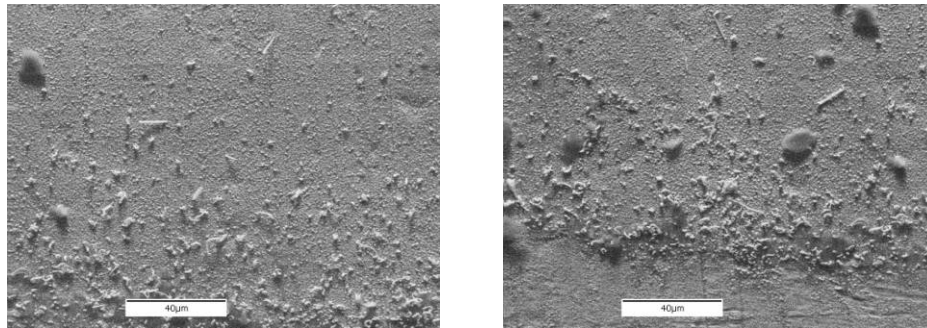


Figure 3.31 Surface of sample incubated at 107 MPa (magnification $\sim 490\times$) close to the source of compressive normal stress exerted by the clamp. This area was excluded from the data set due to the abnormally high number of whiskers, and its close proximity to the fixture clamp.

3.9.2 1500 Å of Tin on Aluminum Substrates

Figures 3.32 – 3.39 show micrographs of the whiskers found on the samples on Al substrates, in order of most compressive (-) to most tensile (+) stress.

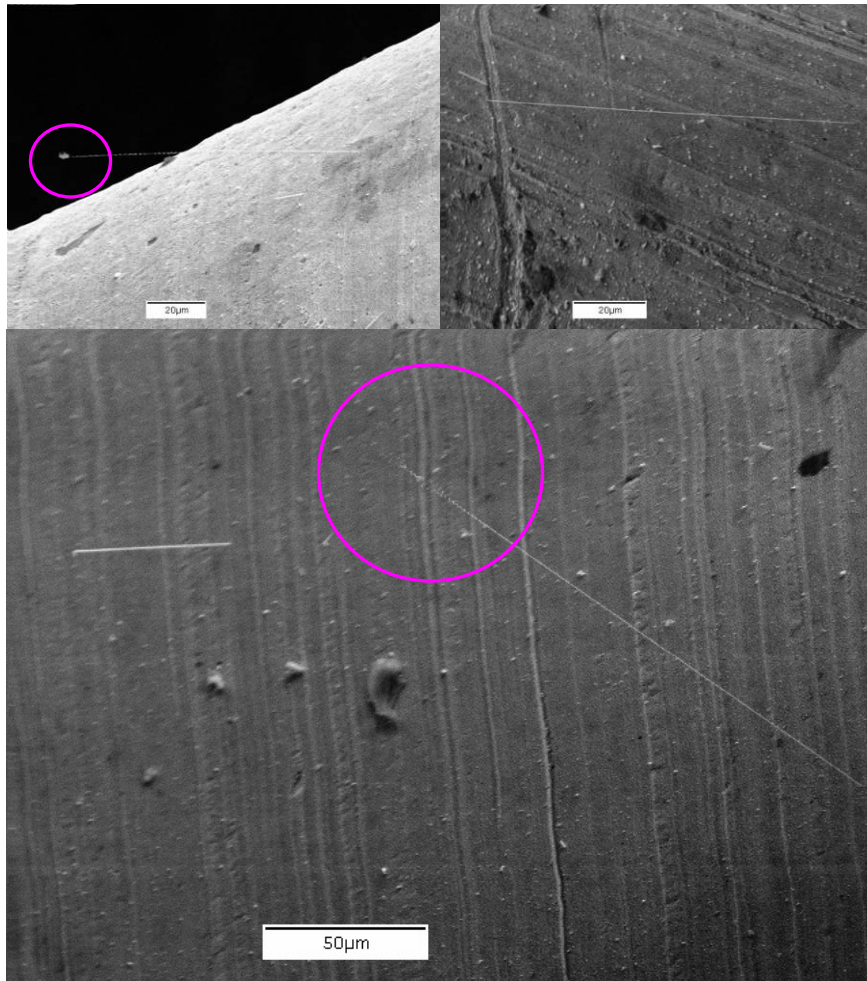


Figure 3.32 Micrographs of whiskers incubated at -432.8 MPa. Notice the dust particle at the tip of the 104 μm whisker (top left); there are also 3 smaller whiskers on the surface. The micrograph on the top right shows a 79 μm whisker and a smaller whisker. The bottom micrograph is enlarged to show a 151 and a 38 μm whisker, the 151 μm whisker has vibration nodes caused by the rastering electron beam from the microscope.

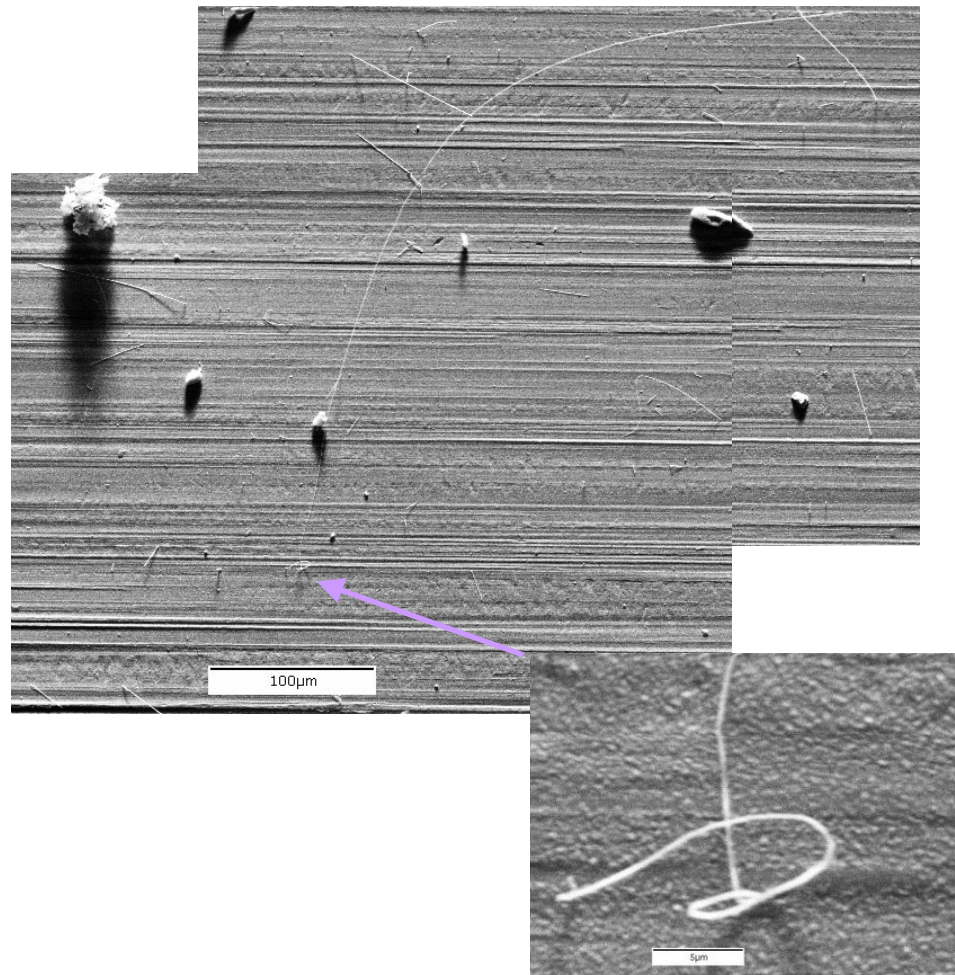


Figure 3.33 Collage of micrographs showing the longest whisker (543 μm) which was found on the sample incubated at -215.3 MPa. The whisker (magnified image of base shown in inset; location on sample indicated by arrow) was one of many long whiskers on the sample.

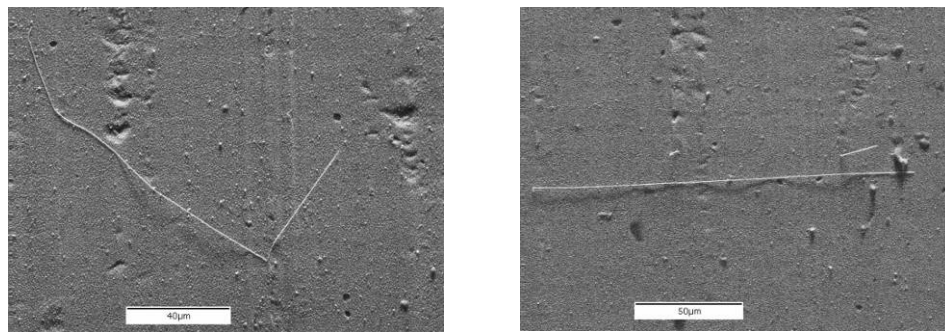


Figure 3.34 Long whiskers on sample incubated at -142.5 MPa.

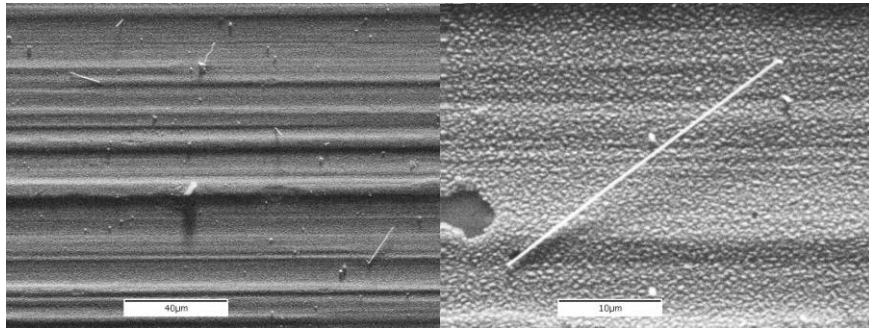


Figure 3.35 Typical whiskers found on sample incubated at -85.5 MPa.

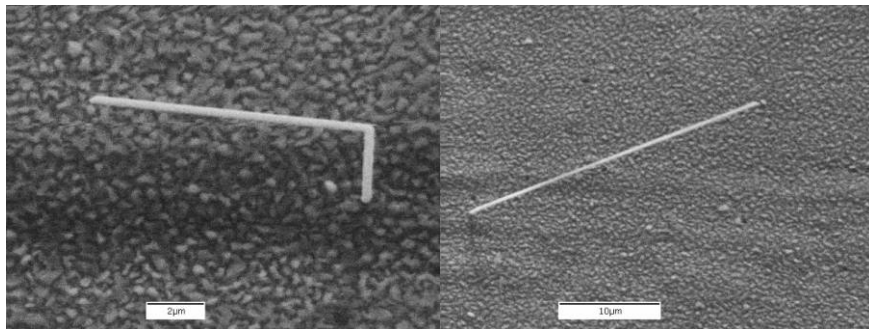


Figure 3.36 Typical whiskers found on sample incubated at 85.5 MPa.

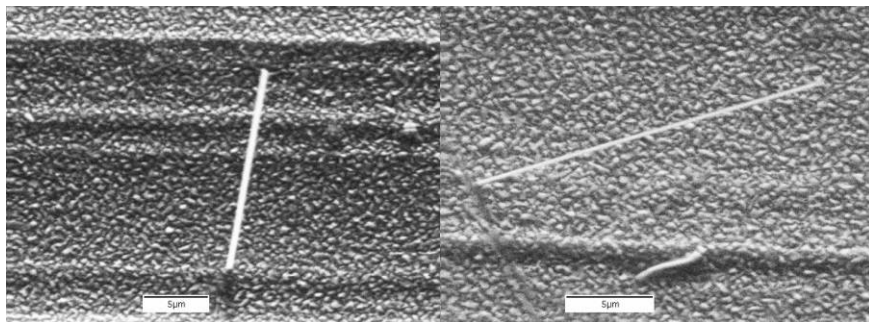


Figure 3.37 Typical whiskers found on sample incubated at 142.6 MPa.

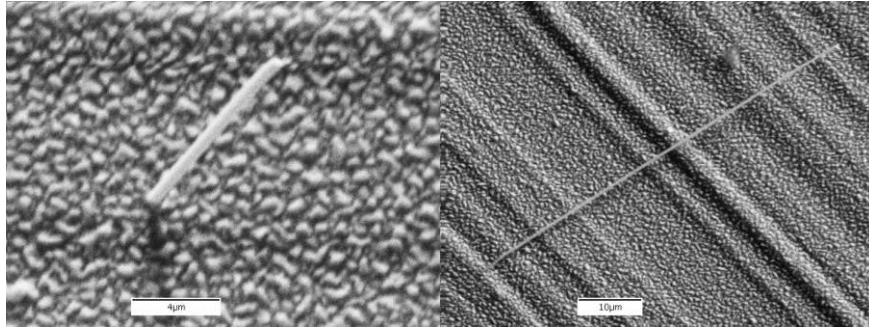


Figure 3.38 Short (left) and long (right) whiskers on sample incubated at 213.3 MPa.

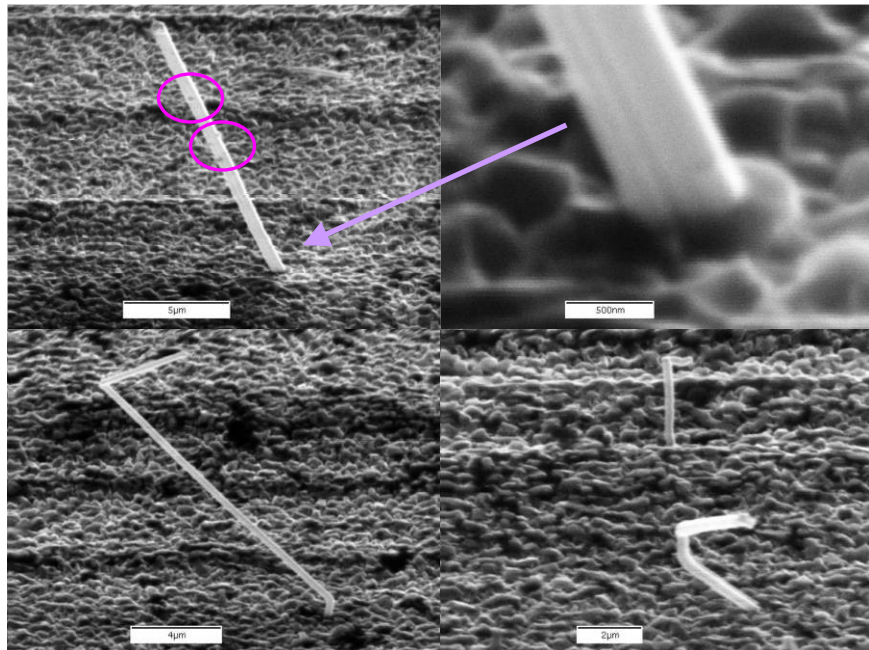


Figure 3.39 Micrographs of whiskers from samples incubated at 425.1 MPa. The top micrographs show striations along the edges and small pieces of debris, presumably picked up from the surface as the whisker grew through it. The top right micrograph is a magnification of the base of the whisker shown in the top left micrograph.

The results are summarized in the table and figures below. The graphs portray a very similar picture to that for samples with the brass substrate, although the scale is very different. In both population density and average length, the Al substrate with 1500Å of Sn proved to be more productive. This observation is contrary to expectations as Al and Sn have no IMC, as discussed earlier in Section 3.3.

Externally Applied Stress (MPa)	Population Density (cm ⁻¹)	Average Length (μm)
-432.8	389.4	32.8
-215.3	6085.3	39.1
-142.5	809.1	36.4
-85.5	4207.1	13.2
85.5	358.3	8.8
142.6	1085.1	9.5
213.3	161.8	17.2
425.1	6287.3	8.9

Table 3.17 Population density and average whisker length at each stress level.

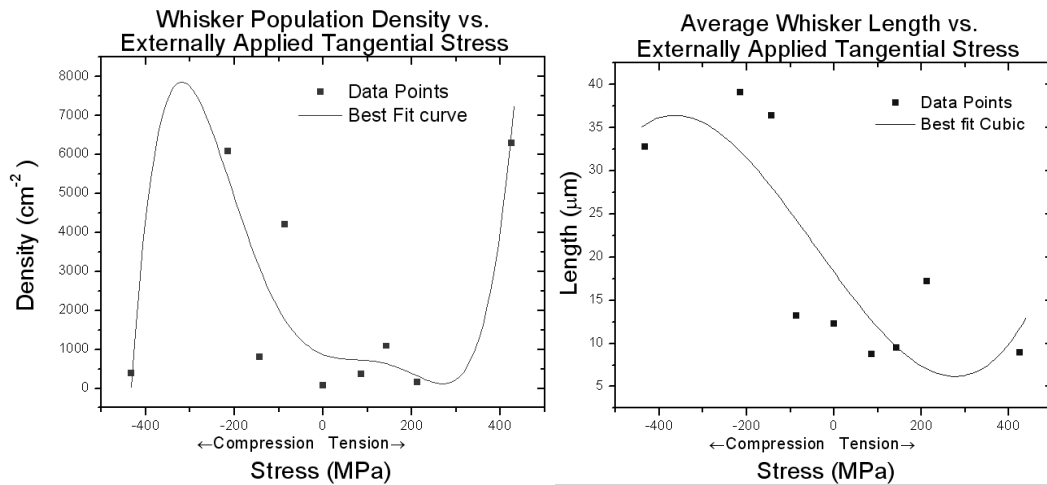


Figure 3.40 Population density (left) and average whisker length (right) as a function of stress for samples with 1500Å of Sn on Al.

3.9.3 6000 Å of Tin on Aluminum Substrates

The series of micrographs below show the whiskers observed on samples with a coating of 6000Å of Sn on Al substrates. They are given in order of most compressive (-) to most tensile (+) stress.

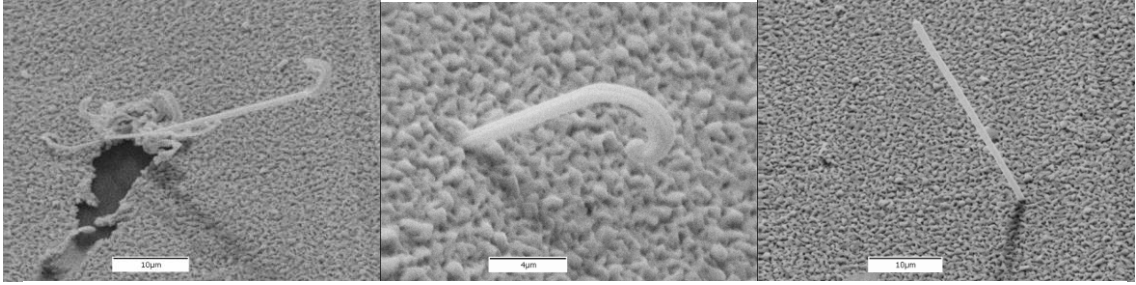


Figure 3.41 Typical whiskers on sample incubated at -432 MPa.

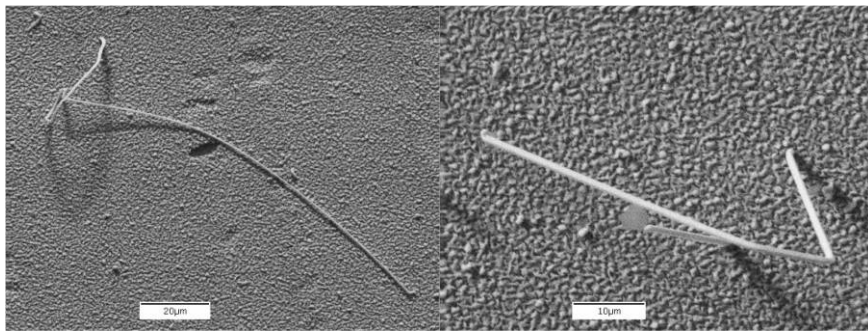


Figure 3.42 Typical whiskers on sample incubated at -215 MPa.

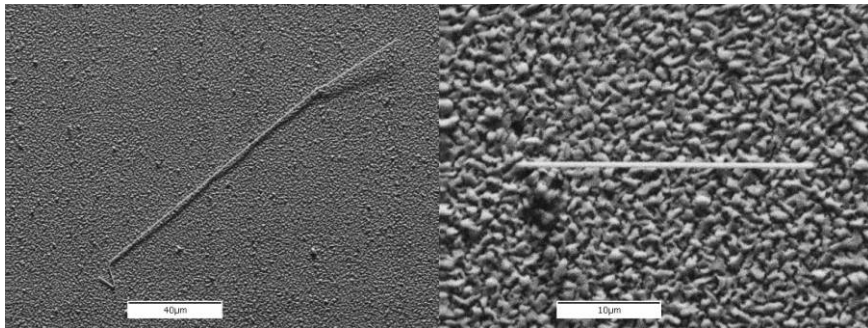


Figure 3.43 Typical whiskers on sample incubated at -142 MPa.

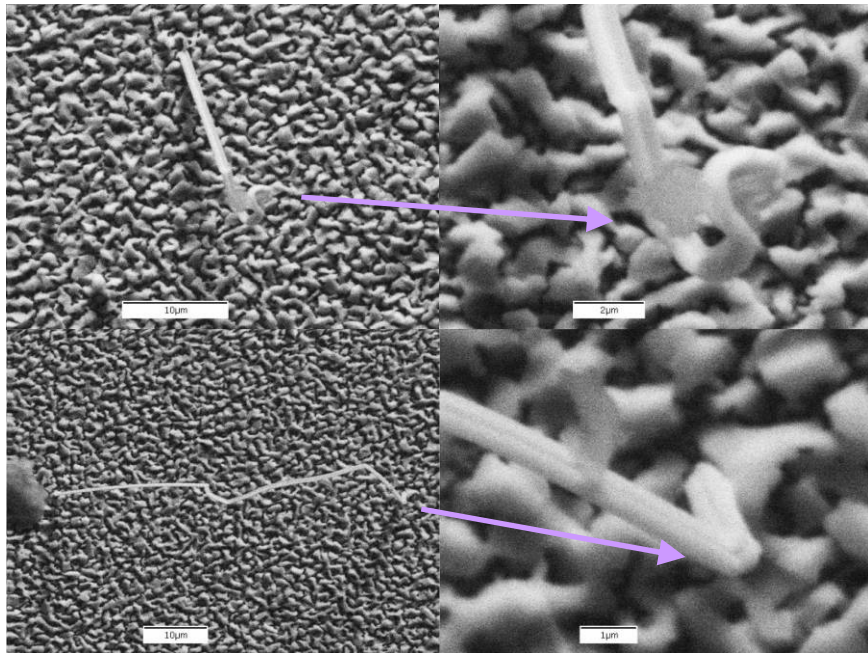


Figure 3.44 Typical whiskers on sample incubated at -85.4 MPa.

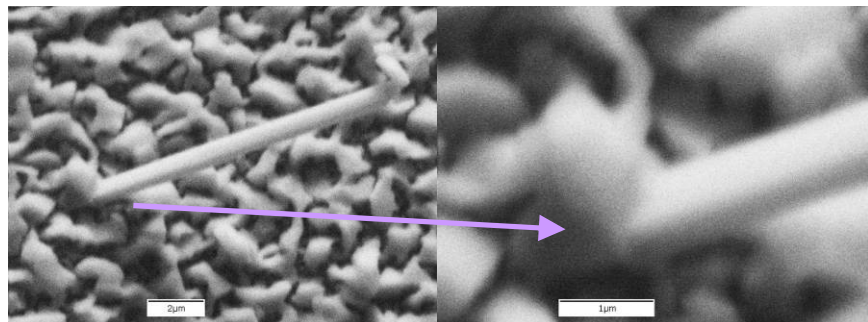


Figure 3.45 Typical whisker on sample incubated at 85.4 MPa.

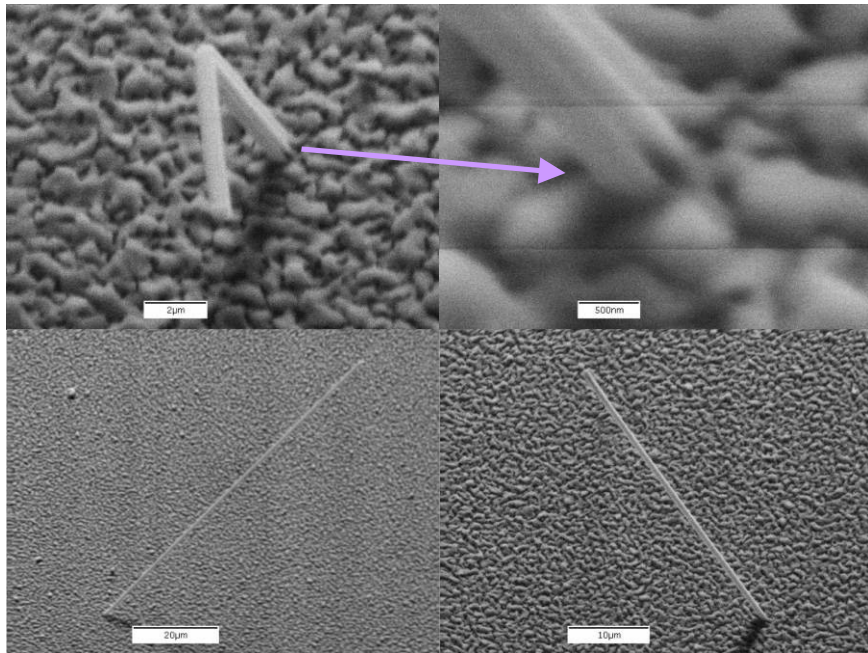


Figure 3.46 Typical whiskers on sample incubated at 143 MPa.

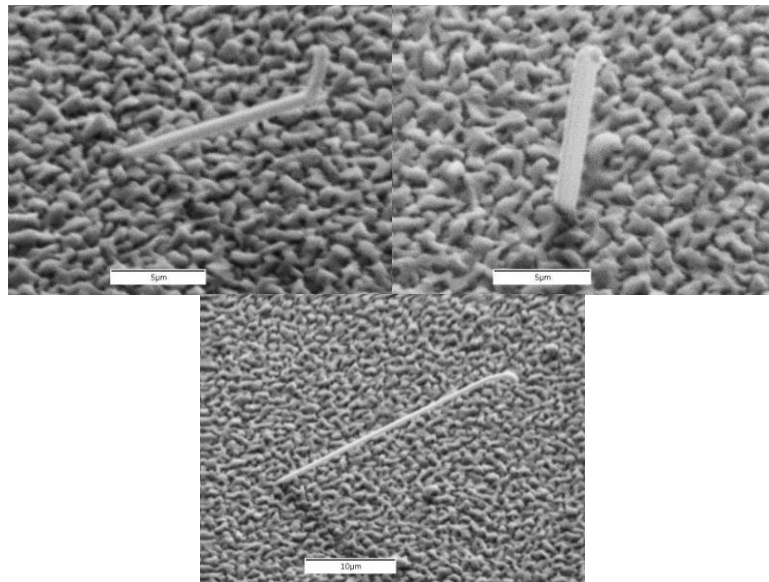


Figure 3.47 Typical whiskers on sample incubated at 213 MPa.

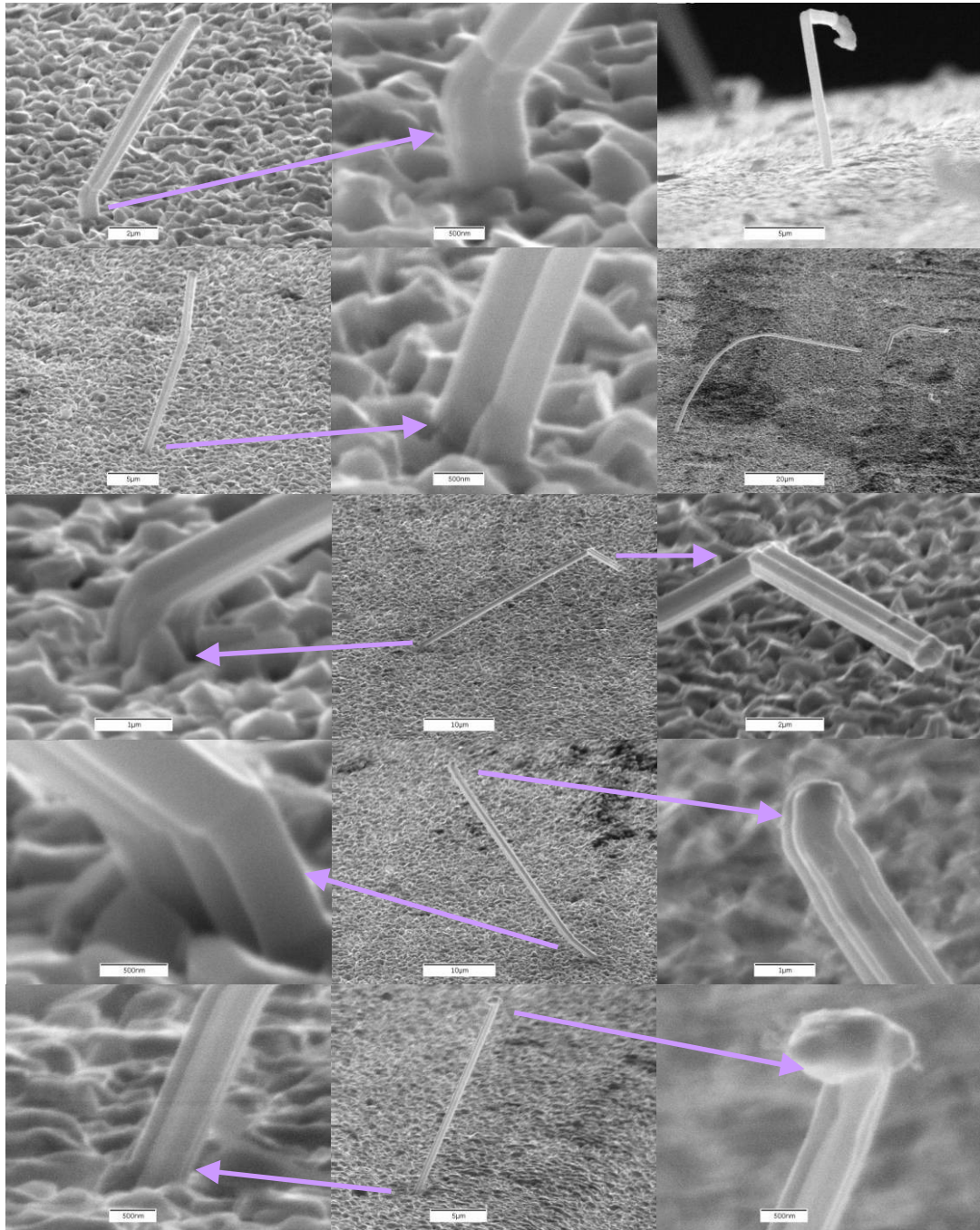


Figure 3.48 Detailed micrographs of typical whiskers on sample incubated at 424.6 MPa. The orientation and shape of the sample allowed excellent resolution, so extra micrographs are provided in the next figure for additional detail.

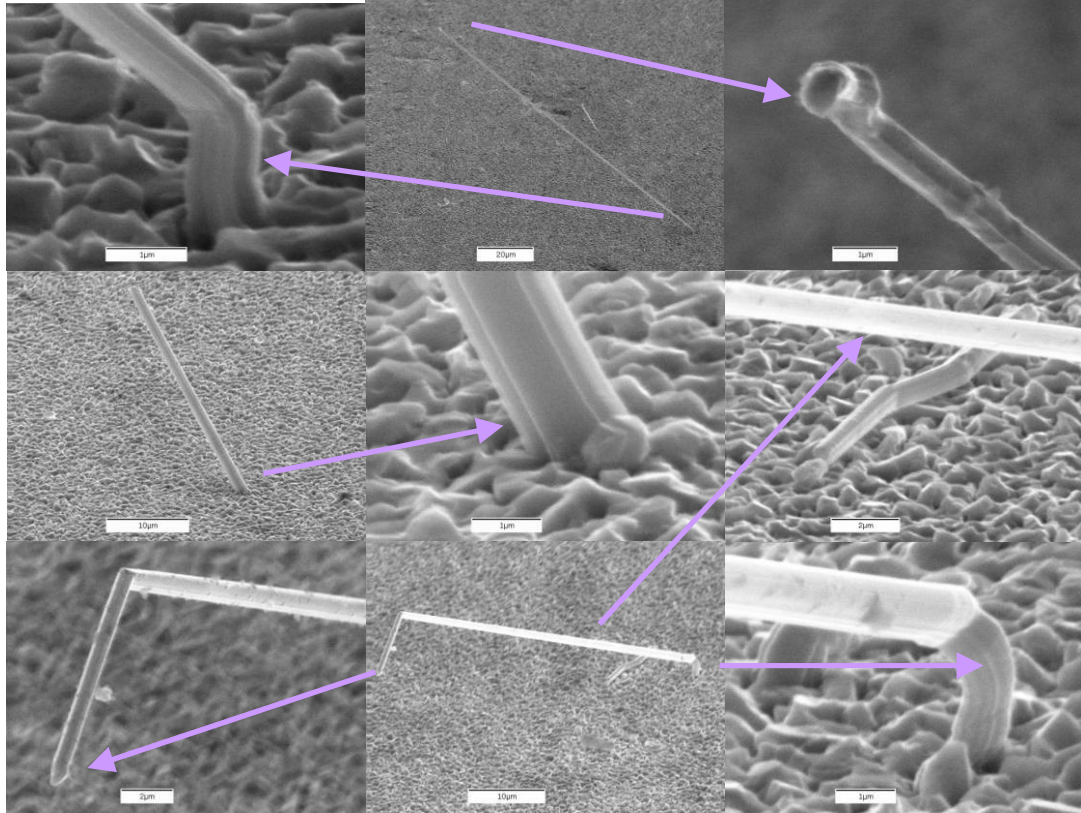


Figure 3.49 Additional micrographs of sample in previous figure.

The results are summarized in Table 3.18 and Figure 3.50 below. The graphs portray a very similar picture to those found in the previous two sections. Again, both the whisker population density and average length were greater than for the comparable brass samples.

Externally Applied Stress (MPa)	Population Density (cm ⁻¹)	Average Length (μm)
-432.4	1206.6	14.7
-215.1	2294.8	46.4
-142.3	363.8	34.3
-85.4	669.1	15.0
85.4	114.4	13.6
142.5	1423.3	14.1
213.1	1045.0	11.8
424.6	3169.4	16.6

Table 3.18 Population density and average whisker length at each stress level.

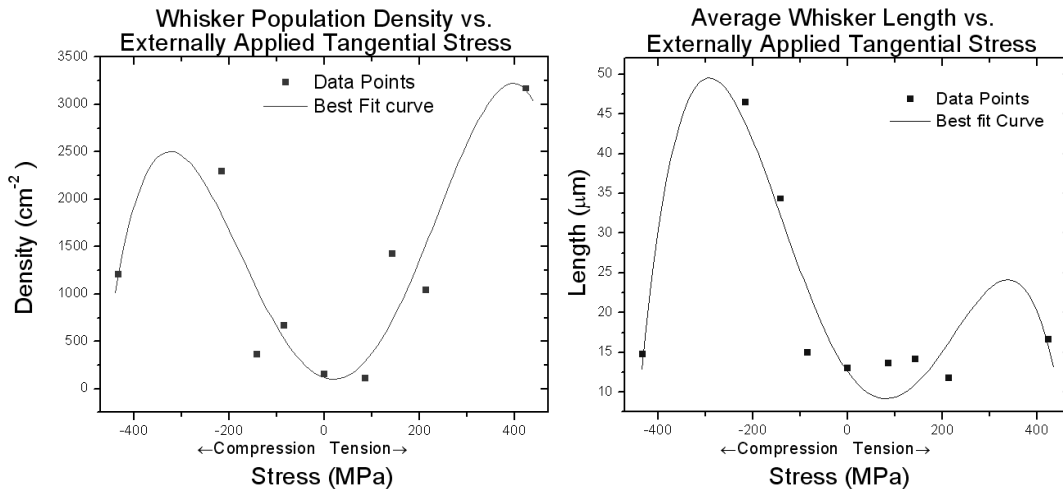


Figure 3.50 Whisker population density (left) and average whisker length (right) as a function of stress for samples with 6000Å of Sn on Al.

In all three sets of samples, both population density and average length generally increased as either compressive or tensile stress increased. This supports the findings presented in Section 3.5 where whisker growth was observed in samples with an intrinsic compressive stress state or an intrinsic tensile stress state. Although general trends may be observed from this data, however, the exact nature of the relationship

between stress and whisker growth is not clear; a more comprehensive study is needed to quantify this apparent relationship. Furthermore the data presented thus far in this section only relates the externally applied stress to whisker growth and does not correlate the total stress state (the 9 element stress tensor, which also needs to take into account all intrinsic stresses) and whisker growth. As a first attempt to find this stress state, a method for finding this total stress state is proposed in Appendix 3, and the data used to find the particular intrinsic stress states of each sample, as well as the resulting total stress states is presented in Section 5.2.

- *Key Result: Whisker growth qualities appear to increase with externally applied compression and tension.*
 - This finding is outlined here, although a larger sample matrix is necessary to strengthen this statement.
- *Key Result: A method for differentiating types of stress sources has been proposed and used.*
 - This method is fully described in Appendix 3, and is applied in section 5.2.
 - This method should be adopted in all future studies in order to fully understand the relationship between stress within the thin film and the

3.10 Influence of Film Thickness

The thickness of the thin film has an effect on the length, number, and type of whiskers formed. This conclusion can be drawn from the findings reported in Section 3.7 (where it is shown that a whisker obtains all of its material from the film) and Section 3.8 (where different whisker qualities are clearly observed with different film thicknesses). This supposition was tested in several of the studies reported in this section, where film thicknesses of 1500Å and 6000Å were deposited on a range of samples which were otherwise the same. Since most of this data was presented in previous data sets, this section focuses on the results in which the only variable was a difference in film thickness. The results shown below in Tables 3.22-3.24 fail to show any overriding effect due to film thickness on population density or average length of whiskers (Sn or otherwise). The results for different substrates are combined in Table 3.22.

Stress	1500Å Film Population Density (cm ⁻²)	6000Å Film Population Density (cm ⁻²)	1500Å Film Average Length (µm)	6000Å Film Average Length (µm)
-433	389.4	1206.6	32.8	14.7
-215	6085.3	2294.8	39.1	46.4
-143	809.1	363.8	36.4	34.3
-86	4207.1	669.1	13.2	15.0
86	358.3	114.4	8.8	13.6
143	1085.1	1423.3	9.5	14.1
213	161.8	1045.0	17.2	11.8
425	6287.3	3169.4	8.9	16.6

Table 3.22 Population density and average whisker length from the study in Section 3.9. The highlighted cells are the larger values. This data shows no conclusive trend.

Conditions	1500Å Film Population Density (cm ⁻²)	5800Å Film Population Density (cm ⁻²)	1500Å Film Average Length (µm)	5800Å Film Average Length (µm)
Al, rough	76.0	154.0	12.0	13.0
Al, Smooth	109.0	144.0	4.0	5.0
Ni, Rough	0.0	4.0	N/A	4.0
Ni, Smooth	248.0	85.0	5.0	5.0
Cu, rough	11.0	51.0	6.0	8.0
Cu, Smooth	1204.0	119.0	4.0	6.0
Ag, Rough	1.51E+06	2.60E+05	1.0	3.0
Ag, Smooth	5.10E+05	1.96E+06	3.0	1.0
Zn, Rough	0.0	1410.0	N/A	7.0
Zn, Smooth	373.0	116.0	6.0	3.0

Table 3.23 Population density and average whisker length from the study in Section 3.3. The highlighted cells are the larger values. This data shows no conclusive trend.

Conditions	1500Å Film Population Density (cm ⁻²)	6000Å Film Population Density (cm ⁻²)	1500Å Film Average Length (µm)	6000Å Film Average Length (µm)
Zn, Smooth	2.78E+05	2.73E+05	1.6	2.3
Cd, Rough	2.54E+05	3.46E+04	1.5	1.5
Cd, Smooth	3.82E+05	9.05E+04	1.5	1.5
Ag, Rough	2.38E+06	3.17E+06	0.5	0.5
Ag, Smooth	1.79E+05	1.19E+05	1.5	1.5
In, Smooth	50	8	7.3	7.0

Table 3.24 Population density and average whisker length from the study in Section 3.8. The highlighted cells are the larger values. This data shows no conclusive trend.

- *Key Result: While the thickness of the metallic film has an effect on the types and quantities of whiskers grown, it currently is not a predictable effect.*
 - The data analysis shows that although thicker films do not always yield longer whiskers or larger population densities, different types of whiskers (different in appearance, and incubation time) can be produced by altering the thickness of the film

CHAPTER 4 CONCLUSIONS

The work reported in this dissertation represents a substantial contribution to our understanding of the formation of metallic whiskers. These significant and original contributions can be summarized as follows:

- *A method for reproducibly growing Sn whiskers with predictable incubation times has been developed and tested.*
 - This technique is fully described in Section 3.1, and was used throughout. The incubation time is 90-110 days.
 - There have been no previous reports (that we are aware of) of a reproducible method of whisker production from a pure Sn film.
- *Surface oxide is not necessary for whisker growth.*
 - The results supporting this finding are described in Section 3.2.
 - This result does not support the hypothesis set forth by Tu [13].
 - This result supports the findings of Moon et al. [20].
- *IMC growth is not necessary for whisker growth.*
 - This conclusion is based on observations of thousands of whiskers grown when a Sn film is placed on an Al substrate (where no IMC is present) in the studies described in Sections 3.3, 3.4, 3.9, and 3.10.
 - This result does not support the hypothesis set forth by Galyon et al. [18].

- *Smoother substrate surface finishes promote whisker growth; polishing the substrate is not an effective whisker mitigation technique, although making the substrate rougher can be effective.*
 - In all cases (except when Ag is in either the substrate or the film), whisker growth qualities (both in population density and average length) are enhanced by smoother substrates (Sections 3.4, 3.8, and 3.10).
 - This result is contrary to certain practices in industry.
 - This work complements and provides more evidence to support results reported by Takeuchi et al. [23].
- *Whiskers grow from both compressive and tensile stress states.*
 - This conclusion is based on the results reported in Sections 3.5 and 3.9.
 - This contradicts the many authors who hypothesized that it is exclusively compressive stress which drives the whisker growth.
- *Sn whiskers are composed of pure Sn, both on their surface and in their bulk.*
 - This is contrary to the findings of Fujiwara and Kawanaka [27].
 - This validates the indirect investigations of other researchers.
- *For Sn on brass, the feedstock of metallic whiskers lies within the film exclusively; the brass substrate does not contribute to whisker production.*
 - The feedstock of Sn whiskers comes from the thin film exclusively. This does not imply that the substrate has no effect on the qualities of whisker growth, as the substrate does have an effect, but simply that the substrate does not contribute any atoms to the whisker (Sections 3.6, 3.7 and 3.8).
 - This finding narrows the range of possible whisker growth mechanisms.

- *There are probably multiple mechanisms of whisker growth depending of the substrate – thin film system.*
 - The findings reported in Section 3. 8 revealed multiple types of whiskers growing from both Cd and Zn films. These types of whiskers could only be produced by different growth mechanisms.
 - There has been no known publications of this finding
- *The film volume consumed by the growth of a single whisker can be estimated by a simple volumetric comparison.*
 - This was confirmed by measurement of an Ag film reported in Section 3.8. The Ag film had an extremely fine and uniform grain structure, clearly revealing changes beneath the surface and showing the area affected by the growth of individual whiskers.
- *Whisker growth qualities appear to increase with externally applied compression and tension.*
 - This finding is outlined in Section 3.9, although a larger sample matrix is necessary to strengthen this statement.
- *While the thickness of the metallic film does have an effect on the types and quantities of whiskers grown, it currently is not a predictable effect.*
 - This finding is presented in Sections 3.8, 3.9, and 3.10. The data analysis shows that although thicker films do not always yield longer whiskers or larger population densities, different types of whiskers (different in appearance, and incubation time) can be produced by altering the thickness of the film

- *As a first attempt, a method for differentiating types of stress sources has been proposed and used.*
 - This method is fully described in Appendix 3, and is applied in Section 5.2.
 - This method should be adopted in all future studies in order to fully understand the relationship between stress within the thin film and the whiskers that grow from that film.

CHAPTER 5 SUGGESTIONS FOR AND DEVELOPMENT OF FUTURE WORK

5.1 IMC Development in a Thin Film-Substrate System

Many Sn whisker end game hypotheses rely on the formation and time-dependent growth of IMC layers [18]. Several focused ion beam (FIB) studies have shown the fully developed IMC layer, but none have yet examined how this layer forms and grows over time for sputtered films in the context of whisker growth.

Studies of the solder-substrate system, which forms a much thicker IMC layer than a sputtered substrate-thin film system, have the potential to address this lack. The thin nature of substrate-thin film IMC layers has prevented such studies in the past, but a more complete understanding of the IMC layer would aid those working on the formation of Sn whiskers.

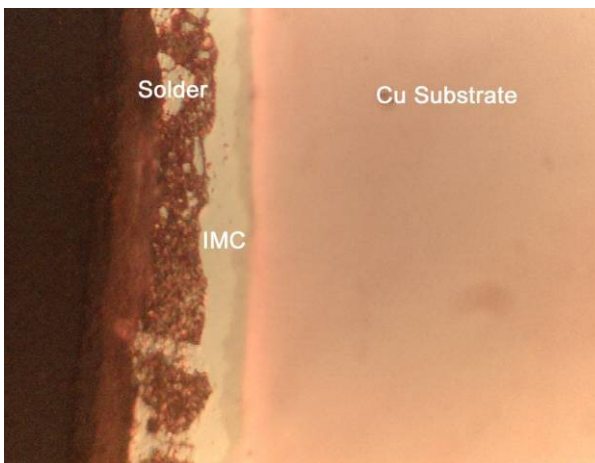


Figure 5.1 The IMC layer developed in a solder-substrate system.

5.2 Intrinsic Stresses in a Thin Film-Substrate System

There are at least seven possible sources of stress in a substrate – thin film system several of these sources have been labeled individually as the underlying cause behind Sn whisker growth [15, 18, 20, 22, 24]. The work presented in this section show that these sources work together to create an overall stress state, which may a driving force underlying the growth Sn whiskers. The seven sources are as follows: 1) atomic peening, 2) coefficient of thermal expansion (CTE) mismatches between the substrate and the film, 3) microstructure stabilization, 4) surface oxidation, 5) grain boundaries oxidation, 6) non-uniform IMC development, and 7) externally applied forces or moments. Factors 1, 3, 4, 5, and 6 are difficult to specify analytically and must be experimentally measured. The first six factors together add to yield a net stress referred to as ‘intrinsic stress.’ Figures 5.2 and 5.3 show the two ways these stresses effect the film-substrate system.

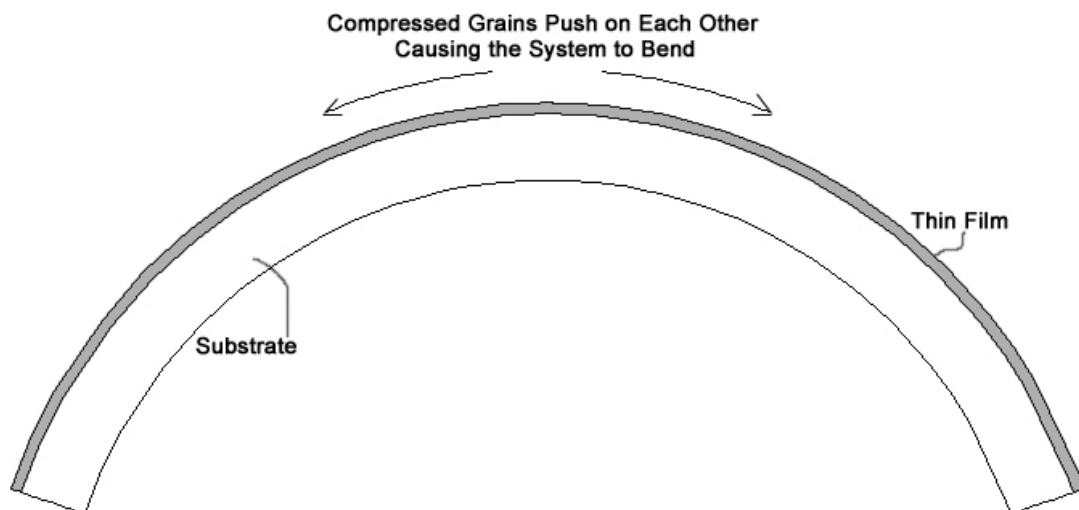


Figure 5.2 Effect of an intrinsic compressive stress on a thin film-substrate system. Notice the curvature is *opposite* to that of a compressive state caused by an external curve shown in Figure 3.18.

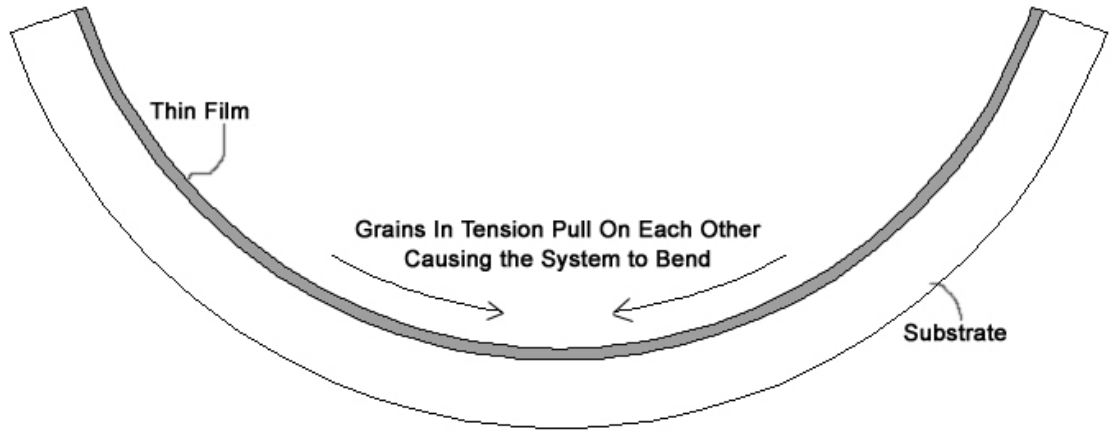


Figure 5.3 Effect of an intrinsic tensile stress on a thin film-substrate system. Notice the curvature is *opposite* to that of a tensile state caused by an external curve shown in figure 3.19.

There have been few studies that have addressed the intrinsic stress state in deposited thin films. One of those studies briefly mentioned that the state of stress changes with time [17]. In a preliminary study we also found this to be true. If whisker growth depends on stress within the Sn film, the nature of the stress needs to be understood. An understanding of stress as a function of time is an integral piece to a complete understanding of Sn whisker growth. Moreover, the exact stress state imposed by background Ar pressure during sputtering should be quantified.

Our preliminary study used brass and Al samples with dimensions 1cm x 10cm. Then a precision slow-speed diamond saw was used to cut a 0.4 mm slit in the middle that went 9 cm along the length of the sample. A cover was made to shield one half of the sample, and a thin metallic film was deposited on the other. Figure 5.4 gives the dimensions of the samples. The dimensions were chosen to ensure two things. First, the large aspect ratio of the individual leaves ensures bifurcation along the length of the leaf. Secondly, the un-coated half of the leaf provides a reference point from which to

measure the amount of displacement caused by the curling coated leaf. A fixture was designed and constructed to mount 8 such samples in such a way as to negate the effects of gravity on the curling of the samples. Figure 5.5 shows the fixture and sputtered samples.

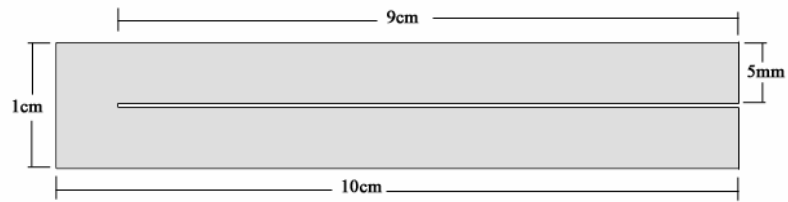


Figure 5.4 Dimensions of samples used to measure intrinsic stresses in a deposited film.



Figure 5.5 Fixture used to mount samples. Eight samples are loaded, and some of the curvatures can clearly be seen.

After a thin film was applied to one leaf of each sample, the displacement between the coated leaf and its uncoated counterpart was measured at regular time intervals over a period of 3,000 hours. Using the equations and methods described more fully in Appendices 1 through 3, the total stress state in the thin films can be experimentally determined. The 8 sample combinations are listed in Table 5.1, and the results of this preliminary study are listed in Tables 5.2-5.9 below.

Film	Film Thickness (μm)	Substrate	Substrate Thickness (mm)
Ag	0.6	Brass	0.125
Zn	0.6	Brass	0.125
Cd	0.6	Brass	0.125
In	0.6	Brass	0.125
Sn	0.6	Brass	0.125
Sn	0.15	Brass	0.125
Sn	0.6	Aluminum	0.25
Sn	0.15	Aluminum	0.25

Table 5.1 Sample matrix used for preliminary study.

This preliminary data clearly shows the wealth of data that can be gleaned from this relatively simple bent beam experiment. The use of this method to find the stress state of a thin film as the Ar pressure is changed would be a nice complement to the experiment listed in Section 3.5, and to any further study. It should be mentioned that the bent beam method has inaccuracies associated with it, also several approximations have been made (outlined in section 5.3). This method needs further revision (as indicated by the high stress and strain values), and is intended to be used as a starting point for future study.

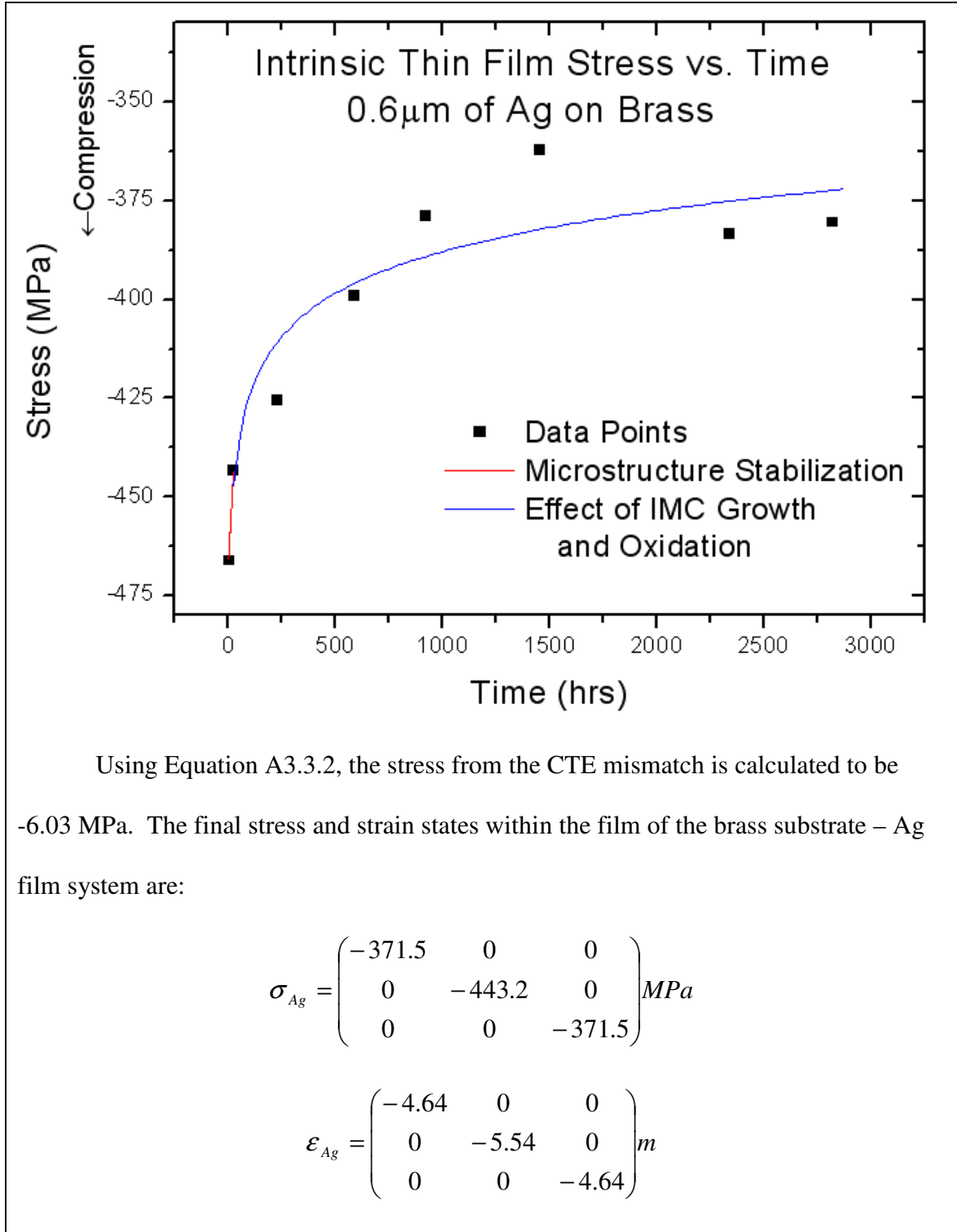
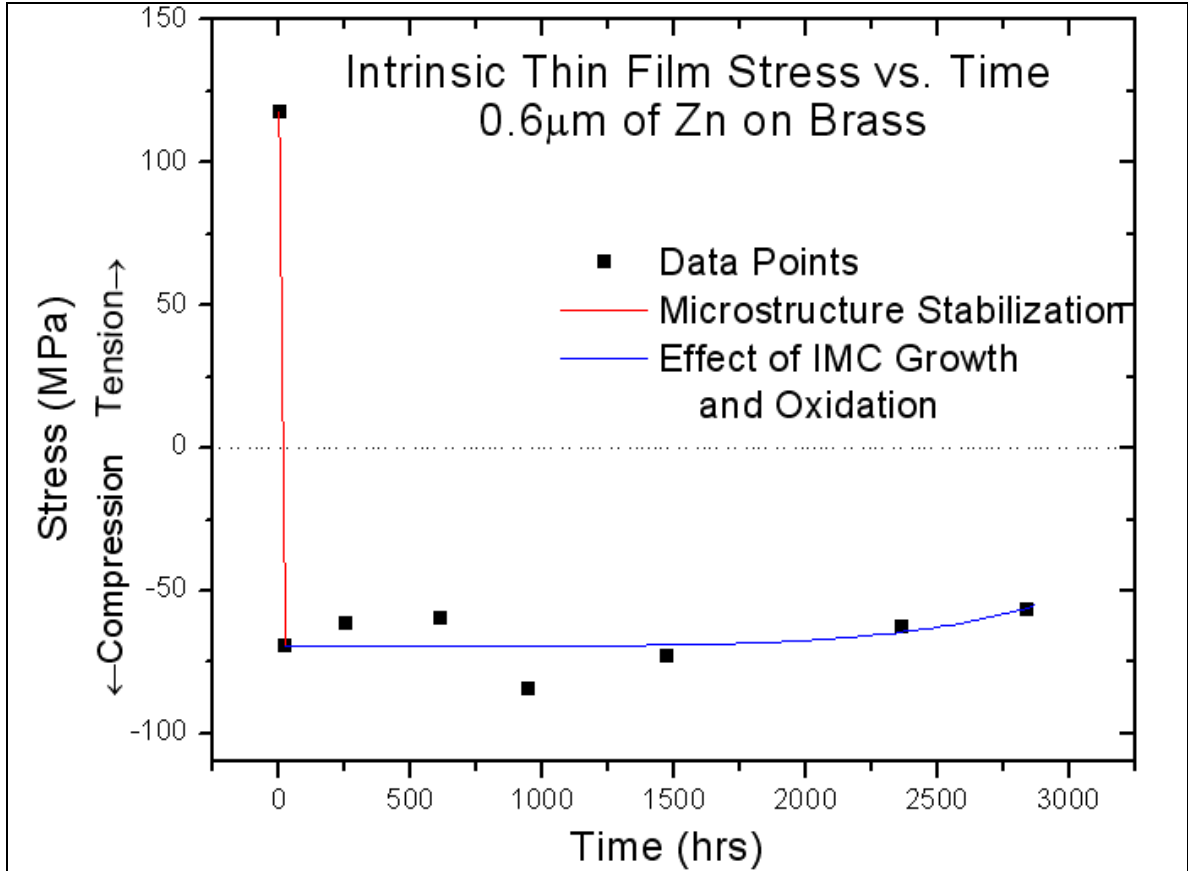


Table 5.2 Stress change over time in a brass substrate – Ag film system The final stress and strain states are also listed.



Using Equation A3.3.1, the stress from the CTE mismatch is calculated to be -41.49 MPa. The final stress and strain states within the film of the brass substrate – Zn film system are:

$$\sigma_{Ag} = \begin{pmatrix} -51.41 & 0 & 0 \\ 0 & -69.06 & 0 \\ 0 & 0 & -51.41 \end{pmatrix} MPa$$

$$\epsilon_{Ag} = \begin{pmatrix} -476 & 0 & 0 \\ 0 & -640 & 0 \\ 0 & 0 & -476 \end{pmatrix} \mu$$

Table 5.3 Stress change over time in a brass substrate – Zn film system The final stress and strain states are also listed.

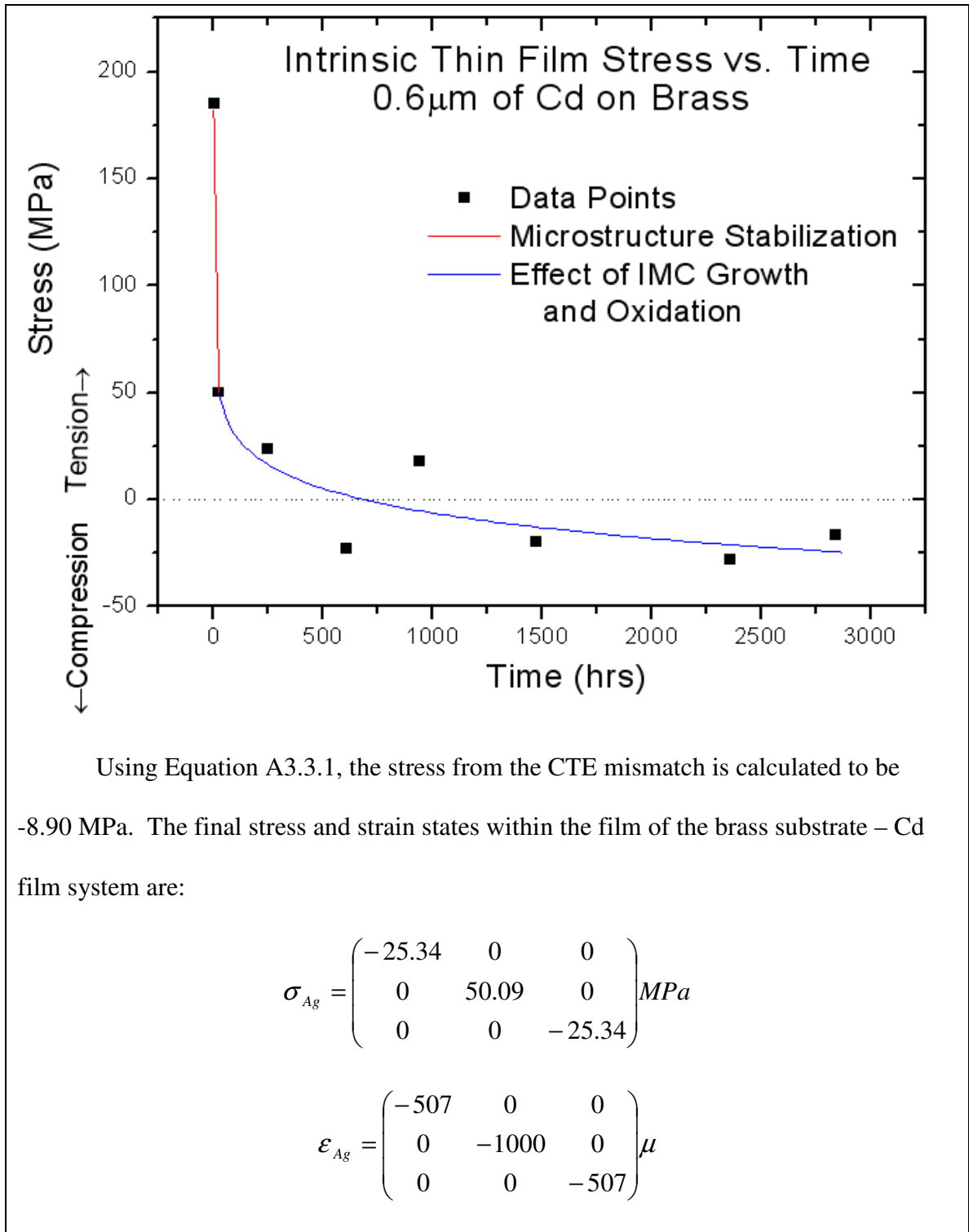
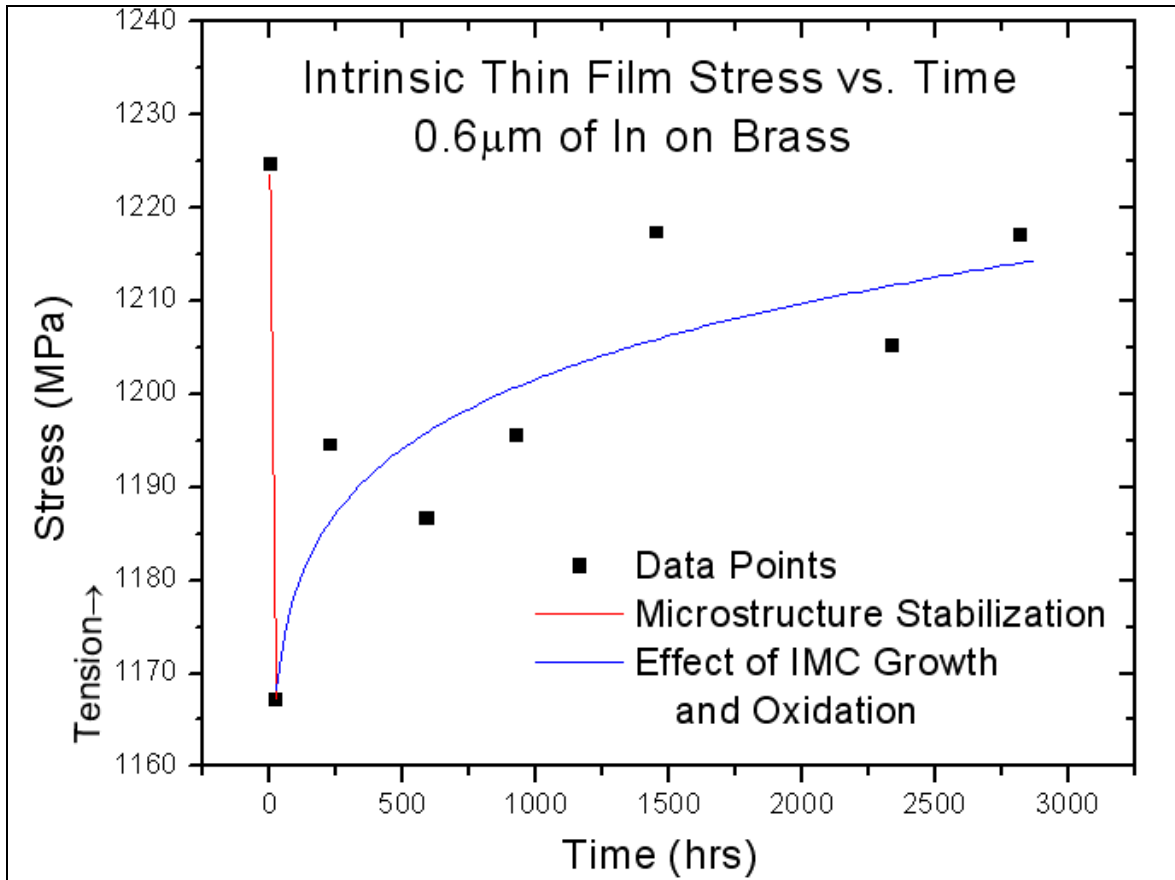


Table 5.4 Stress change over time in a brass substrate – Cd film system. The final stress and strain states are also listed.

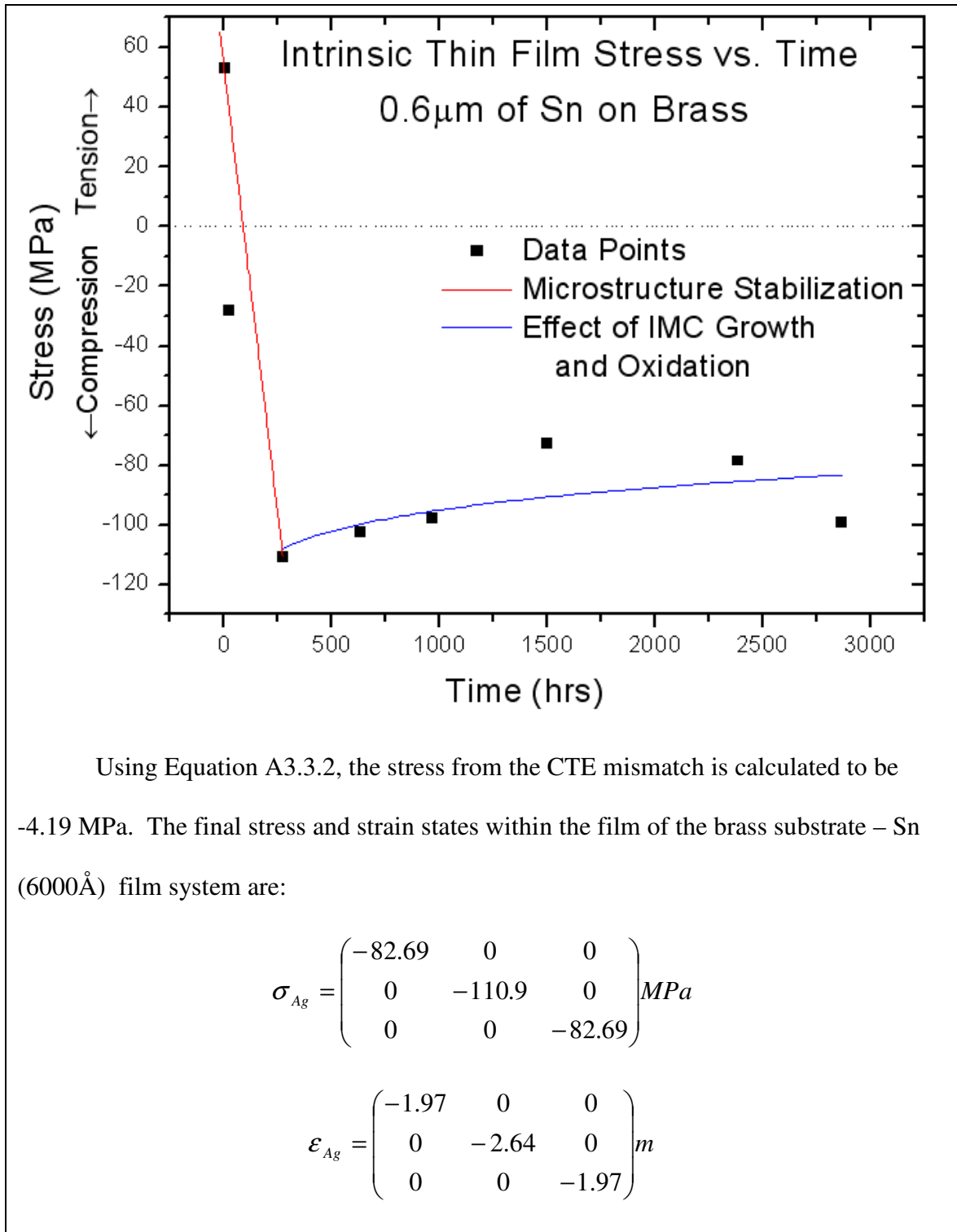


Using Equation A3.3.2, the stress from the CTE mismatch is calculated to be -2.46 MPa. The final stress and strain states within the film of the brass substrate – In film system are:

$$\sigma_{Ag} = \begin{pmatrix} 1215 & 0 & 0 \\ 0 & 1167 & 0 \\ 0 & 0 & 1215 \end{pmatrix} MPa$$

$$\epsilon_{Ag} = \begin{pmatrix} 110.4 & 0 & 0 \\ 0 & 106.1 & 0 \\ 0 & 0 & 110.4 \end{pmatrix} m$$

Table 5.5 Stress change over time in a brass substrate – In film system The final stress and strain states are also listed.

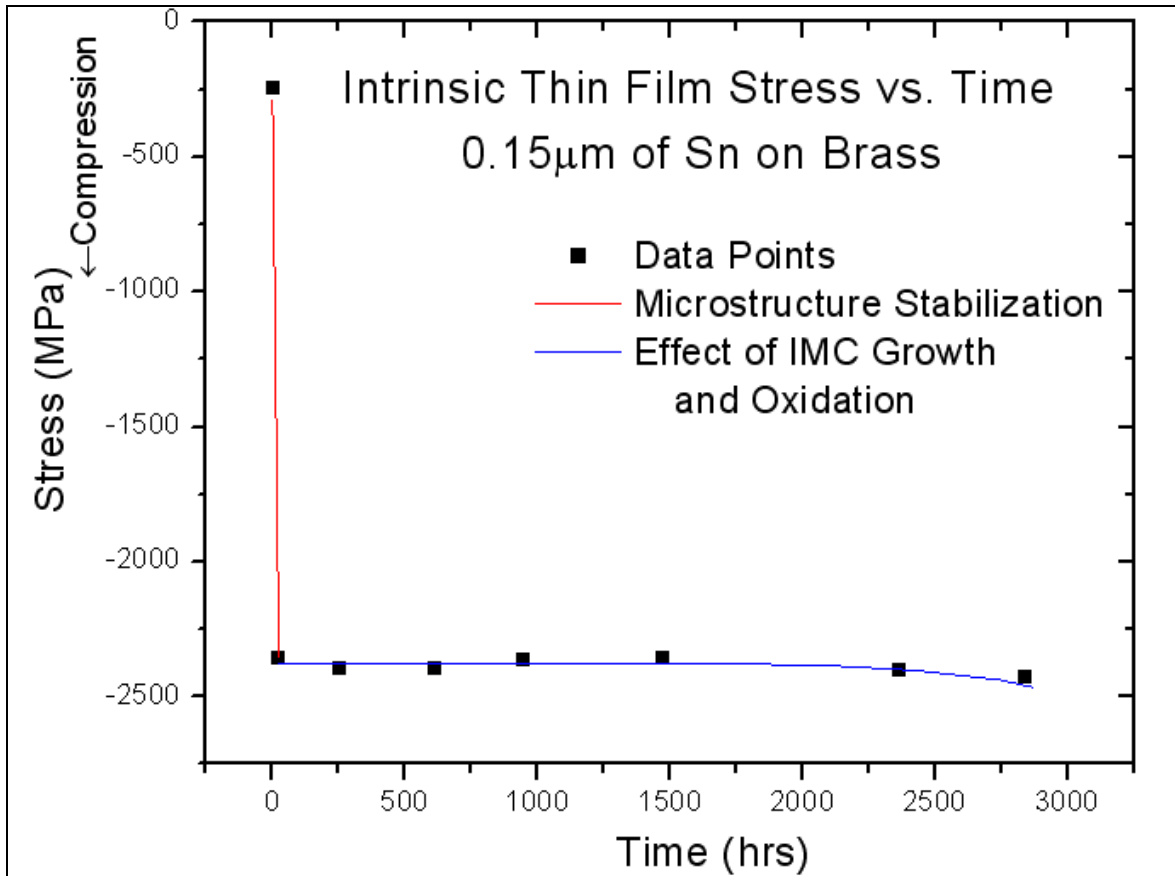


Using Equation A3.3.2, the stress from the CTE mismatch is calculated to be -4.19 MPa. The final stress and strain states within the film of the brass substrate – Sn (6000Å) film system are:

$$\sigma_{Ag} = \begin{pmatrix} -82.69 & 0 & 0 \\ 0 & -110.9 & 0 \\ 0 & 0 & -82.69 \end{pmatrix} MPa$$

$$\epsilon_{Ag} = \begin{pmatrix} -1.97 & 0 & 0 \\ 0 & -2.64 & 0 \\ 0 & 0 & -1.97 \end{pmatrix} m$$

Table 5.6 Stress change over time in a brass substrate – Sn (6000Å) film system. The final stress and strain states are also listed. This work verifies Thornton et al.'s [24] findings.

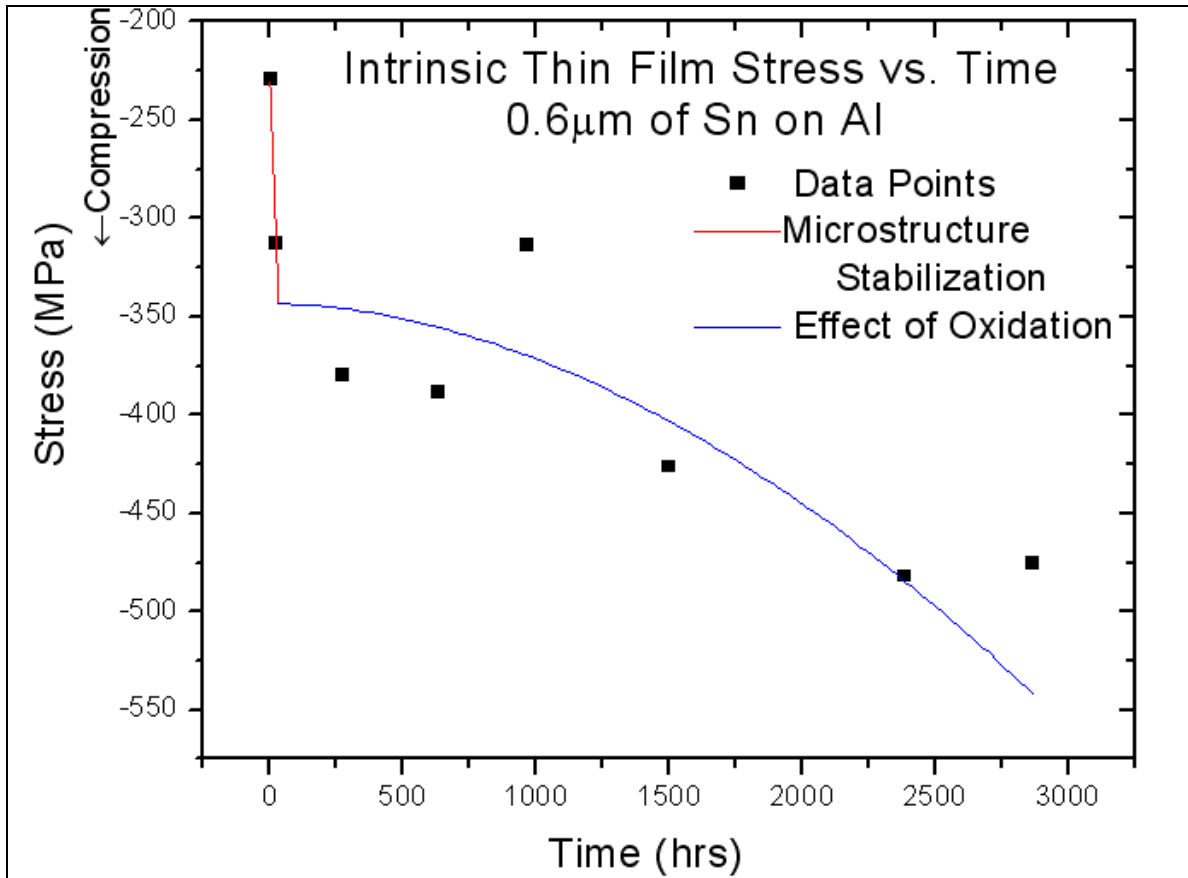


Using Equation A3.3.2, the stress from the CTE mismatch is calculated to be -4.19 MPa. The final stress and strain states within the film of the brass substrate – Sn (1500Å) film system are:

$$\sigma_{Ag} = \begin{pmatrix} -2492 & 0 & 0 \\ 0 & -2357 & 0 \\ 0 & 0 & -2492 \end{pmatrix} MPa$$

$$\epsilon_{Ag} = \begin{pmatrix} -59.3 & 0 & 0 \\ 0 & -56.1 & 0 \\ 0 & 0 & -59.3 \end{pmatrix} m$$

Table 5.7 Stress change over time in a brass substrate – Sn (1500Å) film system. The final stress and strain states are also listed. This work verifies Thornton et al.'s [24] findings.

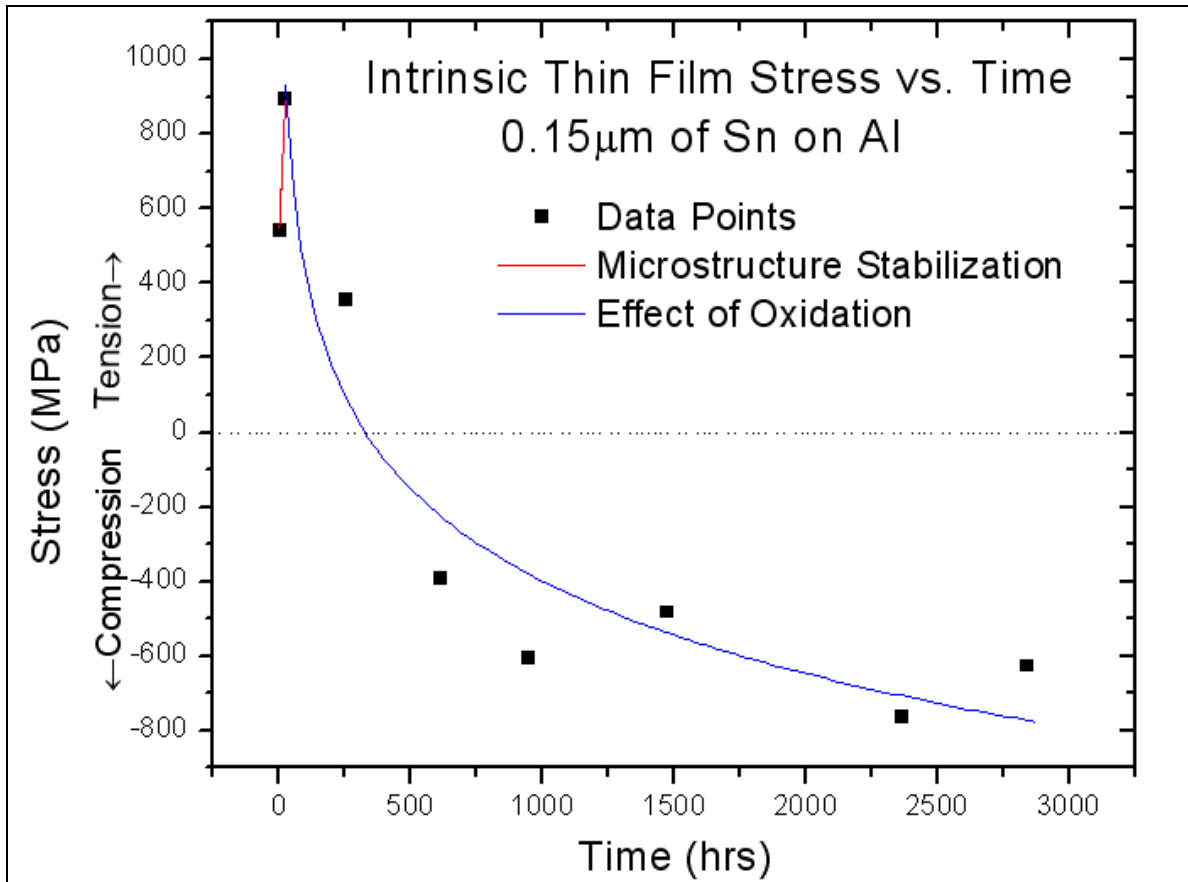


Using Equation A3.3.1, the stress from the CTE mismatch is calculated to be -0.62 MPa. The final stress and strain states within the film of the Al substrate – Sn (6000Å) film system are:

$$\sigma_{Ag} = \begin{pmatrix} -559.0 & 0 & 0 \\ 0 & -312.7 & 0 \\ 0 & 0 & -559.0 \end{pmatrix} MPa$$

$$\epsilon_{Ag} = \begin{pmatrix} -13.3 & 0 & 0 \\ 0 & -7.45 & 0 \\ 0 & 0 & -13.3 \end{pmatrix} m$$

Table 5.8 Stress change over time in a Al substrate – Sn (6000Å) film system. The final stress and strain states are also listed. This work verifies Thornton et al.'s [24] findings.



Using Equation A3.3.1, the stress from the CTE mismatch is calculated to be -0.62 MPa. The final stress and strain states within the film of the Al substrate – Sn (1500Å) film system are:

$$\sigma_{Ag} = \begin{pmatrix} -791.9 & 0 & 0 \\ 0 & 893.8 & 0 \\ 0 & 0 & -791.9 \end{pmatrix} MPa$$

$$\epsilon_{Ag} = \begin{pmatrix} -18.9 & 0 & 0 \\ 0 & 21.3 & 0 \\ 0 & 0 & -18.9 \end{pmatrix} m$$

Table 5.9 Stress change over time in a Al substrate – Sn (1500Å) film system. The final stress and strain states are also listed. This work verifies Thornton et al.'s [24] findings.

As a first attempt to quantify the total stress state in a thin film producing Sn whiskers, the data shown in tables 5.6, 5.8, and 5.9 coupled with the methods shown in Appendices 1-3 has been used to calculate the total stress state inside the film of the samples used in section 3.9 (where an external stress state has been applied). These stress states are presented in tables 5.10 - 5.12. The conjectured results show that the stress state is very different from the externally applied stress. In the two Al cases, the extrinsic stress is not even the dominant factor, as the intrinsic stress is over 150% more than the externally applied stress. Indeed, the σ_{xx} component never switched to the tensile state in either of the sets with Al substrates. The tables also show that even though the shear strain is small, it plays a significant role in the final stress state of the film. For instance, in the case of 1500Å of Sn on Al forced to conform to a 1” compressive curve, the intrinsic σ_{xx} component is -791.9 MPa and the externally applied σ_{xx} is -432.4 MPa, yet the total σ_{xx} is -1936 MPa (which does not equal -791.9 + -432.2). These components cannot be simply added because the shear strain γ_{xy} (imposed by the curvature) is coupled to σ_{xx} via the compliance matrix. This implies that 4 new plots, one for each of the non-zero stress components, are necessary for each set of data. However this new data only shifts and scales the x-axis, thus rendering 24 plots that look extremely similar to the plots already presented; for completeness the plots are provided in Appendix 5.

Total Stress State (MPa)	Population Density (cm⁻¹)	Average Length (μm)
$\begin{pmatrix} -670 & 509 & 0 \\ 509 & -539 & 0 \\ 0 & 0 & -518 \end{pmatrix}$	26.5	17.7
$\begin{pmatrix} -496 & 254 & 0 \\ 254 & -441 & 0 \\ 0 & 0 & -420 \end{pmatrix}$	2.4	19.3
$\begin{pmatrix} -438 & 169 & 0 \\ 169 & -408 & 0 \\ 0 & 0 & -387 \end{pmatrix}$	5.5	6.5
$\begin{pmatrix} -391 & 101 & 0 \\ 101 & -382 & 0 \\ 0 & 0 & -361 \end{pmatrix}$	16.7	7.4
$\begin{pmatrix} -253 & -101 & 0 \\ -101 & -304 & 0 \\ 0 & 0 & -283 \end{pmatrix}$	16.7	3.5
$\begin{pmatrix} -207 & -169 & 0 \\ -169 & -278 & 0 \\ 0 & 0 & -257 \end{pmatrix}$	2.4	1.0
$\begin{pmatrix} -149 & -253 & 0 \\ -253 & -246 & 0 \\ 0 & 0 & -225 \end{pmatrix}$	97.9	5.9
$\begin{pmatrix} 23 & -504 & 0 \\ -504 & -149 & 0 \\ 0 & 0 & -127 \end{pmatrix}$	26.5	10.1

Table 5.10 Whisker data for final stress states for 6000Å of Sn on Brass.

Total Stress State (MPa)	Population Density (cm⁻¹)	Average Length (μm)
$\begin{pmatrix} -2465 & 0.0010 & 0 \\ 0.0010 & -1977 & 0 \\ 0 & 0 & -2159 \end{pmatrix}$	389.4	32.8
$\begin{pmatrix} -2113 & 0.0005 & 0 \\ 0.0005 & -1779 & 0 \\ 0 & 0 & -1961 \end{pmatrix}$	6085.3	39.1
$\begin{pmatrix} -1997 & 0.0003 & 0 \\ 0.0003 & -1714 & 0 \\ 0 & 0 & -1895 \end{pmatrix}$	809.1	36.4
$\begin{pmatrix} -1904 & 0.0002 & 0 \\ 0.0002 & -1661 & 0 \\ 0 & 0 & -1843 \end{pmatrix}$	4207.1	13.2
$\begin{pmatrix} -1626 & -0.0002 & 0 \\ -0.0002 & -1505 & 0 \\ 0 & 0 & -1687 \end{pmatrix}$	358.3	8.8
$\begin{pmatrix} -1534 & -0.0003 & 0 \\ -0.0003 & -1454 & 0 \\ 0 & 0 & -1635 \end{pmatrix}$	1085.1	9.5
$\begin{pmatrix} -1419 & -0.0005 & 0 \\ -0.0005 & -1389 & 0 \\ 0 & 0 & -1570 \end{pmatrix}$	161.8	17.2
$\begin{pmatrix} -1078 & -0.0010 & 0 \\ -0.0010 & -1197 & 0 \\ 0 & 0 & -1378 \end{pmatrix}$	6287.3	8.9

Table 5.11 Whisker data for final stress states for 6000Å of Sn on Al.

Externally Applied Stress (MPa)	Population Density (cm⁻¹)	Average Length (μm)
$\begin{pmatrix} -1936 & 0.0003 & 0 \\ 0.0003 & -390 & 0 \\ 0 & 0 & -1629 \end{pmatrix}$	1206.6	14.7
$\begin{pmatrix} -1584 & 0.0001 & 0 \\ 0.0001 & -191 & 0 \\ 0 & 0 & -1431 \end{pmatrix}$	2294.8	46.4
$\begin{pmatrix} -1467 & 0.0001 & 0 \\ 0.0001 & -126 & 0 \\ 0 & 0 & -1365 \end{pmatrix}$	363.8	34.3
$\begin{pmatrix} -1374 & 0.0001 & 0 \\ 0.0001 & -73.4 & 0 \\ 0 & 0 & -1313 \end{pmatrix}$	669.1	15.0
$\begin{pmatrix} -1096 & 0.0001 & 0 \\ 0.0001 & 82.9 & 0 \\ 0 & 0 & -1157 \end{pmatrix}$	114.4	13.6
$\begin{pmatrix} -1004 & -0.0001 & 0 \\ -0.0001 & 135 & 0 \\ 0 & 0 & -1105 \end{pmatrix}$	1423.3	14.1
$\begin{pmatrix} -889 & -0.0001 & 0 \\ -0.0001 & 199 & 0 \\ 0 & 0 & -1040 \end{pmatrix}$	1045.0	11.8
$\begin{pmatrix} -547 & -0.0003 & 0 \\ -0.0003 & 392 & 0 \\ 0 & 0 & -848 \end{pmatrix}$	3169.4	16.6

Table 5.12 Whisker data for final stress states for 1500Å of Sn on Al.

5.3 A Multi-Media Time Elapsed Comparison of Whisker Growth, Intrinsic Stresses, and IMC Development

IMC growth is thought to be a function of time; it should therefore be possible to collect a sequence of SEM/ optical micrographs documenting this growth that can then be used to construct a time-elased movie of the formation of the IMC layer. Similarly, if stress is a function of time, then a high resolution camera can be used to record changes in the curvature of a bent beam experiment over time and the images used for a time-elased movie. The growth of a Sn whisker takes place over lengthy periods of time, so a movie showing the incubation, initiation and growth could be made using the same approach. Finally, a split-screen time-elased movie showing the simultaneous progress of these three key factors would clearly show any potential links that might affect the growth of a Sn whisker. Such a multi-media production offers a convenient way to view Sn whisker formation. Furthermore, such a tool would clearly show whether or not Sn whiskers actually relieve stress by monitoring the whiskers' growth and simultaneously witnessing the stress relieved, if any.

5.4 Do Alloyed Whiskers Exist?

There have been rumors in the research community that multi-element whiskers have been found, although no formal reports have yet been published in refereed journals. If such a whisker were found to be possible, this would cause new insight in the field and necessitate the rethinking of many of the existing theories of whisker formation. Using a eutectic combination of Sn and Pb in a sputter target, our group is in the process of attempting to grow a Sn-Pb whisker, using the new reliable whisker growth method developed for this study (Section 3.1).

5.5 Development of a Working Model of Whisker Incubation, Initiation, and Growth

Once all of these areas have been fully explored for Sn whiskers, it should be possible to develop a model that explains why and how a Sn (or any elemental) whisker develops. This end game theory must be firmly grounded both theoretically and experimentally, and must be able to account for the observations reported in Chapter 3.

5.6 Confirmation of Model Validity Using a Finite Element Method

Once a Sn whisker model has been established, a finite element model should be used to confirm its validity. Such a model may also be able to explain any similarities or discrepancies between the model and the movie described in Section 5.3.

REFERENCES

- [1] H.L. Cobb, "Cadmium whiskers," *Monthly Rev. Am. Electroplaters Soc.*, vol. 33, no 28, pp. 28-30, Jan. 1946
- [2] B.D. Dunn, "Mechanical and Electrical Characteristics of Tin Whiskers with Special Reference to Spacecraft Systems," *European Space Agency (ESA), Journal* vol 12, pp. 1-17, January 1988
- [3] J. Brusse, "A Discussion of Metal Whisker Formation to the High Reliability Community," *NASA/QSS Presentation*, November 2003, pp. 11
- [4] S.M. Arnold, "The growth of metal whiskers on electrical components," in *Proc. IEEE Electronic Components Technology Conf.*, 1959, pp.75-82
- [5] "Restriction of Hazardous Substances Directive", issued by the European Union. Available from <http://www.rohs.gov.uk>. Accessed 26 May, 2008
- [6] J. Suhling, "Electronics Packaging," course notes packet #6 pp. 33, packet #1 pp. 11, packet #4 pg 55, spring 2007
- [7] G.T. Galyon, "Annotated tin whisker bibliography and anthology," *IEEE Transactions On Electronics Packaging Manufacturing*, vol. 28, no1, Jan. 2005
- [8] M.H. Francombe and J.L. Vossen, "Physics of Thin Films; Contemporary Preparative Techniques," 1989, pp. 32-43
- [9] Q. Sun and G. Selvaduray, "Understanding and minimizing tin whiskers, a review of the literature," *San Jose State University Seminar*, June 2003
- [10] P. Martin, "Adhesion of thin films," *Vacuum Technology and Coating*, pp. 6-12, Feb. 2004
- [11] J. Smetana, "Theory of tin whisker growth: "the end game"," *iNEMI Tin Whisker Workshop at ECTC*, May 31, 2005
- [12] R.M. Fisher, L.S. Darke, and K.G. Carroll, "Accelerated growth of tin whiskers," *Acta Metallurgica*, vol.2 no. 3, pp. 368-372, May 1954
- [13] K.N. Tu, "Irreversible processes of spontaneous whisker growth in bimetallic Cu-Sn thin reactions," *Phys. Rev. B*, vol. 49, no3, pp. 2030-2034, Jan. 1994
- [14] E.N. Hoffman, M.W. Barsoum, W. Wang, R.E. Doherty, and A. Zavaliangos, "Driving force and mechanism for spontaneous metal whisker formation," *Phys. Rev. Let.*, vol. 93, no. 20, pp. 206104-1 – 206104-4, Nov. 2004

- [15] P. Su and M. Ding, "A finite element study of strain energy density distribution near a triple grain junction and its implication on whisker growth," iNEMI Sn Whisker Workshop, May 30, 2006
- [16] M.O. Peach, "Mechanism of growth of metal whiskers," J. Appl. Phys., vol. 23, no. 12, pp. 1401-1403, 1952. Letters to the editor.
- [17] B.Z. Lee and D.N. Lee, "Spontaneous growth mechanism of tin whiskers," Acta Mater. Vol. 46, No. 10, pp. 3701-3714, 1998
- [18] G. T. Galyon and L. Palmer, "An integrated theory of whisker formation: the physical metallurgy of whisker formation and the role of internal stresses," IEEE Transactions on Electronics packaging manufacturing, vol. 28, no. 1 Jan. 2005, pp. 17-29
- [19] K. Chen and G.D. Wilcox, "Observations of the spontaneous growth of tin whiskers on tin-manganese alloy electrodeposits," Physical Review Letters, PRL 94, pg. 066104, (2005), Feb. 18 2005
- [20] K.W. Moon, C.E. Johnson, M.E. Williams, O. Kongstein, G.R. Stafford, C.A. Handwerker, and W.J. Boettinger, "Observed correlation of Sn oxide film to Sn whisker growth in Sn-Cu electrodeposit for Pb-free solders," J. of Electronic Materials, vol. 34, no. 9, pg. L31-L33, 2005
- [21] M.W. Barsoum, E.N. Hoffman, R.D. Doherty, S. Gupta, and A. Zavaliangos, "Driving force and mechanism for spontaneous metal whisker formation," Physical Review Letters, vol. 93, no 20, pg. 206104, Nov. 12 2004
- [22] S. Lin, Y. Yorikado, J. Jiang, K. Kim, K.Suganuma, S. Chen, M. Tsujimoto, and I. Yanda, "Mechanical deformation-induced Sn whiskers growth on electroplated films in the advanced flexible electronic packaging," J. Mate. Re., vol.22, no. 7, pg. 1975-1986, July 2007
- [23] M. Takeuchi, K. Kamiyama, and K. Suganuma, "Suppression of tin whisker formation on fine pitch connectors by surface roughening," J. of Electronic Mater., vol. 35, no. 11, pg 1918-1925, 2006
- [24] J.A. Thornton, and D.W. Hoffman, "Internal stresses in titanium nickel, molybdenum, and tantalum films deposited by cylindrical magnetron sputtering," J. Vac. Sci. Tech., vol. 14, no. 1, Jan./ Feb. 1977 pg. 164-168
- [25] K.G. Compton, A. Mendizza, and S.M. Arnold, "Filamentary growths on metal surfaces – Whiskers," *Corrosion*, vol. 7, no 10, p. 327-334, Oct. 1951
- [26] W. J. Choi, T. Y. Lee, and K. N. Tu, "Structure and Kinetics of Sn Whisker Growth on Pb-free Solder Finish," *Proc. IEEE Elect. Comp. Technol. Conf.*, 2002, pp. 628-633
- [27] K. Fujiwara and R. Kawanaka, "Observation of the tin whisker by Micro-Auger Electron Spectroscopy," J. Appl. Phys. vol. 51, pp. 6231 (1980)
- [28] G.G. Stoney, "The tension of metallic films by electrolysis," Proceedings of the Royal Society of London, vol. 82, no. 553, pg 171-175, May 1909

- [29] T.W. Clyne, "Residual Stresses in Thick and Thin Surface Coatings," Encyclopedia of Materials: Science and Technology, section 4.1.3b, pg. 1-20, 2001
- [30] A. Brenner and S. Senderoff, "Calculation of stress in electrodeposits from the curvature of a plated strip," J. Res. Of Nat. Bur. of Stand., vol.42, (1949) pp.105-123.
- [31] R. W. Hoffman, "Physics of Thin Films," Academic Press Inc, vol. 3 pg. 211, 1966
- [32] R.C Hibbeler, "Mechanics of Materials" 6th Edition, Pearson Prentice Hall, 2005, pg. 291-298, 324-330, 373-386, 585-588, 796-802
- [33] R.G. Budynas, "Advanced Strength and Applied Stress Analysis" 2nd Edition, McGraw-Hill, 1999
- [34] Y. Hada, O. Morikawa, and H. Togami, "Study of tin whiskers on electromagnetic relay parts," in Proc. 26th annu. Relay Conf., Oklahoma State University, Stillwater, OK, April. 1978, pp. 9-1-9-15
- [35] M.Y. Chiang, C.K. Chiang, and W. Wu, "A technique for deducing in-plane modulus and coefficient of a supported thin film," Transactions of the ASME, vol. 124, pg. 274-277, April 2002
- [36] S. Amelinckx, W. Bontinck, W. Dekeyser, and F. Seitz, "On the formation and properties of helical dislocations," Phil. Mag., ser. 8, vol. 2, no. 15, pp. 355-377, Mar. 1957
- [37] R.W. Gedney, "Foreword Special Issue on Tin Whiskers," IEEE Transactions of Electronics Packaging Manufacturing, Vol. 28, No1, pg. 1, January 2005
- [38] E.N. Hoffman, M.W. Barsoum, W. Wang, R.D. Doherty, and A. Zavaliangos, "On the spontaneous growth of soft metallic whiskers," Electrical Contacts, 2005. Proceedings of the Fifty-First IEEE Holm Conference on , vol., no., pp. 121-126, 26-28 Sept. 2005
- [39] J.E. Flinn, J.C. Bae, T.F. Kelley, G.E. Korth, "Microstructure Stabilization in a Rapidly Solidified Stainless Steele," Metallurgical and Materials Transactions, Vol. 23, No. 9, Sept. 1992, pg. 2557-2565

APPENDIX 1 DERIVATION OF STRESS IN A THIN FILM

A1.1 Introduction

Stoney [28] did some of the earliest work in finding stress in a thin film-substrate system. Stoney's equation: $\sigma = \frac{4}{3} E \frac{(h^2 + t \cdot h) \Delta x}{t \cdot L^2}$ (E is the Young's modulus of the

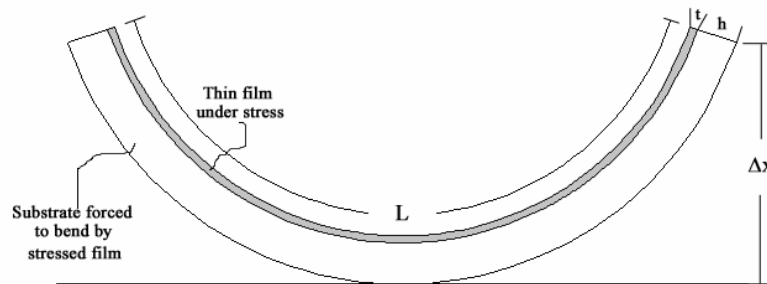


Figure A1.1 Shows an exaggerated bend in a substrate – thin film system and the measurements needed to find the stress in the film.

substrate, h , t , L , and Δx are identified in Figure A1.1) uses several approximations which provide an elegant equation suitable for hand calculations (Stoney's paper was published in 1909, well before computers were available to aid in the multiple tedious calculations required to analyze an experimental data set). A less elegant, but more exact equation is derived in this chapter of the appendix. The equations derived in the

sections below provide a more accurate solution especially in the extreme regimes that are set forth by the experiments discussed in this dissertation. Figures A1.2 - A1.3 show how the two equations compare in Stoney's regime and in the regime of the work presented in this paper.

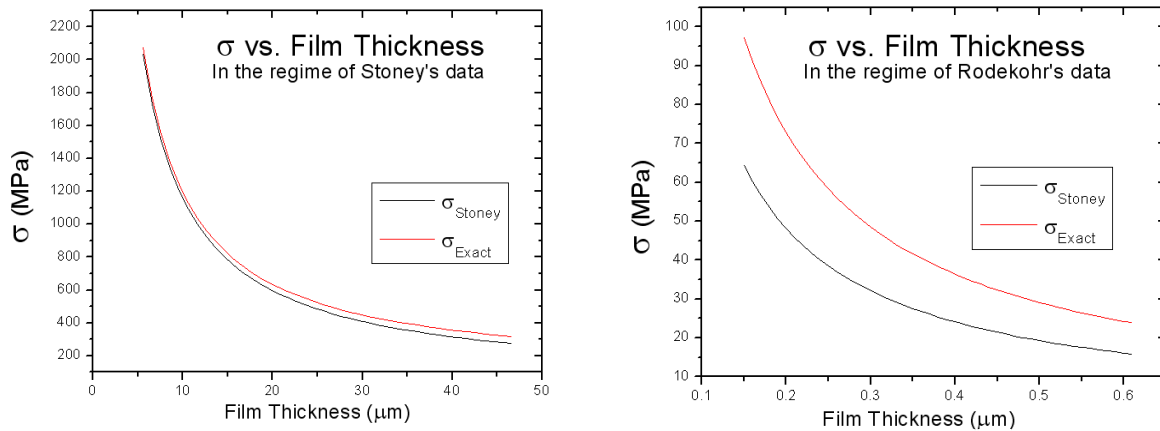


Figure A1.2 Difference between 'exact' stress (derived in this appendix) and Stoney's approximated stress in the film in the regime of Stoney's data where the maximum percent difference is 15% (left), while the maximum difference is 34% in the regime of the work presented here (right).

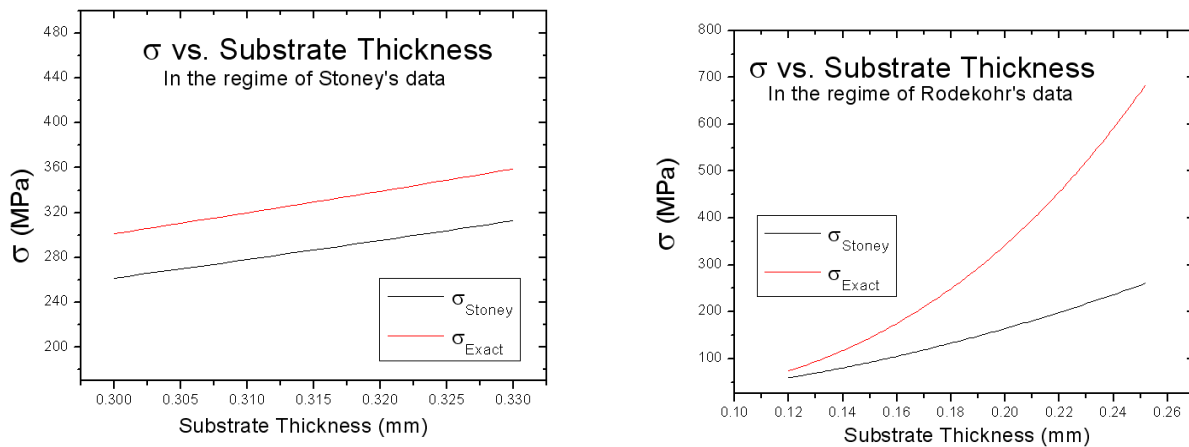


Figure A1.3 Difference between the 'exact' stress and Stoney's approximated stress in the substrate in the regime of Stoney's data, where the maximum percent difference is 13% (left), while it is 62% in the regime of the work presented here (right).

The purpose of Appendices 1-3 is to derive from first principles a ‘first attempt’ to find the total stress state of the film which produces the whiskers, and furthermore to relate that stress state to the various sources of stress which have been indicted as the culprits behind Sn whiskers by various researchers [15, 18, 20, 22, 24].

A1.2 Derivation of Intrinsic Stresses

The equations necessary to find the stress in a thin film adhered to a metallic substrate can be derived from basic mechanics of materials. Starting with a straight beam, one can identify an infinitesimally small distance ds which is displaced from the neutral axis a distance y .

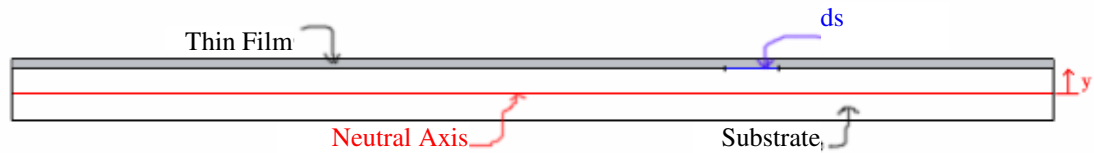


Figure A1.4 Thin film-substrate system that has not undergone bending.

That system can then be forced to conform to a curve (caused either by uniform internal stresses, external moments, or external shear forces), and the length of ds will change to ds' . If ρ (radius of curvature of the neutral axis) is known, then the strain in ds (which is parallel to the length of the sample) can be found:

From the definition of strain:

$$\varepsilon \equiv \lim_{\Delta s \rightarrow 0} \frac{\Delta s' - \Delta s}{\Delta s} = \frac{ds' - ds}{ds}.$$

Since

$$ds = \rho \cdot d\theta,$$

and

$$ds' = (\rho - y) \cdot d\theta \Rightarrow \varepsilon = \frac{\rho \cdot d\theta - y \cdot d\theta - \rho \cdot d\theta}{\rho \cdot d\theta} = \frac{-y}{\rho} .$$

$$\varepsilon = \frac{-y}{\rho} \quad \text{(Equation A1.2.1)}$$

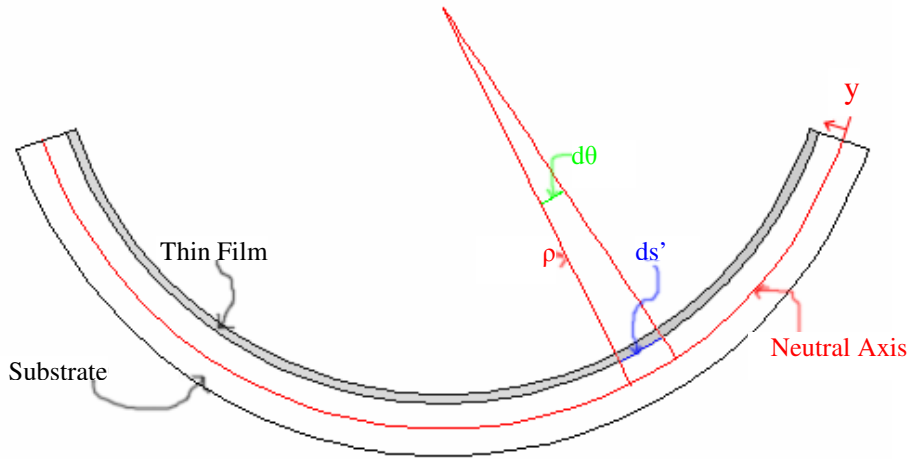


Figure A1.5 Thin film-substrate system that has undergone bending.

The neutral axis (the line where no strain is experienced during bending) is known to be the horizontal centroidal axis (\bar{y}) for a cross section of the width:

$$\bar{y} \equiv \frac{\int y \cdot da}{\int da} .$$

For a bi-metallic system:

$$\bar{y}_{system} = \frac{\sum (\bar{y}A)_i}{\sum A_i} = \frac{n\bar{y}_f A_f + \bar{y}_s A_s}{n \cdot A_f + A_s} = \frac{n \cdot t \cdot h + \frac{n \cdot t^2}{2} + \frac{h^2}{2}}{n \cdot t + h} = \frac{(t+h)(n \cdot t + h) + t \cdot h(n-1)}{2(n \cdot t + h)}$$

Which can also be written as:

$$\bar{y}_{system} = \frac{2 \cdot n \cdot t \cdot h + n \cdot t^2 + h^2}{2(n \cdot t + h)} ; \quad \text{(Equation A1.2.2)}$$

where the transformation factor $n \equiv \frac{E_f}{E_s}$ with E as the Young's Modulus of the film or substrate, and the cross section of the width (w) is shown in Figure A1.6.

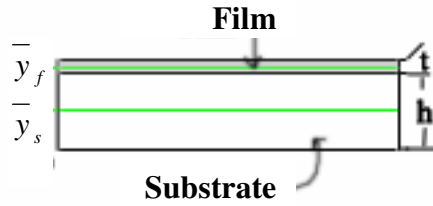


Figure A1.6 Cross section of a substrate – thin film system, viewed along the width. The film thickness t , substrate thickness h , film centroid \bar{y}_f , and substrate centroid \bar{y}_s are all shown.

We can now use Hooke's Law to find the stress at any location along y . This is the stress necessary to bend the system, so we will have to use the Young's modulus of the system:

$$\sigma = E_{system} \cdot \epsilon$$

$$\sigma = \frac{-E_{system} \cdot y}{\rho}; \quad (\text{Equation A1.2.3})$$

where the Young's modulus of the system is approximated via a weighted average:

$$E_{system} = \frac{E_f \cdot t + E_s \cdot h}{t + h}. \quad (\text{Equation A1.2.4})$$

It should be noted that equation A1.2.3 applies when neither the substrate nor the film have undergone expansion due to any intrinsic stress (or stresses). If there is an intrinsic stress in the film, then it will undergo expansion (or contraction). This

expansion will be limited by the substrate, and thus a classic statically indeterminate problem is created. Since the exact nature of the stress is not known, an alternate solution must be used to find the stress. Combining equation A1.2.3 with the famous Flexure Formula

$$\sigma = -\frac{My}{I},$$

one easily finds the Moment Curvature Relationship

$$\frac{1}{\rho} = \frac{M}{E_{system} \cdot I_{system}}.$$

Careful observation of equation A1.2.3 clearly shows gradient stress within the substrate – thin film system (ie. varies with y) as shown in figure A1.7.

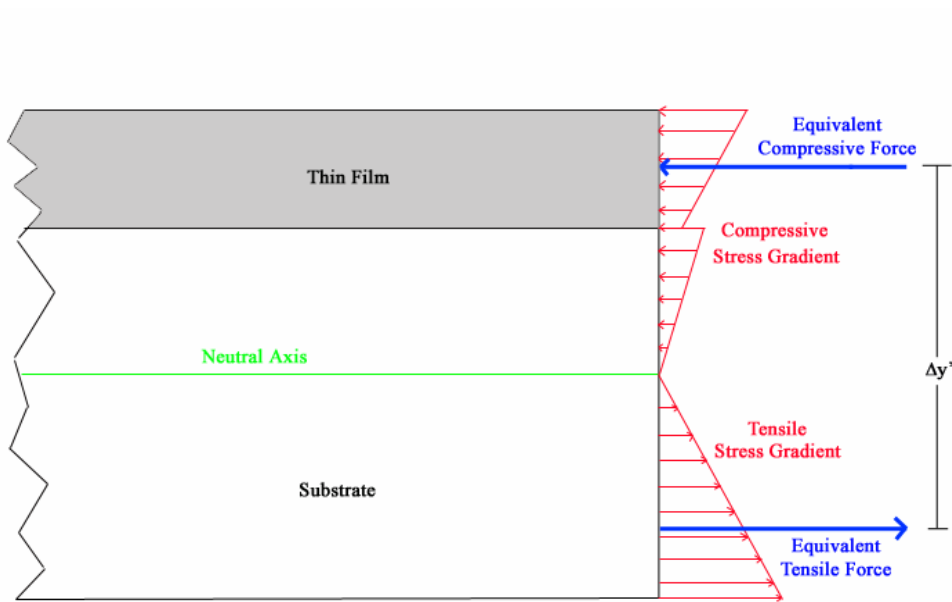


Figure A1.7 Stress gradients and equivalent forces associated with a substrate-thin film system that has undergone bending

The distributed stress gradient in the film can be expressed as a single equivalent force. However since the precise stress gradient is not known, the location where that equivalent force acts is unknown. Stoney and others have approximated this location to be at the centroid of the film, here we will make the same approximation. By Newton's 3rd law, the substrate has an equal and opposite force, however the location of this equivalent force is well known to be one third of the way to the centroid of the system. We can now define the moment which causes the system to bend:

$$M = F \cdot \Delta y'; \quad (\text{Equation A1.2.5})$$

where F is the equivalent force between the stressed film and substrate and $\Delta y'$ is defined in Figure A1.7 to be

$$\Delta y' \equiv \left(h + \frac{t}{2} \right) - \frac{1}{3} y_{system}.$$

This can be re-written in terms of the known quantities:

$$\Delta y' = \frac{2 \cdot E_f \cdot t \cdot (2h + t) + E_s \cdot h \cdot (5h + 3t)}{6(E_s \cdot h + E_f \cdot t)}. \quad (\text{Equation A1.2.6})$$

The bending moment of inertia of the system (I_{system}) can easily be found by using the parallel axis theorem and traditional methods:

$$I_{system} = \sum_i \frac{b_i \cdot h_i^3}{12} + A_i \cdot dy_i^2.$$

This can again be re-written in terms of the desired quantities:

$$I_{system} = \frac{(E_s^2 \cdot h^4 + E_f^2 \cdot t^4 + 2E_f \cdot E_s \cdot h \cdot t \cdot (2h^2 + 3h \cdot t + 2t^2)) \cdot w}{12E_s(E_s \cdot h + E_f \cdot t)}. \quad (\text{Equation A1.2.7})$$

Now the curvature of the neutral axis (ρ) must be written in terms of measurable quantities, namely t , h , and R which are defined in Figure A1.8 below.

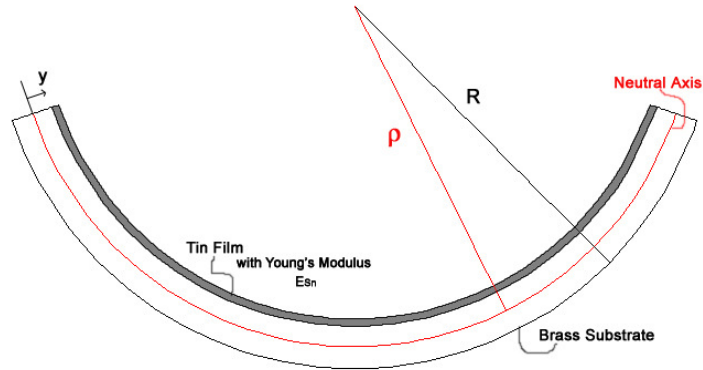


Figure A1.8 Substrate - thin film system with R and ρ labeled.

$$\rho = R - \bar{y}_{(t,h,n)} \quad (\text{Equation A1.2.8})$$

We can approximate R (the quick derivation is in Appendix A2) to be

$$R \cong \frac{L^2}{2(\Delta x + h)}$$

where Δx is the displacement due to bending identified in figure A3.1. Finally it must be noted that whatever intrinsic stress in the thin film is causing the system to bend is a bi-axial stress, in other words it is causing the system to bend in both planar directions. The stress along the width of the sample will have a Poisson effect on the length of the sample, thus there is an effective Young's Modulus:

$$\epsilon_x \cdot E = \sigma_x - \nu(\sigma_y + \sigma_z) = \sigma_x(1 - \nu) \Rightarrow \frac{\sigma_x}{\epsilon_x} = \frac{E}{(1 - \nu)} \equiv E'$$

This effective Young's Modulus is regularly used as a correction factor for substrate – thin film systems [29]. With this knowledge an effective Young's Modulus of the system can be approximated as:

$$E'_{system} = \frac{E_{system}}{(1-\nu_{system})}; \quad (\text{Equation A1.2.9})$$

where

$$\nu_{system} = \frac{\nu_f \cdot t + \nu_s \cdot h}{t + h}.$$

Combining equations A1.2.4 – A1.2.9, and the Moment Curvature Relationship, one can solve for the equivalent force. Since stress is force per area, the average stress in the film can be re-written in terms of the known and measurable quantities:

$$\sigma = \frac{F}{A_{film}} = \frac{E'_{system} \cdot I_{system}}{\rho \cdot A_{film}}$$

Which yields:

$\sigma =$

$$\frac{\left\{ (E_s \cdot h + E_f \cdot t)^2 [E_s^2 \cdot h^4 + E_f^2 \cdot t^4 + 2E_s \cdot E_f \cdot h \cdot t(2h^2 + 3h \cdot t + 2t^2)] \cdot (h + \Delta x) \right\}}{\left\{ E_s \cdot t [2E_f \cdot t(2h + t) + E_s \cdot h(5h + 3t)] [E_s \cdot h[h(h + \Delta x) - L^2] + E_f \cdot t[2(h + t)(h + \Delta x) - L^2]] \right\} \cdot [t(\nu_f - 1) + h(\nu_s - 1)]}$$

(Equation A1.2.10)

At this point, this first attempt derivation must become less general and move to the two specific cases in which R is measured differently depending on the direction of curvature, and measurement capabilities. These two specific cases are outlined in the following tables.

Intrinsic Tensile Stress in the Thin Film Forcing a Concave Curve on the System

R is measured to the outside edge of the curve, so equation A1.2.8:

$$\rho = R - \bar{y}$$

is used. Using equations A1.2.4 – A1.2.9, and the Moment Curvature Relationship will yield equation A1.2.10: $\sigma =$

$$\frac{\left\{ (E_s \cdot h + E_f \cdot t)^2 [E_s^2 \cdot h^4 + E_f^2 \cdot t^4 + 2E_s \cdot E_f \cdot h \cdot t(2h^2 + 3h \cdot t + 2t^2)] \cdot (h + \Delta x) \right\}}{\left\{ E_s \cdot t [2E_f \cdot t(2h + t) + E_s \cdot h(5h + 3t)] [E_s \cdot h[h(h + \Delta x) - L^2] + E_f \cdot t[2(h + t)(h + \Delta x) - L^2]] \right\} \cdot [t(\nu_f - 1) + h(\nu_s - 1)]}$$

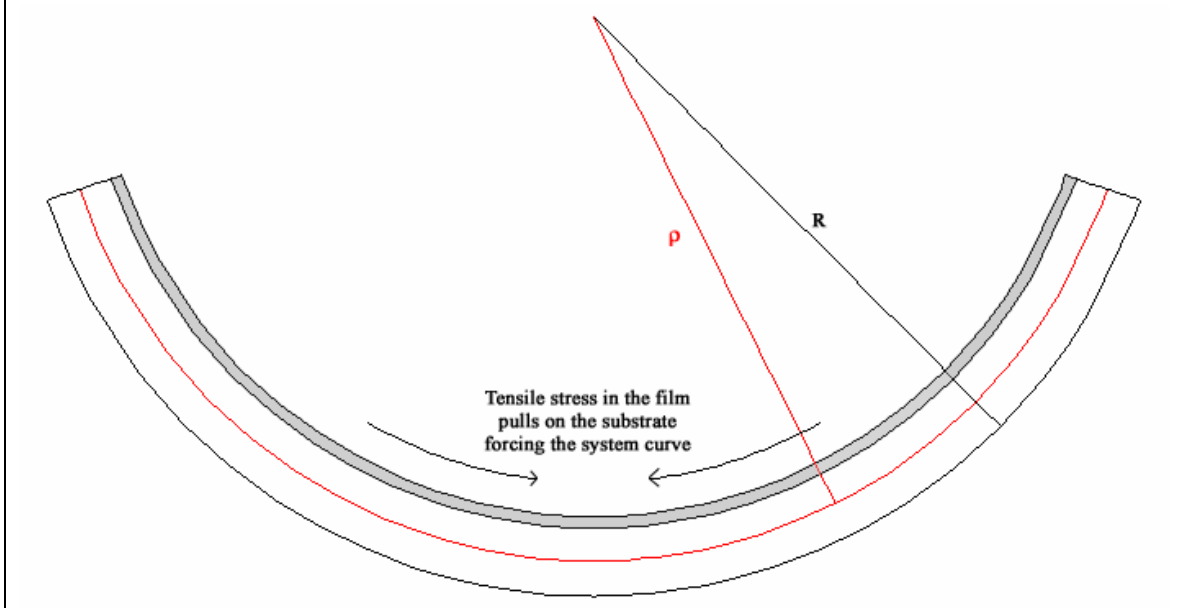


Table A1.1. Equations describing the effect of internal tensile stress(es) in a thin film force the system to conform to a concave curve.

Intrinsic Compressive Stress in the Thin Film Forcing Convex Curve on the System

In these cases R was measured from the outside of the curve which gives:

$$\rho = R - (t + h) + \bar{y}. \quad (\text{Equation A1.2.11})$$

Using equations A1.2.4 – A1.2.9, and the Moment Curvature Relationship will yield:

$\sigma =$

$$\frac{\left\{ (E_s \cdot h + E_f \cdot t)^2 [E_s^2 \cdot h^4 + E_f^2 \cdot t^4 + 2E_s \cdot E_f \cdot h \cdot t(2h^2 + 3h \cdot t + 2t^2)] \cdot (h + \Delta x) \right\}}{\left\{ E_s \cdot t [2E_f \cdot t(2h + t) + E_s \cdot h(5h + 3t)] [L^2 - E_f \cdot t(t(h + \Delta x)) + E_s \cdot h[L^2 - (h + 2t)(h + \Delta x)]] \right\} \cdot [t(\nu_f - 1) + h(\nu_s - 1)]}$$

(Equation A1.2.12)

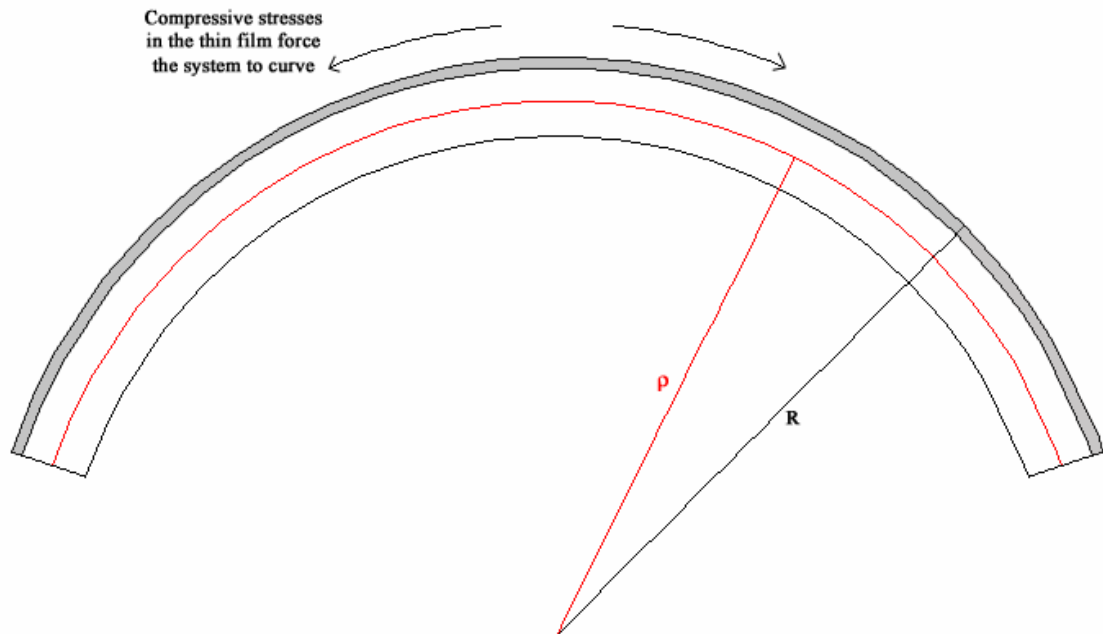


Table A1.2 Equations describing the effect of internal compressive stress(es) in the thin film that force the system to conform to a convex curve.

A1.3 Derivation of Externally Imposed Stresses

For the cases when a substrate – thin film system is forced by an external source to conform to a curve, the equations to find the stress in the film become much simpler, due to the fact that the problem is not statically indeterminate. Therefore one can begin with equation A1.2.1:

$$\varepsilon = \frac{-y}{\rho}.$$

To find the stress one must notice two things: 1) the stress is along the length of the sample only, so the effective Young's Modulus is not needed, and 2) we are only looking for the stress in the film, so we simply apply Hooke's Law to A1.2.1 and obtain:

$$\sigma = \frac{-E_f \cdot y}{\rho}. \quad (\text{Equation A1.3.1})$$

The distance from the neutral axis (y , which is shown in Figure A1.8) must now be written in terms of known and measurable quantities:

$$y = h - \bar{y} + x, \quad (\text{Equation A1.3.2})$$

where x is any additional distance into the film beyond substrate – thin film interface.

Like the intrinsic stresses, ρ is closely tied to the value of R (the radius of curvature at the outside of the curve beam), but in this case R is well known.

Upon inspection one can easily verify that equation A1.3.1 can be found from the Flexure Formula

$$\sigma = -\frac{My}{I}$$

and the Moment Curvature Relationship

$$\frac{1}{\rho} = \frac{M}{E_{system} \cdot I_{system}}.$$

By similar inspection, the shear stress (τ) can be found:

$$\tau = \frac{E_{system} \cdot Q}{\rho \cdot L \cdot w} \quad \text{(Equation A1.3.3)}$$

by comparing The Shear Formula:

$$\tau = \frac{V \cdot Q}{I \cdot w},$$

the Moment Curvature Relationship, and by noting that:

$$V = \frac{dM}{dx} = \frac{M}{L}$$

if M is uniform along the length of the sample. In equation A1.3.3, Q is the first moment of the area (A') above y (as defined in figure A1.3.1)

$$Q \equiv \int_{A'} y \cdot dA.$$

For the case of finding the shear stress at the interface between the substrate and the film becomes

$$Q = y'_{film} \cdot A'_{film}.$$

When this is put into terms of known and measurable quantities, it can be written as:

$$Q = \left[\left(h - \bar{y}_{system} \right) + \frac{t}{2} \right] \cdot \left(\frac{E_f}{E_s} \cdot t \cdot w \right).$$

Q is shown in figure A1.9.

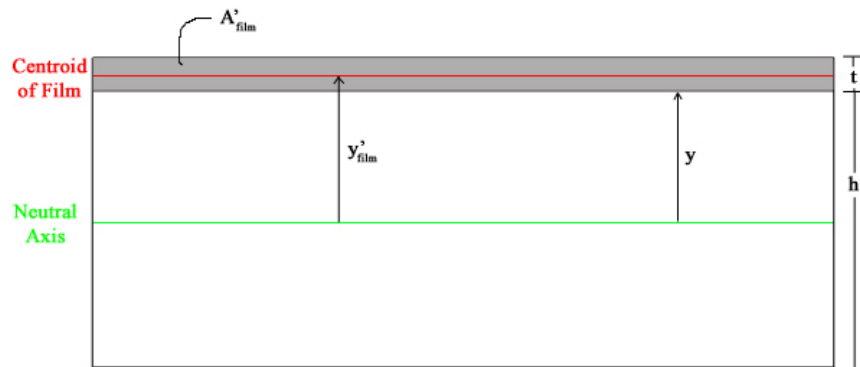


Figure A1.9 Dimensions needed to determine Q of the film at the interface between the film and the substrate.

As with the intrinsic stress, we must now break this down into compressive stress and tensile stress to actually obtain the equations of stress. These equations of known and measurable quantities are shown in the following two tables. It should be noted that R is measured directly from the curve around which the samples were forced to conform, so R is not approximated nor is it a function of Δx as it was in the intrinsic stress cases (see Appendix 4 for precise values of R).

External Source Forcing a Compressive Stress in the Thin Film

R is measured to the outside edge, this yields:

$$\rho = R - \bar{y}. \quad (\text{Equation: A1.3.5})$$

This combined with equations A1.3.1, A1.3.2, A1.2.2, and A1.2.4 yields:

$$\sigma = \frac{E_f (E_f \cdot t(t-2x) - E_s \cdot h(h+2x))}{E_f \cdot t(2R-t-2h) + E_s \cdot h(2R-h)}. \quad (\text{Equation A1.3.6})$$

Also combining A1.2.2, A1.2.4, A1.3.4, and A1.3.5 yields:

$$\tau = \frac{E_f \cdot h \cdot t \cdot (E_s \cdot h + E_f \cdot t)}{L \cdot [E_s \cdot h \cdot (2R-h) + E_f \cdot t \cdot (2R-2h-t)]}. \quad (\text{Equation A1.3.7})$$

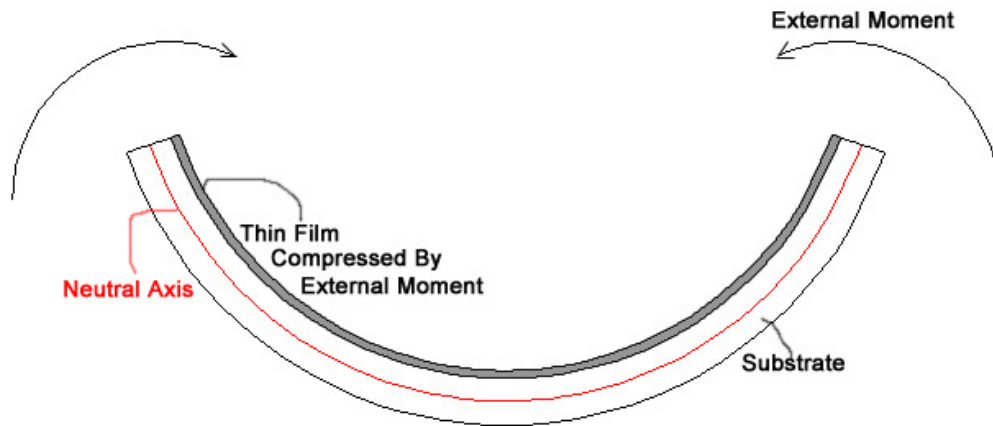


Table A1.3 Equations describing the normal and shear stress that arise when an external source is used to force a compressive stress state in the thin film.

External Source Forcing a Tensile Stress in the Thin Film

In these cases, R is measured based on the inside curve, yielding:

$$\rho = R + \bar{y}. \quad (\text{Equation A1.3.8})$$

Using this and equations A1.3.1, A1.3.2, A1.2.2, A1.2.4 the definition of n, and the fact that this stress must be in the tensile stress state will yield:

$$\sigma = \frac{E_f (E_f \cdot t(2x-t) + E_s \cdot h(h+2x))}{E_f \cdot t(2R+2h+t) + E_s \cdot h(2R+h)}. \quad (\text{Equation A1.3.9})$$

Also combining A1.2.2, A1.2.4, A1.3.4, and A1.3.8 yields:

$$\tau = \frac{E_f \cdot h \cdot t \cdot (E_s \cdot h + E_f \cdot t)}{L \cdot [E_s \cdot h \cdot (h-2R) + E_f \cdot t \cdot (2h-2R+t)]}. \quad (\text{Equation A1.3.10})$$

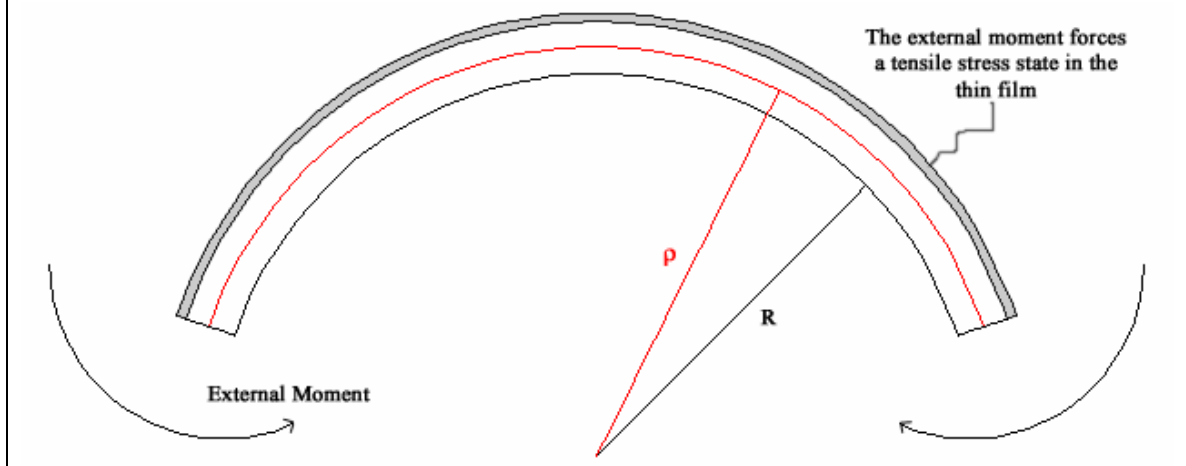


Table A1.4 Equations describing the effect of an external moment applied to force a tensile stress state in the thin film.

APPENDIX 2 DERIVATION AND JUSTIFICATION OF THE RADIUS OF CURVATURE FROM A MEASURED DISPLACEMENT

Since R is well known in the extrinsic stress study (Section 3.9), this derivation is only necessary for the intrinsic stress study described in Section 5.2. When one leaf is

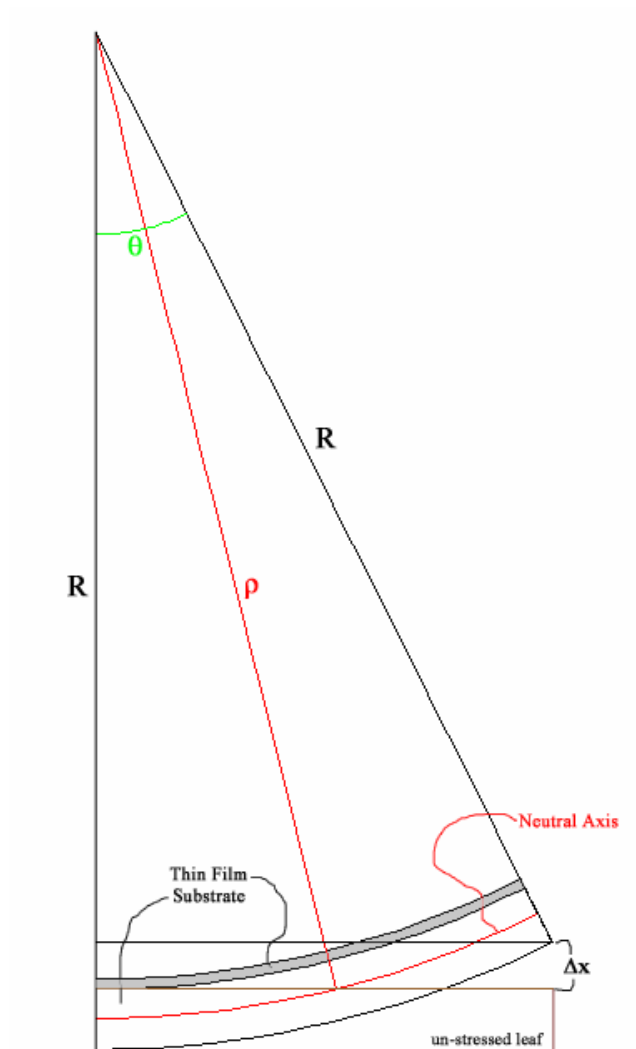


Figure A2.1 Measurement of Δx relative to each leaf of the samples.

stressed, it will conform to a curve and its tip will be displaced from the un-stressed leaf a distance Δx .

From this displacement, the radius of curvature R can be calculated. Starting with the arc length formula,

$$L = R\theta \Rightarrow \theta = \frac{L}{R},$$

where L is the length (or arc length) of a leaf. Also, basic trigonometry says:

$$\text{Cos}(\theta) = \frac{R - (\Delta x + h)}{R};$$

where h is the thickness of the substrate. Combining these two equations yields:

$$\text{Cos}\left(\frac{L}{R}\right) = \frac{R - (\Delta x + h)}{R}. \quad (\text{Equation A2.1})$$

Directly solving equation A2.1 for R as a function of L and Δx is not algebraically possible. The solution to this equation must be solved numerically using computer software (Mathematica was used for table A2.1) or one can assume that $R \gg L$ and a small angle approximation (valid when $\theta \approx < 20^\circ$) can be made (ie. $\text{Cos}(\theta) \cong 1 - \frac{\theta^2}{2}$, which are the first two terms from Taylor's expansion of $\text{Cos}(\theta)$).

If the small angle approximation is made, then R can be solved for:

$$1 - \frac{\left(\frac{L}{R}\right)^2}{2} \cong \frac{R - (\Delta x + h)}{R} \Rightarrow 1 \cong \frac{R - (\Delta x + h)}{R} + \frac{L^2}{2R^2} \Rightarrow R^2 \cong R^2 - R(\Delta x + h) + \frac{L^2}{2} \Rightarrow$$

$$R \cong \frac{L^2}{2(\Delta x + h)}. \quad (\text{Equation A2.1})$$

To show the validity of this approximation, it needs to be shown that R is indeed much greater than L. Table A2.1 shows the validity of this approximation for the two extreme (smallest and largest) measured values of Δx .

Δx (m)	h (m)	L (m)	Low end Numerical Solution of R (m)	High End Numerical Solution of R (m)	Approximate solution of R (m)	Ratio of S to R (θ in radians)	Percent Error (%)
2.032×10^{-5}	1.25×10^{-4}	0.09	27.87	27.87	27.87	3.229×10^{-3}	6.882×10^{-4}
1.201×10^{-2}	1.25×10^{-4}	0.09	0.3316	0.3316	0.3336	2.700×10^{-1}	6.162×10^{-1}

Table A2.1 Extreme measured values of Δx . This table shows that the small angle approximation is valid for this experiment, as the largest angle is 0.27 radians (or 15°). This is reasonable as the worst percentage error is 0.6% (i.e. ± 2 mm). Notice that Δx was measured to ± 0.0025 mm (± 0.0001 inches), so all the values in this chart have 4 significant figures.

APPENDIX 3 A DISCUSSION ON THE ORIGINS OF FILM STRESS

A3.1 Introduction

The stress discussed so far in Appendices 1 and 2 apply to bent beam systems. Appendix 3 will attempt to distinguish (as much as possible) the seven different types of stress sources as mentioned throughout this paper and by various Sn whisker authors. The only necessary information for this distinction is a plot of stress vs. time. The plots in this paper were obtained via bent beam analysis, however there are other more accurate methods to obtain such plots. The goal of this appendix is to: 1) show that intrinsic stresses play a very significant and complicated role in the internal stress state of a thin film, 2) show that the entire stress state (not just one of the 9 components) needs to be considered when discussing whisker motivation, and 3) to shed some light on the results of section 3.9. It should also be noted that the discussion of this appendix makes several approximations, and only yields 'ball-park' solutions.

It is possible for any combination of the seven stress sources to be influencing the total stress state at any point in time. Furthermore some of the stress sources are functions of time, and thus have a varying effect on the total stress state of the film. Some of the stresses act differently than others (i.e. some are normal to the surface, some are tangential to the surface, and some are shear stresses). If the stress of interest can be safely approximated as uniform, then a direct summation with stresses from other uniform sources is possible.

Seven potential sources of stress in the substrate – thin film systems are as follows: 1) atomic peening, 2) differences coefficient of thermal expansion (CTE) mismatch between the substrate and the film, 3) microstructure stabilization, 4) oxidation on the surface, 5) oxidation within the grain boundaries, 6) non-uniform IMC development, and finally 7) any externally applied forces or moments. Before detailed descriptions of these stresses can be made, it is necessary to first define the elements of our stress state. Here we will use the standard Cartesian notation of stress:

$$\underline{\underline{\sigma}} = \begin{pmatrix} \sigma_{xx} & \sigma_{xy} & \sigma_{xz} \\ \sigma_{yx} & \sigma_{yy} & \sigma_{yz} \\ \sigma_{zx} & \sigma_{zy} & \sigma_{zz} \end{pmatrix},$$

where x is in the lengthwise direction of the sample, y is in the direction which is normal to the surface of the film, and z parallel to the width of the film (as shown in figure A3.1).

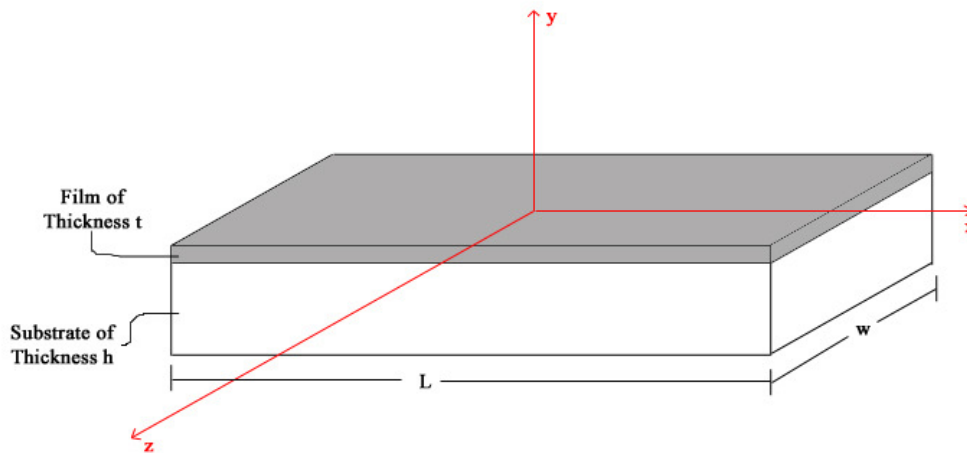


Figure A3.1 Definition of Cartesian Coordinate system used for samples in this study.

Because of shear strain coupling to normal stresses within the compliance matrix, it is best to discuss the strains (as opposed to discussing the stresses) whenever

shears are involved (such as in the case of externally applied forces). Then Hooke's law can be applied to find the total stress state.

A3.2 Atomic Peening

The first stress introduced to a sample in a sputtering process is due to atomic peening. Atomic peening may also occur in electroplating; indeed this may be the primary factor influencing Lee and Lee's [17] study of stress as a function of voltage. Although stress from atomic peening in sputtering has been experimentally observed to be roughly proportional to the square root of the film's atomic mass [24], there is currently no analytical method for determining this stress. The value of this stress can only be found by experimentally measuring the *initial* stress state of a system and subtracting out the stress caused by the CTE mismatch. Due to crystallographic symmetry, the stress from atomic peening is approximated to cause equal stresses in the normal and both tangential directions, ie.:

$$\sigma_{Peening} = \begin{pmatrix} \sigma_{exp} & 0 & 0 \\ 0 & \sigma_{exp} & 0 \\ 0 & 0 & \sigma_{exp} \end{pmatrix}; \quad (\text{Equation A3.2.1})$$

where 'exp' stands for 'experimentally determined.'

A3.3 Coefficient of Thermal Expansion Mismatch

Stresses caused by differences in the CTE between the substrate and the film can be calculated if the following assumptions are made: 1) perfect adhesion is made between the film and the substrate, and 2) the film does not crack to relieve the stress. We will assume both of these assumptions in order to find a solution, however they may not be safe assumptions. Once these assumptions are made, stress determination

becomes an elementary statically indeterminate problem. It can be solved upon making the following two observations: 1) the force of the film on the substrate is equal to the force of the substrate on the film

$$F_f = F_s$$

(which is Newton's 3rd law), and 2) the total change in length (δ) of the film (caused by both F_s and ΔT) is equal to the total change in length of the substrate. This can be written in equation form as:

$$(\delta_f)_{\Delta T} \pm (\delta_f)_{F_s} = (\delta_s)_{\Delta T} \mp (\delta_s)_{F_f};$$

where the top signs are chosen if the substrate has the greater coefficient of thermal expansion

$$\alpha_s > \alpha_f.$$

The expansion due to change in temperature can be found by:

$$\delta_{\Delta T} = L \cdot \alpha \cdot \Delta T,$$

where L is the original length and α is the coefficient of thermal expansion. The expansion due to the approximately axial force is:

$$\delta_F = \frac{F \cdot L}{A \cdot E};$$

where F is the applied force, A is the cross sectional area and E is the Young's Modulus.

All of these equations can be combined to find the stress in the film due to the CTE mismatch:

$$L \cdot \alpha_f \cdot \Delta T \pm \frac{F_s \cdot L}{t \cdot w \cdot E_f} = L \cdot \alpha_s \cdot \Delta T \mp \frac{F_f \cdot L}{h \cdot w \cdot E_s} \Rightarrow$$

$$F_s = F_f = F = \frac{h \cdot t \cdot E_s \cdot E_f \cdot L \cdot \Delta T (\mp \alpha_f \pm \alpha_s)}{t \cdot E_f + h \cdot E_s}$$

Since

$$\sigma \equiv \frac{F}{A} \Rightarrow \sigma_f = \frac{F}{t \cdot w} = \frac{h \cdot E_s \cdot E_f \cdot \Delta T (\mp \alpha_f \pm \alpha_s)}{t \cdot E_f + h \cdot E_s};$$

for simplicity this equation can be broken into two equations:

for the cases when $\alpha_s > \alpha_f$;

$$\sigma_f = \frac{h \cdot E_s \cdot E_f \cdot \Delta T (\alpha_s - \alpha_f)}{t \cdot E_f + h \cdot E_s}, \quad (\text{equation A3.3.1})$$

and for the cases when $\alpha_f > \alpha_s$;

$$\sigma_f = \frac{h \cdot E_s \cdot E_f \cdot \Delta T (\alpha_f - \alpha_s)}{t \cdot E_f + h \cdot E_s}. \quad (\text{equation A3.3.2})$$

Thermal expansion occurs in all three dimensions, but is only resisted by the substrate in the x and z directions, thus equations A3.3.1 and A3.3.2 apply to the σ_{xx} and σ_{zz} components only. These equations can be written in terms of strain by simply dividing out the Young's Modulus of the film. Although there is expansion in the y direction and thus there is a ε_{yy} component (found by:

$$\varepsilon_{yy} = \alpha_f \cdot \Delta T),$$

it is free expansion, so there is no resulting stress. At this point the stress state of a substrate – thin film system due to CTE mismatch can be written as:

$$(\sigma_f)_{CTE} = \begin{pmatrix} \frac{h \cdot E_s \cdot E_f \cdot \Delta T (\mp \alpha_f \pm \alpha_s)}{t \cdot E_f + h \cdot E_s} & 0 & 0 \\ 0 & 0 & 0 \\ 0 & 0 & \frac{h \cdot E_s \cdot E_f \cdot \Delta T (\mp \alpha_f \pm \alpha_s)}{t \cdot E_f + h \cdot E_s} \end{pmatrix}$$

(Equation A3.3.3)

One should observe that the effects of CTE mismatch occur as soon as the temperature changes. For the purposes of this study, we have assumed that the CTE and Young's Modulus do not change over time as Chiang et al.'s [30] study may indicate. To gain a better understanding of how stress interacts with whiskers, a full understanding of the time dependence of the CTE mismatch must be acquired, however that concept is beyond the scope of this study.

A3.4 Microstructure Stabilization

Little is known about microstructure stabilization [39], although it is commonly accepted that basic material data such as creep, Young's Modulus and even the overall appearance of the microstructure are affected by the phenomena. This effect occurs as the atoms within the recently sputtered film move to vacant locations in the atomic lattice to lower the potential energy of the film. The results of this stabilization are dramatic, but occur over a relatively short time period after sputtering. Again there is no analytical method for determining these stresses: they must be measured experimentally and are assumed (for simplicity) to be crystallographically symmetrical. The stress state due to microstructure stabilization is:

$$\sigma_{stabilization} = \begin{pmatrix} \sigma_{exp} & 0 & 0 \\ 0 & \sigma_{exp} & 0 \\ 0 & 0 & \sigma_{exp} \end{pmatrix}. \quad (\text{Equation A3.4.1})$$

A3.5 Surface Oxidation

As oxygen from our planet's atmosphere interacts with the film, an oxidation layer builds on the surface of the film. Little is known about the magnitude of the resulting stress (if one exists at all). To our knowledge, there is no analytical method to determine this stress, and the bent beam method cannot measure its effects. It will not be considered in this study.

A3.6 Oxidation Within the Grain Boundaries

Isometric expansion of the film that results due to oxygen seeping into the grain boundaries and forming an oxide within the film is a stress which has been investigated by Barsoum et al.[21]. In that study they approximated an analytical method for determining this stress at the atomic level, and used this method to run a finite element analysis (FEA) of such a stress. Despite this excellent work, there is no analytical method for determining this stress on a macroscopic level; thus, it must be determined experimentally. This stress state is time dependent as the oxidized atoms develop slowly over a long time period. This stress state can only act bi-axially, and is outlined by

$$\sigma_{Oxydation} = \begin{pmatrix} \sigma_{exp} & 0 & 0 \\ 0 & 0 & 0 \\ 0 & 0 & \sigma_{exp} \end{pmatrix}. \quad (\text{Equation A3.6.1})$$

A3.7 Intermetallic Development

Galyon and Palmer [18] hypothesized that non-uniform development of the IMC layer creates a tangential stress in the film which in turn forces the whisker growth. It should be noted that IMC growth is non-uniform in all three directions (x, y, and z), thus there will be local σ_{yy} components (neglected by Galyon and Palmer). It is the view of

this author that the σ_{yy} cannot be neglected in the study of whisker development. However, this component (which is not crystallographically symmetric) cannot be accounted for either analytically or by the bent beam experimental method, thus by necessity it will be neglected in this study as well. Although uneven IMC development happens on a local level and creates local stress gradients, the bent beam method can be used to find the average bi-axial stress caused IMC growth.

$$\sigma_{IMC} = \begin{pmatrix} \sigma_{exp} & 0 & 0 \\ 0 & 0 & 0 \\ 0 & 0 & \sigma_{exp} \end{pmatrix}. \quad (\text{Equation A3.7.1})$$

A3.8 Externally Applied Stress

Stresses can be externally applied in a myriad of ways. These stresses can usually be measured via strain gauges or some known force, or in some cases can be determined analytically. The stress state from these sources can effect any of the 9 components.

$$\sigma_{IMC} = \begin{pmatrix} \sigma_m^1 & \sigma_m^4 & \sigma_m^5 \\ \sigma_m^4 & \sigma_m^2 & \sigma_m^6 \\ \sigma_m^5 & \sigma_m^6 & \sigma_m^3 \end{pmatrix}, \quad (\text{Equation A3.8.1})$$

where the subscript m stands for measured, and the superscript indicates the 6 independent elements.

A3.9 Intrinsic Stress State

All of the sources of stress described in sections A3.2-A3.7 are collectively known as ‘intrinsic stress’. It is this intrinsic stress which can be measured with the bent beam method described in Section 5.2. The bent beam method measures the σ_{xx}

component of intrinsic stress exclusively. Once the σ_{xx} component is known, one can extrapolate to the other components based on knowledge of the source stress. To distinguish how much each source contributes to the total stress state, a careful analysis of the stress as a function of time must be undertaken. To illustrate this process we will now consider the case where 1500Å of Sn have been deposited onto a 0.25 mm thick strip of Al. The basic material data for all the materials used in this paper are listed in Table A3.1, the data needed for this example are highlighted. A plot of the σ_{xx} stress as a function of time which was measured by our bent beam method for the case of 1500Å of Sn on Al is shown in figure A3.2.

Material	Young's modulus (Gpa)	Poisson's Ratio	CTE (α) (parts/million.°C)	Sputter Temperature (°C)
Sn	42	0.36	23.0	58
Ag	80	0.37	18.9	75
Cu	124	0.34	16.9	Not Sputtered
In	11	0.45	32.1	40
Zn	108	0.25	30.2	~60
Cd	50	0.3	30.8	38
Brass	103	0.34	20.3	Not Sputtered
Al	70	0.35	23.4	Not Sputtered

Table A3.1 Characteristics of materials used in this study. Sn and Al are highlighted because they are used in the example

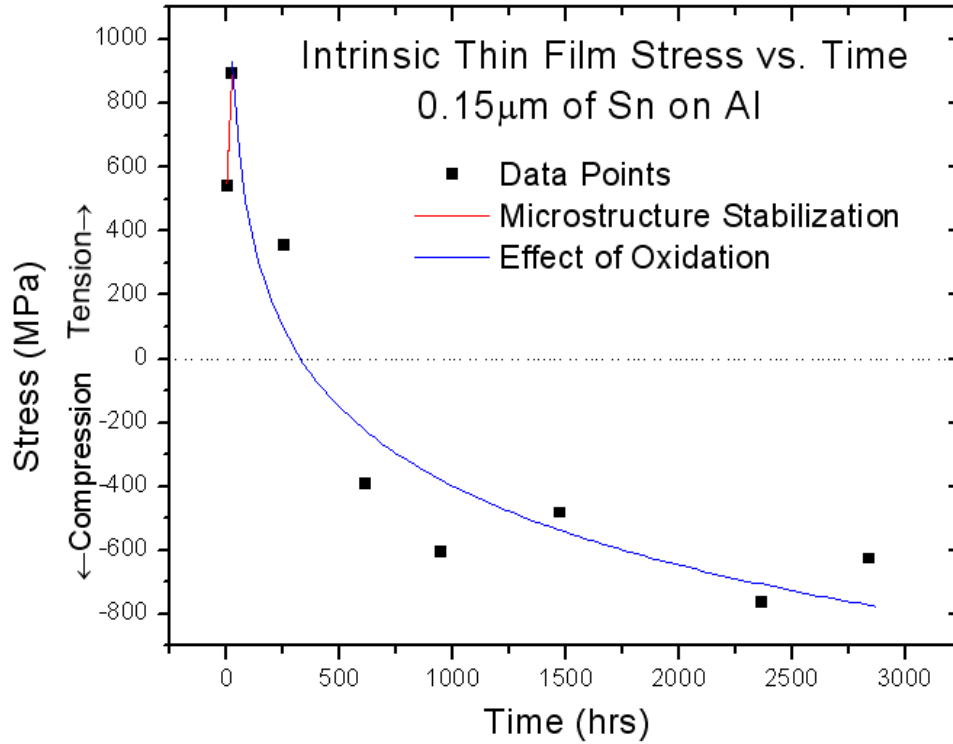


Figure A3.2 The σ_{xx} component of intrinsic stress as a function of time in 1500Å of Sn on an aluminum substrate.

If there were no intrinsic stresses, then the stress as a function of time would be on top of the horizontal dashed line in the middle of the plot. The first point indicates the σ_{xx} component of stress measured in the first 30 minutes. This point is nonzero due to atomic peening and CTE mismatch. The substrate warmed to a temperature of 58°C during the sputtering process, and room temperature is 21 °C. Using equation A3.3.1 (because $\alpha_s > \alpha_f$), the stress due to CTE mismatch is calculated to be -0.62 MPa. The initial stress point is observed to be 541.83 MPa, thus the stress due to atomic peening (at 2 mTorr Ar pressure) when 1500Å of Sn are deposited must be 542.45 MPa;

$$\sigma_{Peening} + \sigma_{CTE} = \sigma_{initial} \Rightarrow \sigma_{Peening} = \sigma_{initial} - \sigma_{CTE}.$$

This result is contrary to the prediction of Thornton and Hoffman^[26], although that study was probably looking at the final stress state rather than isolating the effects of atomic peening, as in this analysis. If one only considers the final stress state (as Thornton and Hoffman probably did), our results concur with theirs.

The effects of microstructure stabilization can be noted by the red line in Figure A3.2. The equation for this line fully describes the effects of microstructure stabilization. In this case the effects of microstructure stabilization continue the trend of atomic peening, and make the stress state more tensile. The equation for line in this case is

$$\sigma_{stabilization} = 14.66 \frac{MPa}{hr} \cdot t + 541.83 MPa .$$

It should be noted that it is impossible to separate the effects of atomic peening and microstructure stabilization, thus the equation for $\sigma_{stabilization}$ reflects its starting point which is set by the previously imposed stresses (atomic peening and CTE mismatch).

The effects of oxidation in the grain boundaries can be noted by the blue portion of the curve. Although oxidation begins as soon as the sample is exposed to the atmosphere, this factor does not dominate the stress state immediately. In this case, it is the effects of oxidation that bring the σ_{xx} component of stress into the compressive regime. The equation for this curve is:

$$\sigma_{Oxidation} = 525238.08 MPa - 523173.87 \frac{MPa}{hr} \cdot t^{0.0007} .$$

The effects of IMC growth on the σ_{xx} stress state in this case are zero because Al and Sn have no IMC. This shows that the blue curve is entirely due to oxidation. Again,

attention needs to be drawn to the fact that effects of oxidation cannot be separated from previously imposed stresses (those of CTE mismatch, atomic peening, and microstructure stabilization), thus the equation for $\sigma_{Oxidation}$ reflects its starting point.

Now that this information has been gathered, we can now extrapolate the entire stress state of the film. First we note that there are no shear stresses in this example, so all the components can be added straight away due to the lack of shear coupling in the compliance matrix. Then we note that atomic peening and microstructure stabilization happen in all three normal components (σ_{xx} , σ_{yy} , and σ_{zz}). CTE mismatch occurs via equation A3.3.1 in the σ_{xx} and σ_{zz} components while the third component is zero. Lastly the effects of oxidation in within the grain boundaries effect only the σ_{xx} and σ_{zz} components. Thus the final stress state can be stated as

$$\sigma = \begin{pmatrix} \sigma_{Intrinsic} & 0 & 0 \\ 0 & \sigma_{Before_Oxidation} & 0 \\ 0 & 0 & \sigma_{Intrinsic} \end{pmatrix};$$

where $\sigma_{Intrinsic}$ is found by evaluating the $\sigma_{Oxidation}$ equation when $t = 3000$ hrs, and $\sigma_{Before_Oxidation}$ is simply the stress state of the system before the oxidation became the dominant factor (the 2nd point on the plot for this case). In numbers, the final stress state for this example is:

$$\sigma = \begin{pmatrix} -791.89 & 0 & 0 \\ 0 & 893.82 & 0 \\ 0 & 0 & -791.89 \end{pmatrix} MPa.$$

In the cases where an external shear stress is applied (such as section 3.9), the final stress cannot be found through basic addition, because σ_{xx} , σ_{yy} , and σ_{zz} are

coupled by the shear strains through the compliance matrix. Thus, it is also necessary to find the intrinsic strain state:

$$\underline{\underline{\varepsilon}}_{\text{Intrinsic}} = \frac{\underline{\underline{\sigma}}}{E_f} = \frac{1}{42\text{GPa}} \begin{pmatrix} -791.89 & 0 & 0 \\ 0 & 893.82 & 0 \\ 0 & 0 & -791.89 \end{pmatrix} \text{MPa}.$$

$$= \begin{pmatrix} -18.9 & 0 & 0 \\ 0 & 21.3 & 0 \\ 0 & 0 & -18.9 \end{pmatrix} \cdot m$$

Once the strain state is found, the externally applied strain state can be added directly and converted to look like a six dimensional vector

$$\left(\underline{\underline{\varepsilon}}_{\text{Intrinsic}} + \underline{\underline{\varepsilon}}_{\text{External}} \right) \rightarrow \left(\underline{\underline{\varepsilon}}_{\text{Intrinsic}} + \underline{\underline{\varepsilon}}_{\text{External}} \right),$$

then the final stress state can be found through the generalized Hooke's Law

$$\underline{\underline{\sigma}}_{\text{Final}} = \underline{\underline{S}} \left(\underline{\underline{\varepsilon}}_{\text{Intrinsic}} + \underline{\underline{\varepsilon}}_{\text{External}} \right);$$

where $\underline{\underline{S}}$ is the 6x6 compliance matrix.

APPENDIX 4 EXTERNAL STRESS FIXTURE DESCRIPTION, DIMENSIONS, AND DIAGRAMS

In order to produce a uniform tangential (σ_{xx}) stress throughout a given substrate, two fixtures were manufactured for this study. These two fixtures had to accomplish three main goals; 1) have multiple constant and well known curvatures, 2) enable easy sample removal and replacement (for intermediate examinations), and 3) inflict minimal sample damage (particularly to the film). These fixtures were designed to have diameter curvatures of -1", -2", -3", -5", 5", 3", 2", and 1", and to hold 3 1 cm x 5.08 cm samples at each curvature. The samples were designed to be held in place by aluminum clamps. These clamps apply no normal stress to the films of the compressive samples, and only apply a normal stress to the very edges of the tensile samples.

The concentric curves of the compressive fixture were milled from a solid piece of 6061 Al 3" x 3.25" x 6". The solid piece was mounted on a mill, and each of the successive steps were milled into place and the 1" hole was milled. Then the fixture was mounted on a precision turn table fixed to the mill table such that the 1" hole was centered precisely in the center of the turn table. The y-axis of the mill was adjusted so that as the turn table was rotated, the 1" mill bit acted as a bore, and each of the successive curves were bored in this manner. Finally the holes for the clamps were drilled and hand-tapped.

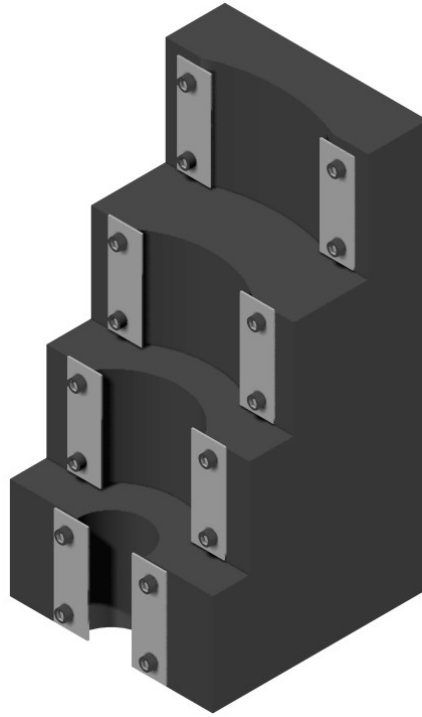


Figure A4.1 Computer aided drawing of the fixture used to impose external compressive stress.

The concentric curves of the tensile fixture were all made from a single cylindrical piece of 6061 Al (5.25" x 7"). This cylinder was mounted on a lathe and each of the steps were cut to size. Finally a 1" hole was bored into the bottom of the fixture so that it could be mounted on the precision turn table which was fixed on the mill. As with the compressive fixture, this fixture was mounted concentrically with the turn table. Once it was mounted on the mill, the holes for the clamps were drilled by rotating the precision turn table to the calculated angle (to a precision of ± 5 arc-seconds) which ensured arc lengths of 2" (5.08 cm) precisely.

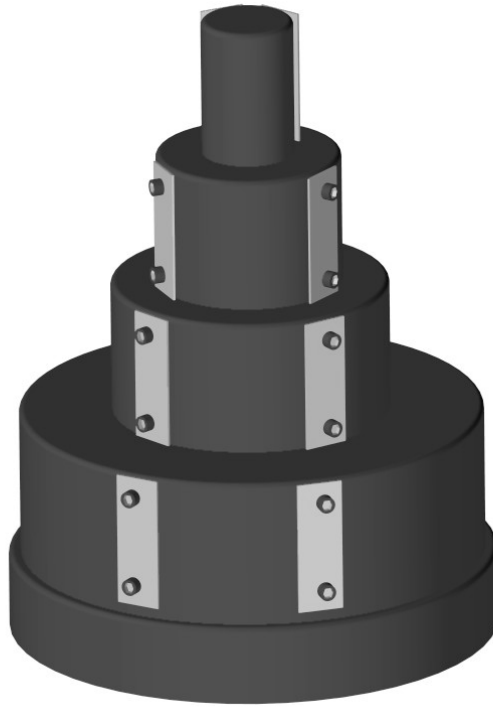


Figure A4.2 Computer aided drawing of fixture used to impose external tensile stress.

These two fixtures are geometrically pleasing as they are exact volumetric negatives of each other. This artistic element is embodied in the fact that the tensile fixture fits precisely inside of compressive fixture with no extra space. This feature is not only artistically pleasing, but also serves the practical function of minimizing storage space when not in use. The post production measured dimensions are shown in Figures A4.3 and A4.4 below.

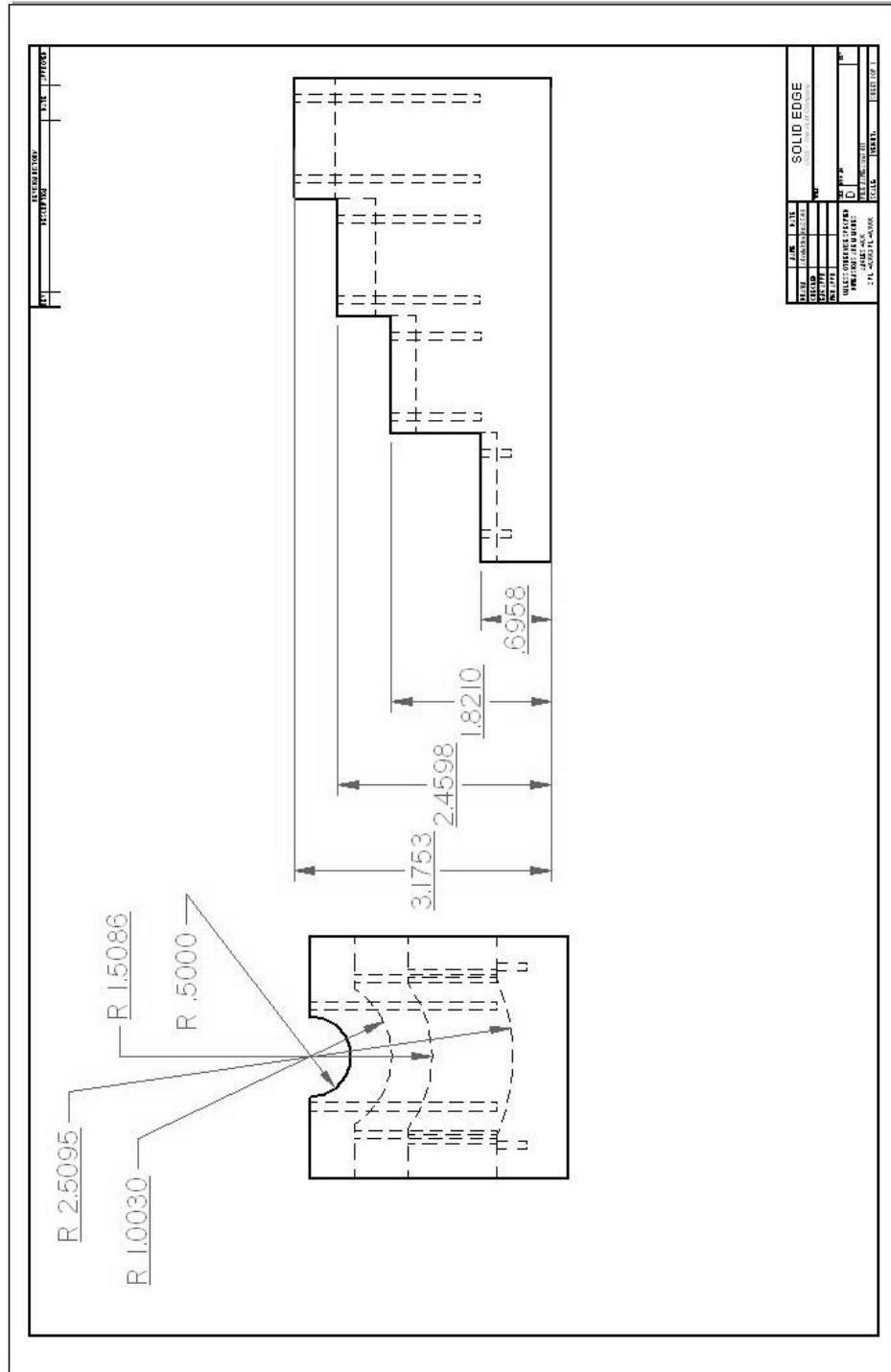


Figure A4.3 Physical dimensions of fixture used to produce externally applied compressive stress.

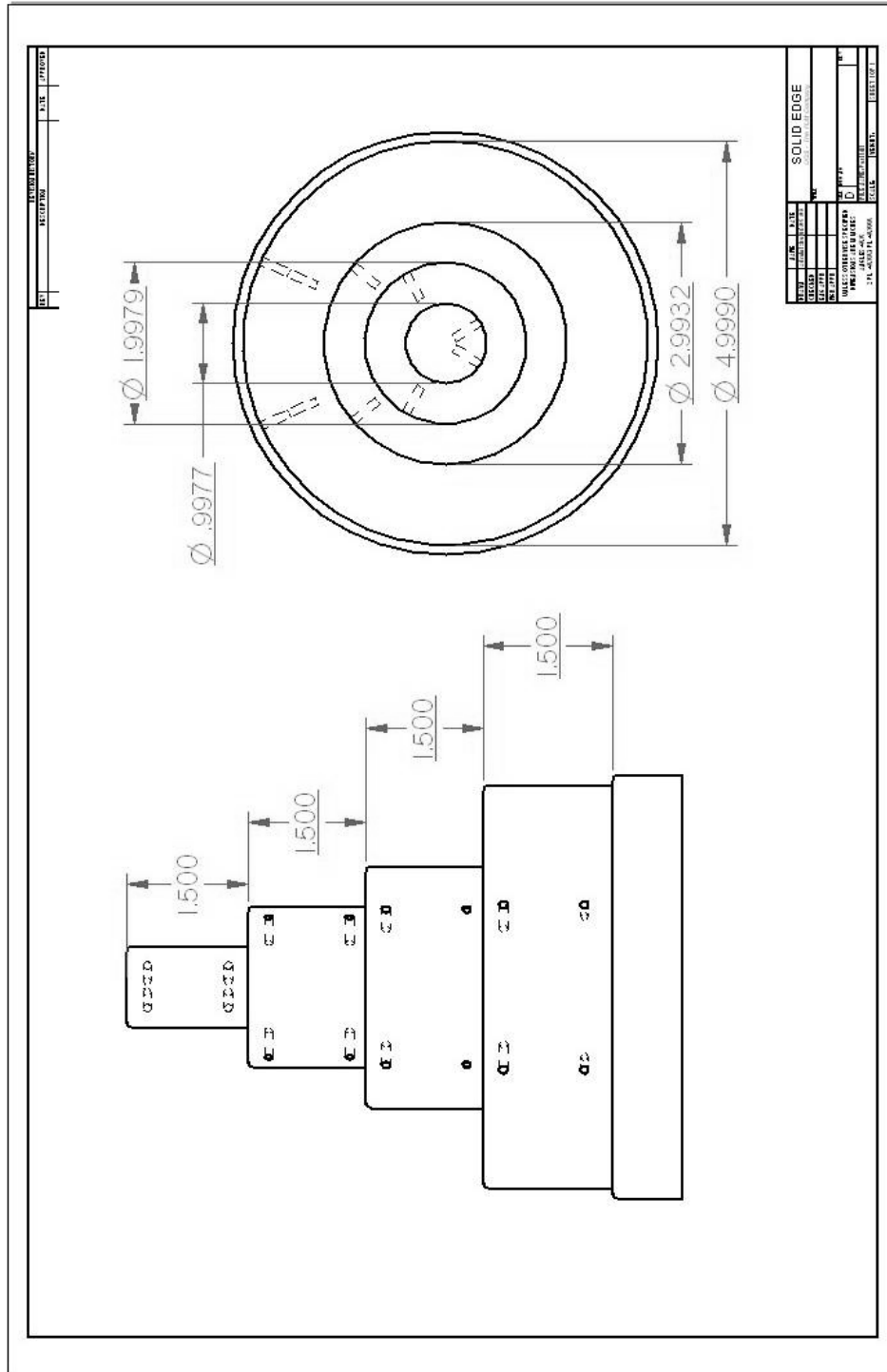


Figure A4.4 Physical dimensions of fixture used to produce externally applied tensile stress.

APPENDIX 5 PLOTS OF TOTAL STRESS STATE VS QUALITIES OF WHISKER GROWTH WHEN EXTERNAL STRESS IS VARIED

A5.1 6000Å of Tin on a 0.125 mm Brass Substrate

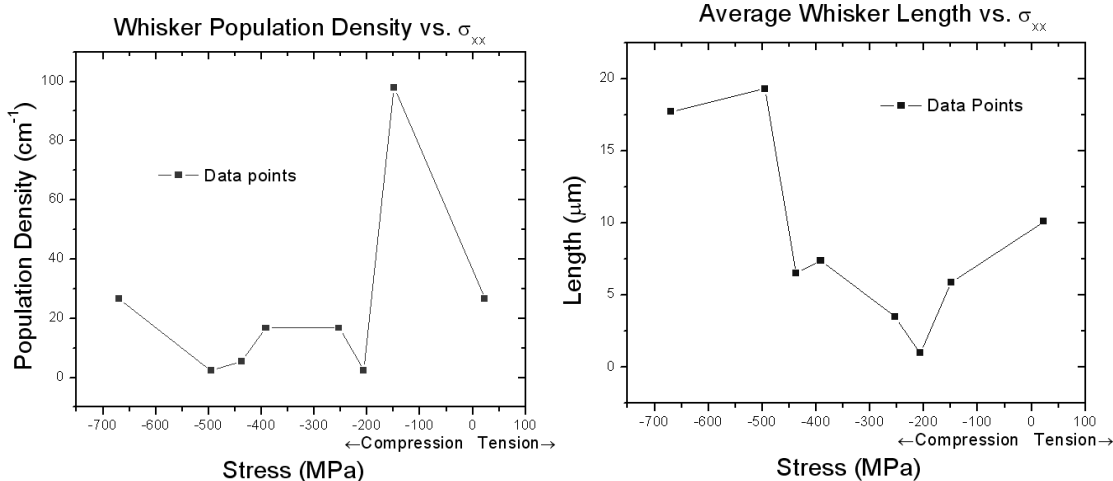


Figure A5.1 Whisker growth as a function of the σ_{xx} component of total stress.

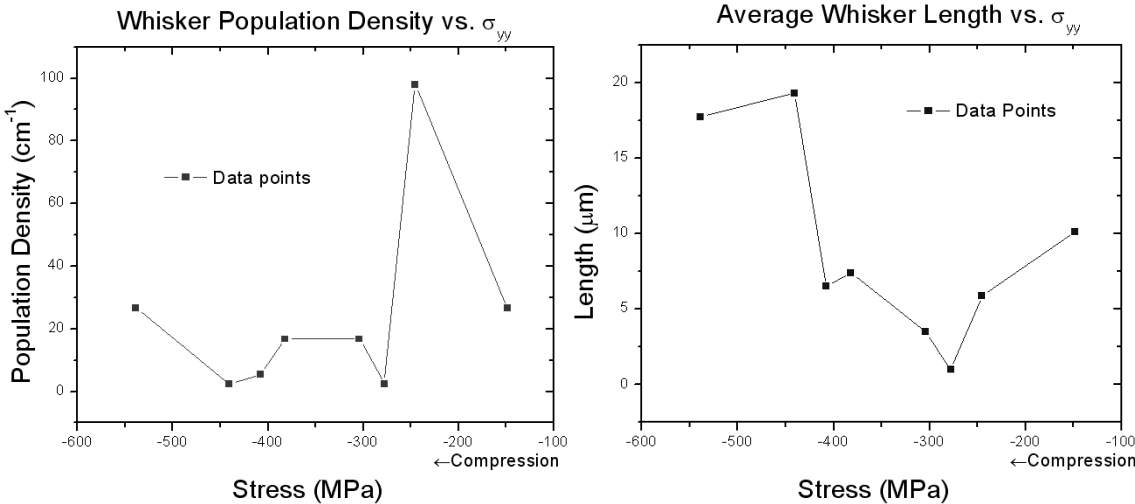


Figure A5.2 Whisker growth as a function of the σ_{yy} component of total stress.

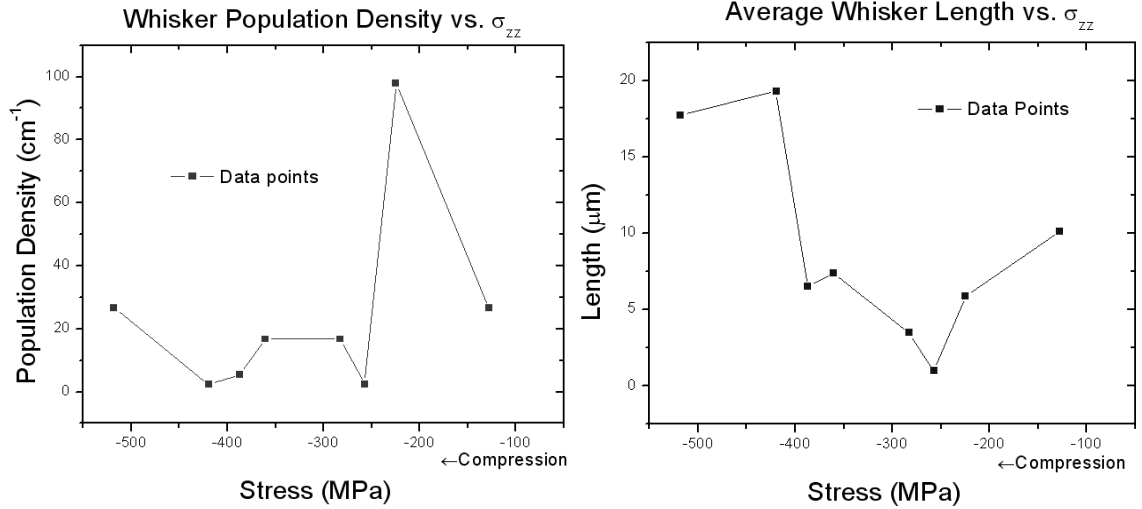


Figure A5.3 Whisker growth as a function of the σ_{zz} component of total stress.

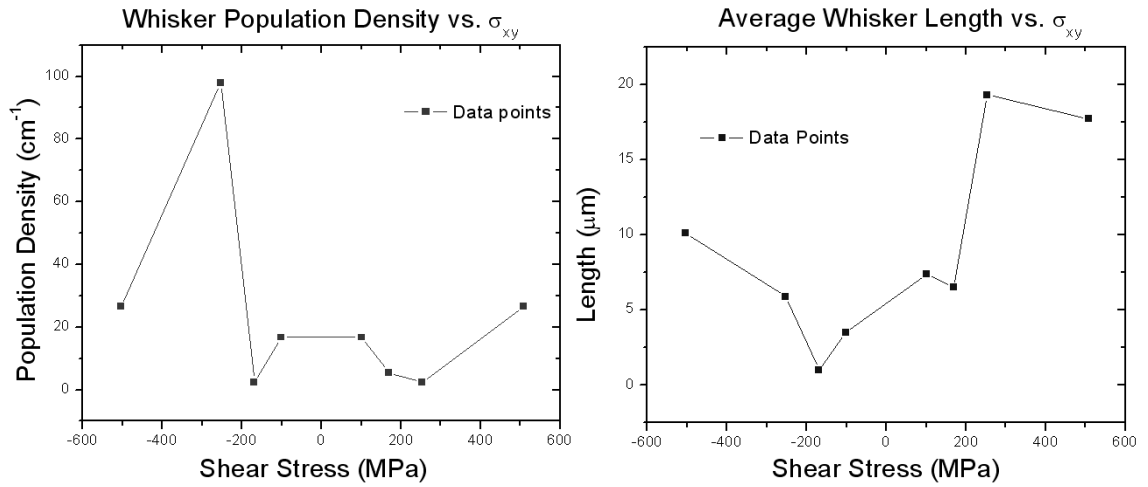


Figure A5.4 Whisker growth as a function of the σ_{xy} component of total stress.

A5.2 6000Å of Tin on a 0.25 mm Aluminum Substrate

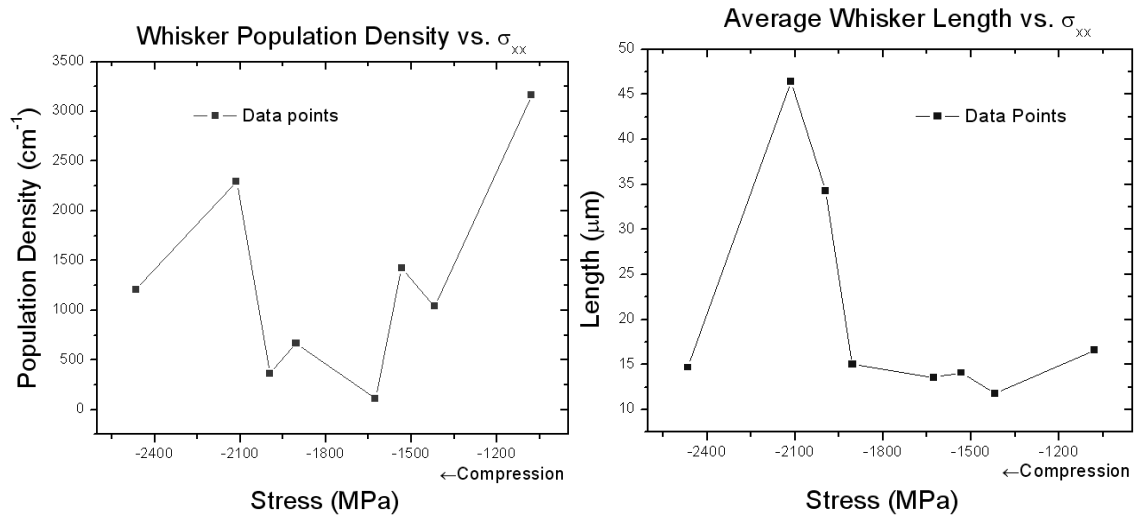


Figure A5.5 Whisker growth as a function of the σ_{xx} component of total stress.

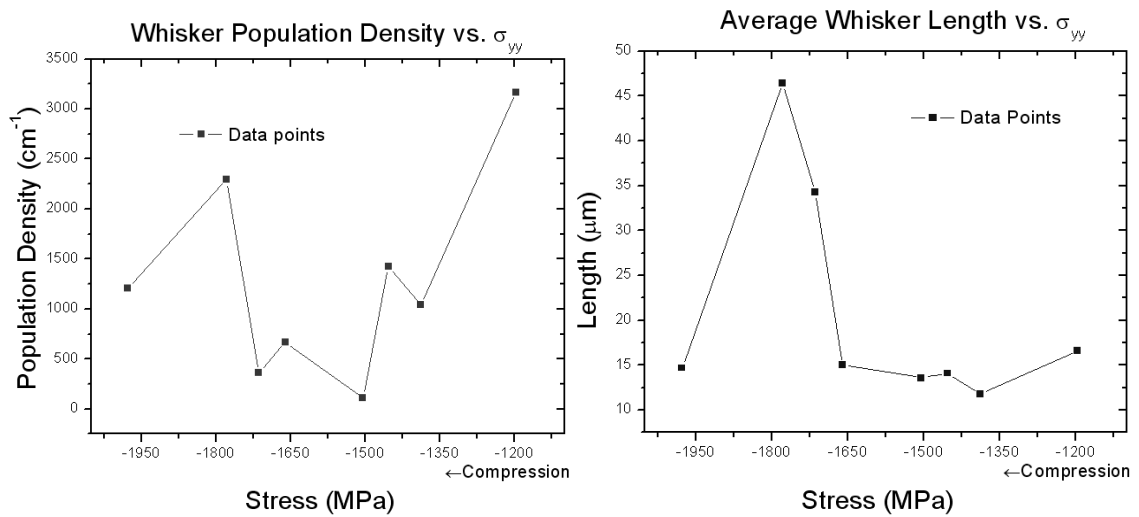


Figure A5.6 Whisker growth as a function of the σ_{yy} component of total stress.

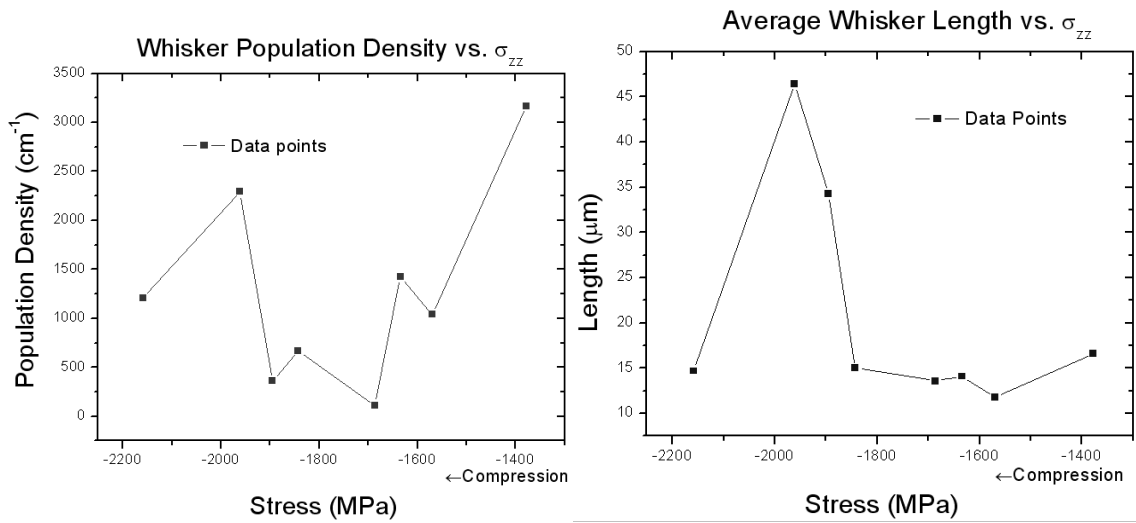


Figure A5.7 Whisker growth as a function of the σ_{zz} component of total stress.

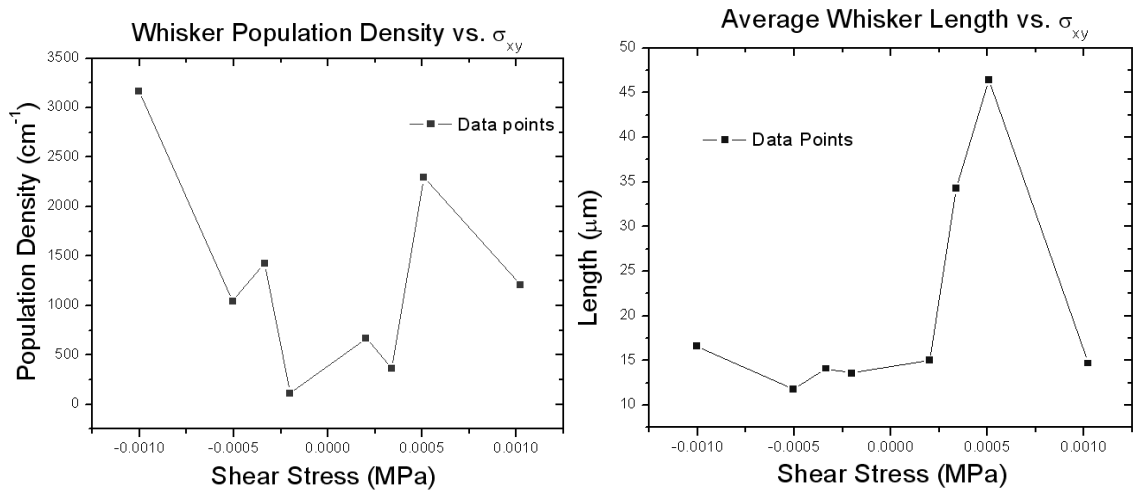


Figure A5.8 Whisker growth as a function of the σ_{xy} component of total stress.

A5.3 1500Å of Tin on a 0.25 mm Aluminum Substrate

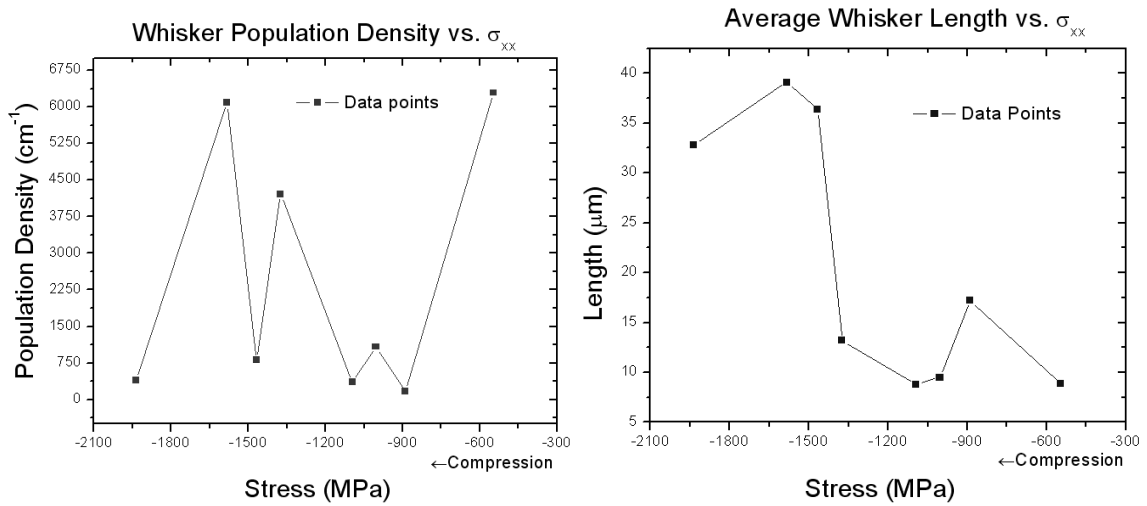


Figure A5.9 Whisker growth as a function of the σ_{xx} component of total stress.

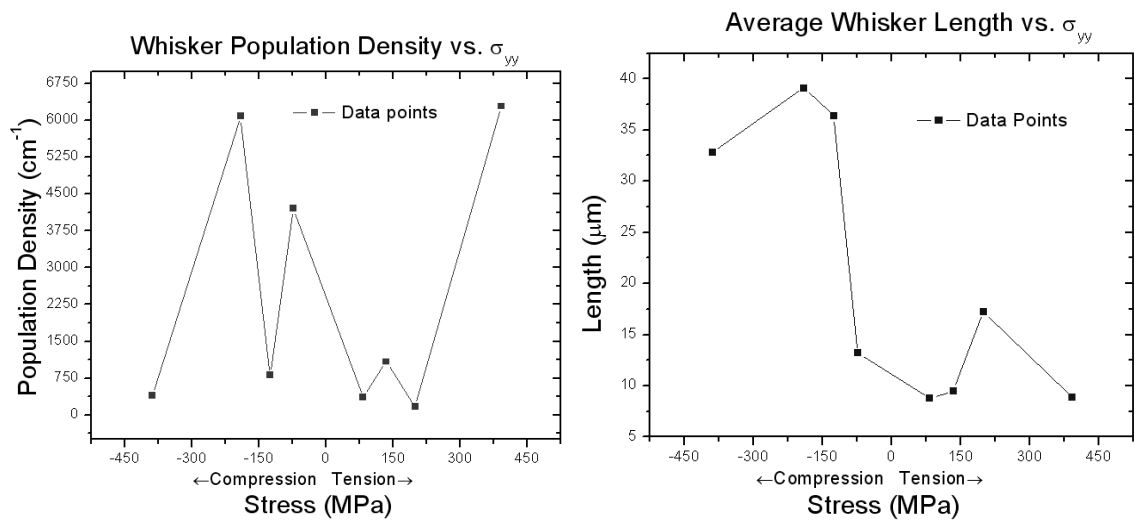


Figure A5.10 Whisker growth as a function of the σ_{yy} component of total stress.

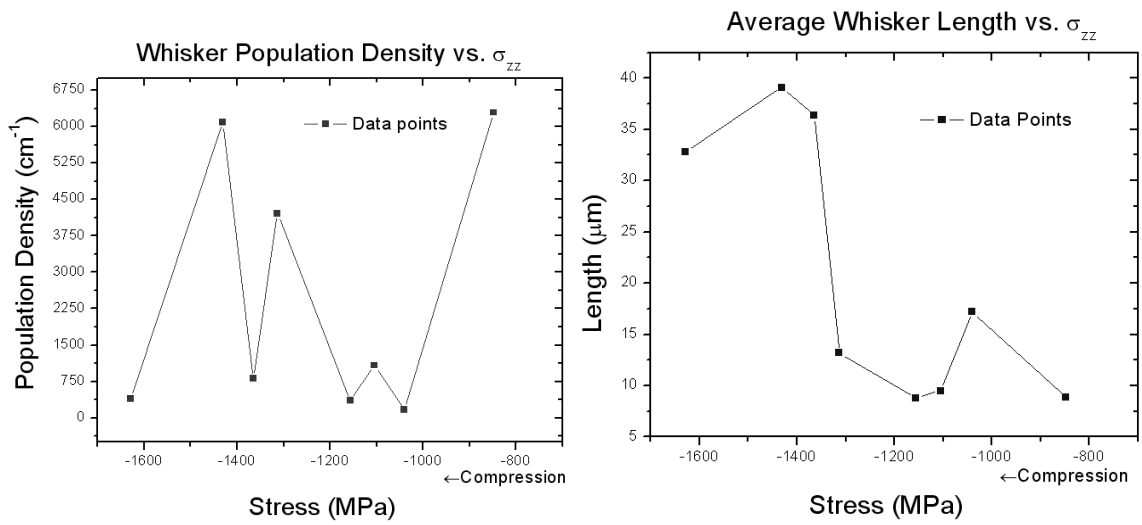


Figure A5.11 Whisker growth as a function of the σ_{zz} component of total stress.

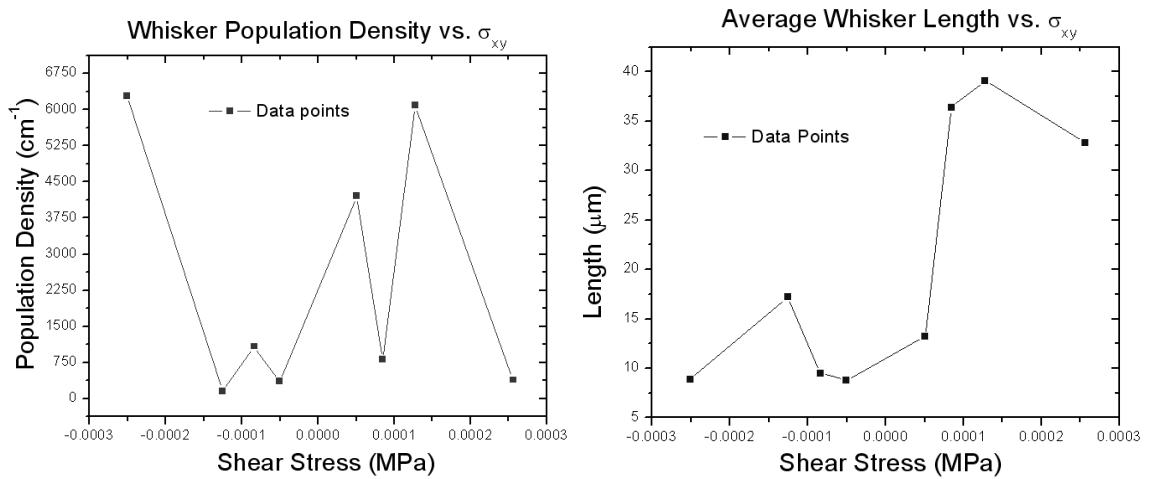


Figure A5.12 Whisker growth as a function of the σ_{xy} component of total stress.